TUHH
Technische Universität Hamburg-Harburg

Project Work Thesis

TONGJI UNIVERSITY
COLLEGE OF MECHANICAL ENGINEERING

TECHNISCHE UNIVERSITÄT
HAMBURG-HARBURG
INSTITUT FÜR REGELUNGSTECHNIK

Prof. Dr. Liu Haijiang
Prof. Dr. Herbert Werner

Development of a Control System for the Shànghǎi Subway Flood Gate System

Author
B.Sc. Christian Hoffmann

Supervising Tutor
M.Sc. Pan Zhenhua

June, 29th 2009

Ich versichere, diese Arbeit im Rahmen der am Arbeitsbereich üblichen Betreuung selbstständig angefertigt und keine anderen als die angegebenen Quellen und Hilfsmittel benutzt zu haben.

I hereby affirm the sole authorship of this thesis, that it has been completed under the supervision common to the institute and that no sources or auxiliary means have been used other than specified.

Hamburg-Harburg, June, 29$^{\text{th}}$ 2009

Abstract

In this thesis a control system for the Shànghǎi subway flood gate system is developed. The system has been realised utilising discrete position sensors and a simple but efficient control logic implemented on a SIEMENS *S7-200 programmable logic controller. A more sophisticated control algorithm for continuous position control by means of a digital RST sensitivity shaping controller is suggested, designed and compared against the discrete positioning solution. By further generalisation, position control of common wire-rope hoist driven lifting devices carrying unknown loads is considered. An adaptive control algorithm scheme utilising recursive least squares online identification and subsequent controller adaptation is developed and analysed.*

Keywords: Shànghǎi subway flood gate system, programmable logic controller, RST sensitivity shaping controller, wire-rope hoist driven lifting device, unknown load, adaptive control algorithm, recursive least squares online identification

TONGJI UNIVERSITY
COLLEGE OF MECHANICAL ENGINEERING

Mr. B.Sc. Christian Hoffmann
Student ID at Technical University Hamburg-Harburg: 20522587

Task description for a Project Work Thesis

Subject:

Development of a Control System for the
Shànghǎi Subway Flood Gate System

As part of the contribution of TONGJI University to the safety of the citizens and the protection of the metro network of the city of Shànghǎi, a team of three students at the COLLEGE OF MECHANICAL ENGINEERING has been assigned to develop and realise the control system of the Shànghǎi flood gate security system. The mechanical engineering and design of the gate has been finished prior to the beginning of the research and implementation of the control system. The imposed constraints are thus twofold: To effectively make use of the preexisting mechanical parts and to intelligently add a simple, feasible and robust control system with all components needed. It has been Mr. Hoffmann's task to give aid in the realisation and to further investigate a more sophisticated position control structure and algorithm of the flood gate. More specifically, his task has been comprised of the following items:

- Aid in the realisation and documentation of the flood gate control system.
- Support in the experimental testing of a control system prototype.
- Development of a new position measurement paradigm.
- Detailed derivation, assessment and documentation of a control algorithm suited to the new paradigm under given hardware constraints and the inclusion of possible new hardware components.
- Conduction of a preliminary controller design and its analysis under realistic assumptions and necessary means, i.e. mathematical modelling, experiments, etc.
- Extension of the control problem to investigate applicability under uncertain conditions, i.e. unknown loads, in order to enable the development of a more widely applicable standard lifting device position control solution.

Shànghǎi, June, 29th 2009

Prof. Dr. Liu Haijiang

Contents

Nomenclature

Control Systems Nomenclature

$\boldsymbol{\Phi}$	Discrete time system matrix.
$\boldsymbol{A}$	Continous time system matrix.
$\boldsymbol{\Gamma}$	Discrete time input gain vector.
$\boldsymbol{b}$	Continous time input gain vector.
a_i	Discrete time transfer function denominator polynomial coefficients.
b_i	Discrete time transfer function numerator polynomial coefficients.
$\boldsymbol{C}$	Continous/discrete time output gain vector.
$\boldsymbol{D}$	Continous/discrete time feedthrough gain vector.
$e(t)$	Control error in continuous time domain.
$e_k, e(k)$	Control error in discrete time domain — k^{th} sample.
f	Frequency.
$G(s)$	Continuous time transfer function of plant model.
$H(z^{-1})$	Discrete time transfer function of plant model.
ω_0	A second order system's natural frequency.
$r(t)$	Controller reference input in continuous time domain.
$r_k, r(k)$	Controller reference input in discrete time domain — k^{th} sample.
s	Continuous time transfer function independent variable (LaPlace-Transform)
$S_{21}(z^{-1})$	Sensitivity transfer function from 2 to 1.
$\theta_i(t)$	Time-varying parameter.

$\boldsymbol{\theta}(t)$	Time-varying parameter vector.
$u(t)$	Controller output in continuous time domain.
$u_k, u(k)$	Controller output in discrete time domain — k^{th} sample.
$\boldsymbol{x}$	State vector.
$y(t)$	Plant output in continuous time domain.
$y_k, y(k)$	Plant output in discrete time domain — k^{th} sample.
ζ	Damping parameter.
z^{-1}	Discrete time transfer function independent variable (z-Transform) and time shift operator

General Measures

$\Delta\alpha$	Difference in rotation.
φ	Angle.
b	Damping coefficient.
d	Diameter.
η	Coefficient of performance.
i	Transmission factor.
k	Gain.
M, m	Mass.
T	Torque.
T_s	Sampling time.
Δx	Difference in location.

Abbreviations

AC	Alternating Current
ARX	Auto Regressive Exogenuous
ARMAX	Auto Regressive Moving Average Exogenuous
DC	Direct Current
DI	Digital Input
DO	Digital Output
DSP	Digital Signal Processor
I/O	Input/Output
ICR	Instantaneous Center of Rotation
LPV	Linear Parameter-Varying
PC	Personal Computer
PLC	Programmable Logic Controller
RMB	Rénmínbì - Chinese Currency (People's Currency)
SFC	Sequential Function Chart
SISO	Single-Input-Single-Output
MIMO	Multiple-Input-Multiple-Output
VFD	Variable Frequency Drive

1. Introduction

The main part of Shànghǎi and its subway in particular is below mean sea level. Therefore the local government has taken precautionary measures to ensure higher safety and less economic losses during flood season from June until September. In 2007 about 19 million RMB have been invested to improve the storm drainage system to prevent certain districts from suffering frequent inundation [6].

Furthermore, as climate change progresses, until the year 2050 the sea level may rise by 20 to 60 cm as predicted by the Tiānjīn-based National Marine Data and Information Service (NMDIS) [7], which increases the risk of inundation even more.

Additional means are taken to protect Shànghǎi's vast Metro network, of which the most part is build underground. Flood gates have been installed on the subway, which are supposed to protect all parts of the network, that — in case of a major flood — have not yet been submerged. While some of the protective gates are already in place, their control systems are not.

It is the task of a team of three students led by Prof. Liu Haijiang of Tongji University, Shànghǎi, to develop a solution for the control system and its practical realisation including the selection and utilisation of all gear. As a further step thorough investigations have been made on how to improve the position control portion of the overall system with regard to gate movement speed and sensor layout efficiency.

1.1. Overall System Description and Purpose

The flood gate's purpose is to secure parts of the Metro network from inundation. In case of imminent threat, the gate is operated from a control room directly beside the gate. All maintenance is also done directly in the gate's main control room. From there, the gate has to be unlocked manually, before it can be controlled to block the water's way. Once unlocked, basic actions can also be exerted from a remote control room at the nearest subway station. In addition, the remote station yields a simple surveillance system to monitor the flood gate's status. An even higher instance, like a Shànghǎi disaster control center, is considered to directly communicate with the individual flood gates' control systems in the future, but this addition to the overall communication scheme will not be dealt with in this thesis. Figure 1.1.1 illustrates the general arrangement.

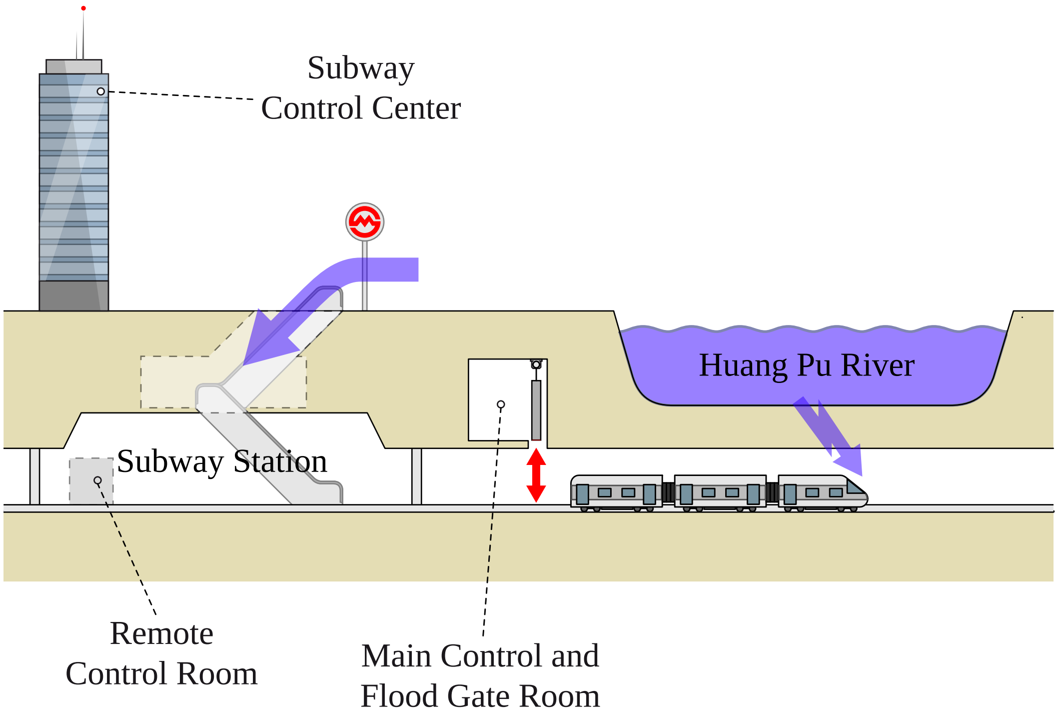

Figure 1.1.1.: Flood Gate System Illustration

Since some flood gates have already been installed on the subway network, the design of the mechanical apparatus is already considered final. The next section explains the design.

1.2. The Flood Gate Electro-Mechanical Device

The gate is lifted or lowered by a hoist, which is driven by an electric motor. The hoist is located above the gate and the lifting force is transmitted via two steel cables furled up on two separate windlasses as part of the hoisting device. Linear guidance is kept simple by employing strong rubber tubes.

To each side of the gate, there are two v-shaped support clamps, mounted on stands. They are connected to the stands by a free hinge which allows the clamps to rotate freely in 360°. The support devices can be latched onto corresponding brackets attached to the gate's sides, which prevent the clamps from rotating. The jamming can only be resolved by an upward motion of the gate, such that in *opened* position, the gate is fully carried by all four clamps.

The support clamps' center of gravity is located in the center of both arms of the v-shape and is sufficiently detached from the hinge, such that the clamps turn over and form an upside-down v, when they are not wedged against the gate's brackets. The free rotational movement of the support clamps in this case is vital for the execution of all basic movements.

An experimental version of the flood gate has been manufactured, which is reduced in size, but employs the same mechanisms. Figures 1.2.1 to 1.2.3 show fotos of the experimental setup.

(a)

(b)

Figure 1.2.1.: Experimental Flood Gate: (a) Front View, (b) Support Clamps in Latched Position

(a)

(b)

Figure 1.2.2.: Experimental Flood Gate: (a) Automatic Lock Solid Cylinder, (b) Automatic Lock Notch in Flood Gate

The mechanical design is strongly coupled to the possible basic motions and key positions of the flood gate, which are the subject of the next section.

Figure 1.2.3.: Experimental Flood Gate: Linear Bearing

1.2.1. Final Key Positions

The flood gate is able to assume three basic final key positions as follows. In a final key position the electric hoist is not required to apply force for the gate to retain its position.

Opened Position is defined as the gate being supported by all four pairs of clamps and brackets.

Closed Position is defined as the gate being supported by the ground. The gate is supposed to seal the complete subway's passageway.

Maintenance Position is defined as the gate being lifted beyond the opened position, while it is supported by the automatic lock's solid cylinder bolt.

Other positions, which require the electric hoist to hold the gate, are also used for maintenance purposes. These will be denoted **intermediate (key) positions**, in order to distinguish them from the final key positions.

The flood gate's support device mechanism is best explained by describing the basic motions, which are necessary to open, close or repairing it.

1.2.2. Basic Motions

Figure 1.2.5 illustrates consecutive closing and opening phases in a series of intermediate steps. There is also an even more illustrative animation on the accompanying disc. A dynamical simulation has been done with the help of an educational version of AUTODESK INVENTOR 2008 PROFESSIONAL. Damping, friction and material coefficients have been estimated for this purpose. In the following description, numbers refer to the corresponding intermediate step in figure 1.2.5.

When opened, the gate is supported by four clamps latched in corresponding brackets attached to the side of the gate (1). Lifting the gate up from the opened and latched

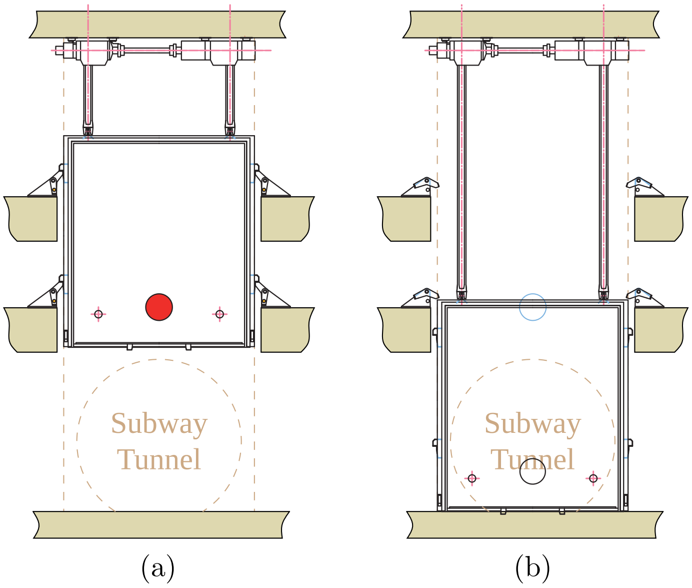

Figure 1.2.4.: Flood Gate Final Key Positions: (a) Opened Position, Automatic and Support Device Locks Engaged, (b) Closed Position, (c) Maintenance Position, Automatic Lock Supports Gate

position will eventually cause the support clamps to slide off (3) the brackets and oscillate into their loose equilibrium positions (4). At this point the gate can again be lowered completely, due to the brackets now passing the clamps without any hindrance (5 – 10).

The gate can be opened again by lifting it up, until the clamps slip by the protruding parts of the brackets (12 – 17), then lowering it into latched position (18 – 1). This simple, yet effective, purely mechanical mechanism is designed to ensure a maximum of operability even under total loss of power. To enable this, the hoist can also be operated manually.

While the gate is opened, it is also secured by a massive lock. This lock comes in the form of a solid cylinder, which can be manually or automatically inserted into a notch in the gate. Furthermore, the support clamps are secured by bolts, that have to be removed manually, in order to enable them to hinge away from latched position.

For maintenance, the gate can be lifted up further from *opened* position. While the gate is undergoing maintenance, it is supported by the solid cylinder of the automatic lock rather than by the support clamps. The bolt of the lock can be extended to go underneath the gate.

For additional maintenance work, the gate is also able to assume any desired intermediate position by controlling the electric hoist.

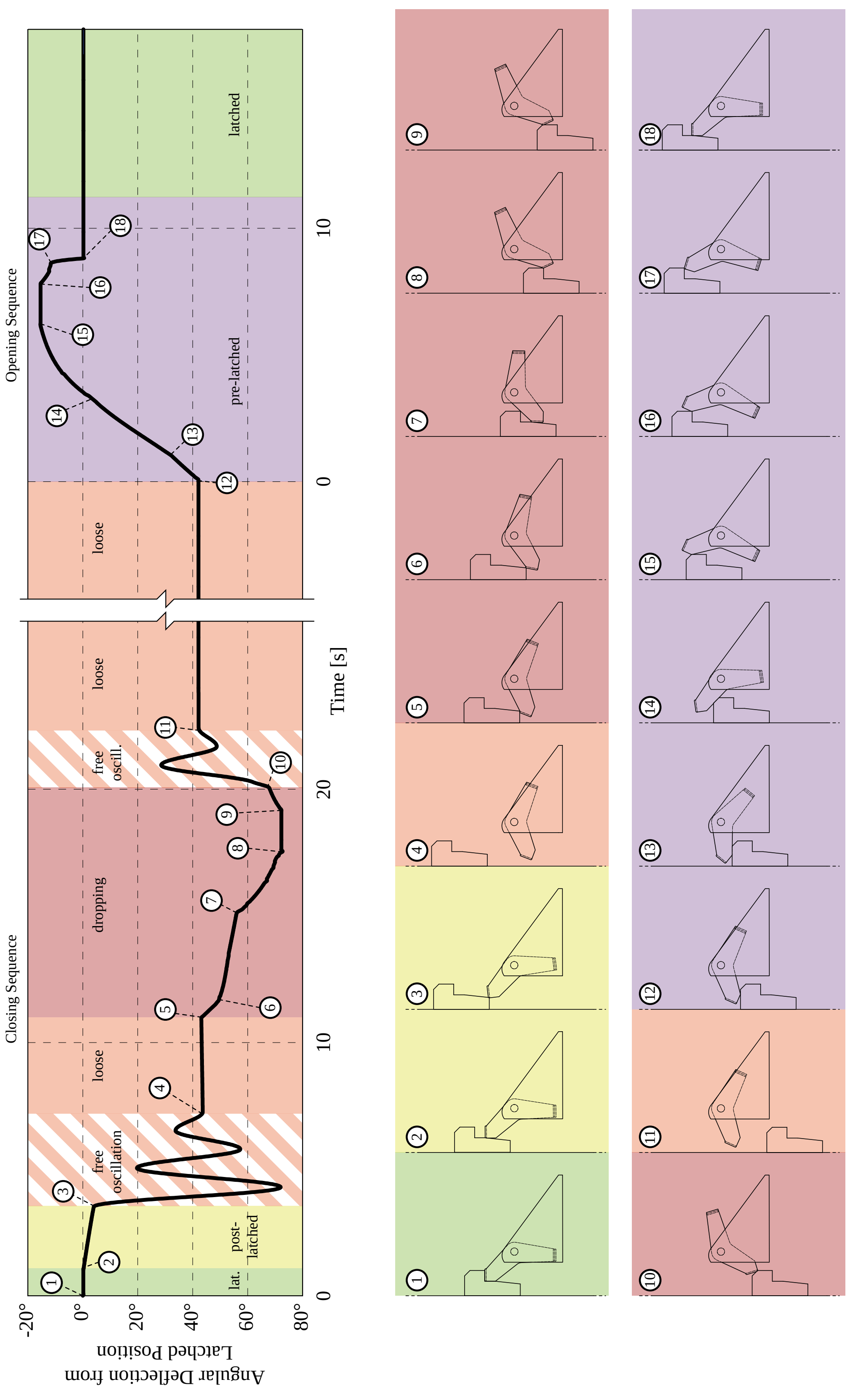

Figure 1.2.5.: Support Device Latching Mechanism (Based on dynamical simulation data generated by AUTODESK INVENTOR 2008 PROFESSIONAL Educational Version)

1.3. Summary — System Abstract

In order to provide a first general overview of the control problem, the before-mentioned and additional design requirements are summarized in note form. The items are intentionally kept detached from implementation issues, as to enable for the development of multiple approaches with regard to the implementation of algorithms, from which the most efficient may be selected.

1.3.1. Control Task Definition

- A programmable logic controller[1] controls the flood gate position and automatic locks.
- In nominal operation the PLC can let the gate assume *closed*, *opened* and *maintenance* position.
- The transition from one position to another can be overrided and the PLC brings the gate back to the former position.
- The gate's speed of movement is adjusted according to its position, such that hard impacts are prevented.
- The control system provides a convenient interface via a manual control panel and by communicating with a remote control panel. A camera is used for surveillance from the remote control room.
- The status of manual security locks attached to the flood gate's support devices are supervised by the PLC.
- An additional maintenance mode allows to position the flood gate at any desired intermediate position.

1.3.2. Design Philosophy

- The main control room containing the PLC device and manual control panel is located above the subway.
- The support devices' manual security locks, as well as the manual control panel are operated from the main control room.
- A remote control room is located at the nearest subway station. Its purpose is to supervise the gate's current status, perform the remote control of the gate's operation, while the manual security locks are disengaged, and report some relevant information to the Shànghǎi subway control center.

[1] In the following, "programmable logic controller" will be called "PLC" for short

- While no water is spilling into the subway's network, the flood protection gate system may *under no circumstances* pose any threat to the nominal operation of the subway, let alone to the life of any human being.
- In case of doubt, the system should rather fail to secure the subway's network than accidentially block the path of any incoming subway train.

1.3.3. Objectives

- The positioning of the gate in predefined *opened*, *closed* and *maintenance* positions should be carried out quickly and efficiently under consideration of all possible causes of failures.
- The arbitrary positioning of the gate should be tolerated to be precise within error bounds of $\pm 10\,\mathrm{mm}$.
- The individual components' reliability properties should not demand for maintenance intervals shorter than half a year.
- The control interface should be designed, such that it provides an intuitive and safe way of operation for both operating personell and subway passengers.
- The control system should be robust against any breakdown in power supply. In case of power supply failure, fail-safe operation should be guaranteed and vital information is either to be stored in persistent memory or has to be readily available at the next system startup.

1.4. Aims of the Thesis

It has been the project's aim to develop and extend the Shànghǎi flood gate control system. The realisation of a switch logic based control system has been carried out, while in parallel a more sophisticated discrete rotary encoder based feedback control synthesis approach has been utilised to design and evaluate benefits of a potential upgrade to the control system. This thesis documents the results of the project work.

More specifically, the aims of this thesis are comprised of the following items:

Documentation of the Realised Control System A rough but insightful documentation of the engineering work done with regard to the switch logic PLC based control system shall be given.

Issues of the Realised Control System Possible issues of the realised control system shall be pointed out and discussed to evaluate the necessity of improvement.

Suggestions on Improvements Suggestions on Improvements shall be given and investigated in particular with respect to a position control algorithm and its according sensor layout.

Investigation of a Feasible Synthesis Approach A suitable control algorithm synthesis approach shall be explained and carried out. Given hardware constraints will be taken into account to ensure a cost-effective implementation.

Controller Design and Simulation With a suitable mathematical model, simulations of controller designs shall be conducted and evaluated. Disturbances will be employed to reflect real world conditions and the controller design shall be refined to cope with this.

Generalisation to Lifting Device Position Control with Uncertain Load Conditions The derived control algorithm shall be extended to be applicable to lifting device position control problems with uncertain load conditions. This is intended to be the basis of further research on developing a dedicated lifting device position control module with extended functionality.

1.5. Outline of the Thesis

This thesis is comprised of two main parts: The documentation of the current realisation of the Shànghǎi flood gate system in chapter 2 and the development of an improved position control algorithm and its extension to uncertain plants from chapter 3 to 5.

Chapter 2 begins with a description of the system configuration in section 2.1. As part of the system configuration, the arrangement of all control system components on workstation level is sketched (2.1.1) followed by a configuration diagram of the PLC equipment and its connection scheme (2.1.2). The system's arrangement analysis and illustration is concluded by a sensor layout diagram (2.1.3). Types and quantities of the sensors and their purpose are listed, which is vital for a deeper understanding of the control mechanisms and logic explained in section 2.2. First, the basic motions imposed by the mechanical design of the flood gate support devices and the sensor layout is depicted. This is followed by a sequential function chart of the gate's operating modes. Detailed flowcharts of the processes on switch logic level are omitted in this thesis, since they would not add to the overall understanding of the flood gate control system's functionality. Instead, the control panel's design is briefly illustrated (2.2.1) and the requirements with respect to the control cabinet are listed, rounding off the overall picture of the control system as it has been realised.

The thesis continues with a short report on the prototypical testing of the control system on a smaller size flood gate in section 2.3. Special attention is paid to the problems, that occurred during the initial testing phase (2.3.1). A separate section 2.4 is dedicated to listing and developing ideas on how to improve the existing control system, in particular by introducing a new position measurement paradigm based on rotary encoders (2.4.1) and pointing out its possible advantages over the old design (2.4.2). This leads to the second part of the thesis, which deals with the development of a feasible control algorithm by approaches and rigoros computation procedures common to control theory.

Chapter 3 provides the basis for the following chapters. Before the mathematical model is derived in terms of differential equations in section 3.2, assumptions are made with regard to the instrumentation, drive and transmission system in section 3.1 and discussed for their viability. Special attention is paid to the derivation of a symbolic discrete transfer function representation via transformation of the continuous transfer function (3.2.2). This will be used later in the thesis to develop and optimise an adaptive controller synthesis algorithm. The notion of linear parameter-varying state space modelling is briefly described and a corresponding model is derived for simulation purposes (3.2.3).

The next chapter deals with the synthesis and design of a so-called discrete RST-structure controller. After the RST controller structure is explained, the necessary notation and formulae for the sensitivity functions are defined in section 4.1, the synthesis approach followed in this thesis presented (4.2). The synthesis approach is a mixture of applying pole placement and sensitivity shaping techniques in the framework of solving a Bezout Identity by a simple matrix inversion. To be able to properly evaluate the controller synthesis' results and in order to supply the user with tools on how to achieve a robust controller design, templates for upper and lower bounds on the sensitivity function plots are given in section 4.3. The actual controller design for the flood gate lifting device is carried out in section 4.4, followed by a discussion on possible implementation issues with a special focus on the control algorithms feasibility to the already existing equipment (4.4). This concludes the controller design investigation for the new flood gate position measurement paradigm.

Chapter 5 further expands on the ideas and approaches developed this far. It deals with the design of an adaptive controller for general lifting devices and in the case, that the lifted load mass may be unknown to a certain extent. First, the general adaptive controller scheme of an explicit self-tuning controller is reproduced, to provide a well-defined framework for the following derivations. After that, the recursive least squares online identification algorithm is briefly explained (5.2) and taken as a fixed part of the adaptive controller scheme employed, because it has been succesfully applied even to mechanical systems with fast dynamics in the literature [11]. For online use, the RST structure controller synthesis has to be optimised, with the aim not to depend on matrix inversions in every sampling instant. In section 5.3 the synthesis is actually reduced to a simple function evaluation, which then, however, is substituted in favour of a lookup table solution to avoid numerical instabilities. The controller is successfully applied to the simulated plant in the concluding section 5.4.

The final chapter 6 of this thesis summarises all results presented and provides an outlook on necessary adjustments to the flood gate control system, in order to realise the improved instrumentation and control paradigm. A possible development of a dedicated lifting device control module, which could also include an adaptive controller is also briefly discussed.

2. Current Realisation of the Flood Gate Control System Using PLC Logic

The Shànghăi flood gate security system, which has been briefly introduced in the previous chapter has already been well into the testing phase, when the theoretical work on an improved control system documented in chapter 4 and 5 was finished. The engineering work done to realise the flood gate control system in its current state has also been a part of the project. The following sections give a more detailed insight into the system's structure concluding with a discussion on a number of issues that occurred during testing and possible improvements.

2.1. System Configuration

A general overview of the complete control system's components, instrumentation and system arrangement will illustrate the flood gate system's design. Various literature helped in understanding and identifying the important structures and components of a PLC control system and its programming [2], [5], [4], [1].

2.1.1. System Arrangement

Figure 2.1.1 depicts the control system's arrangement. It is comprised of three control and surveillance locations: The subway control center, the remote control room and the main control and flood gate room. Only the main control and flood gate room has been subject to prototype testing as this is written. Therefore, following sections will focus on the components and structures present in this location.

Main Control and Flood Gate Room This location is directly adjacent to the flood gate. It contains the control cabinet, which holds the PLC and all necessary peripherals, including the control panel on the cabinet's door. The flood gate system components, like power supplies, switches and motors are all wired to the PLC in their respective ways within relatively short distance.

Normally the flood gate is operated from here, while the remote control room is only meant for emergencies.

The flood gate is monitored by a surveillance camera, which guarantees certainty over the gate's current status via visuals. The PLC is also programmed to detect malfunctions and sets an alarm in case of failure.

If an alarm occurs, maintenance personell has to enter the room and remove the cause of failure. In addition to the control panel, it is also possible to operate the flood gate manually without all electric components. A chain winch is attached to the hoisting device to enable lowering or raising, though at very low speeds. The automatic lock can also be operated manually by a crank lever.

Subway Control Center and Remote Control Room The subway control center and the remote control room are intended to enhance the operator's safety, rendering him more remote from possibly hazardous environments. They have yet to be fully planned and engineered. Thus the illustration 2.1.1 only contains the author's rough idea of these locations.

2.1.2. Configuration Diagram

The configuration diagram in 2.1.2 illustrates the way, how the system components are attached to the PLC. It becomes obvious, that simplicity and ease of maintenance has been a major rule during the design phase. All the system's interaction and event handling takes place via digital I/O. No bus system is needed, because no other intelligent devices are involved other than the PLC.

A Siemens S7-200 PLC is powered by a 24 V DC power supply. Because of the number of the limited number of connections the Siemens S7-200 has been extended by a digital I/O device, which is powered by the PLC. The switches and control panel buttons and LEDs are directly connected to the PLC. They and the motor switching relays comprise the device network as a set of components, whose binary states are directly controlled or read by the PLC.

A 380 V AC power supply powers two motors, which are designed to move the flood gate in rapid or slow motion, respectively. The power supplies are secured by fuses and are engineered to both have a redundant counterpart, which is automatically switched on, in case of power loss by the primary supply.

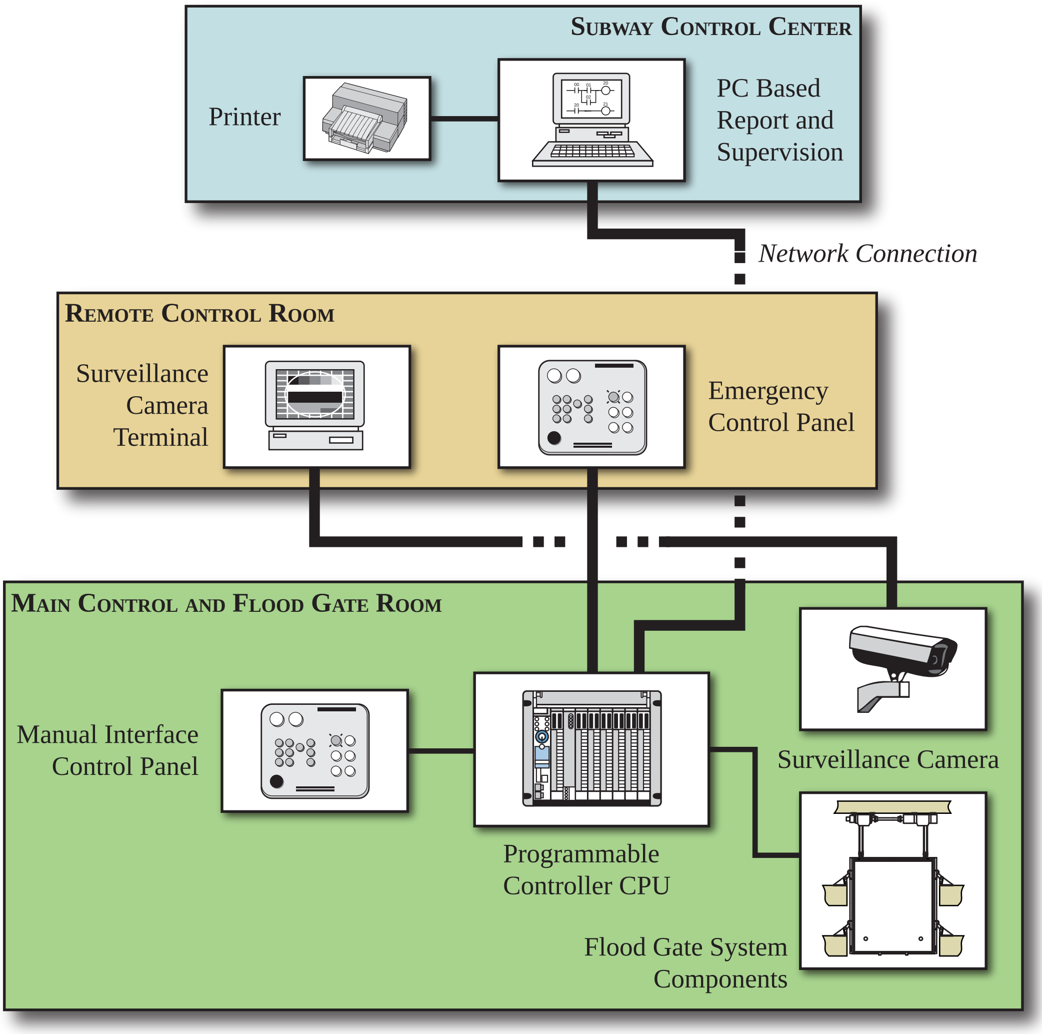

Figure 2.1.1.: System Arrangement Diagram (diagram symbols courtesy of Industrial Text & Video)

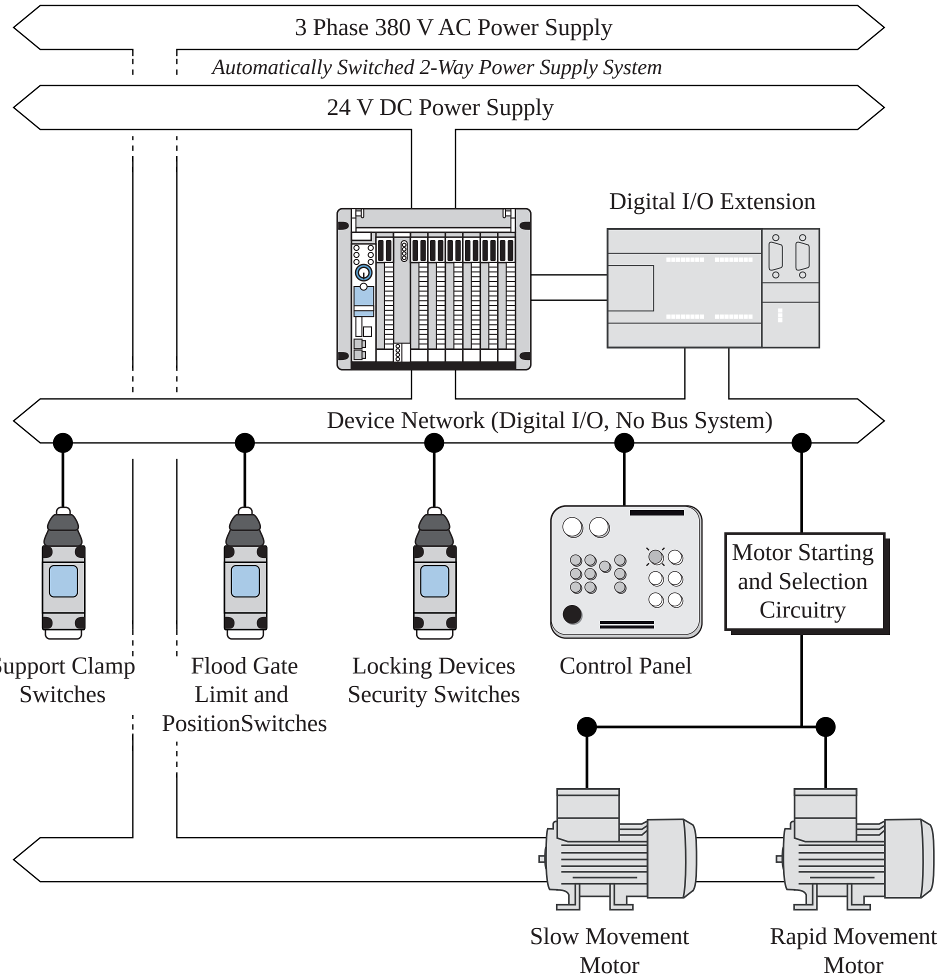

Figure 2.1.2.: Simplified System Configuration Diagram (diagram symbols courtesy of Industrial Text & Video)

2.1.3. Instrumentation

Figure 2.1.3 shows the basic sensor layout and substantiates the switches' quantity, positions and use. The sensors have been divided into three groups:

Gate Position To acquire information about the gate's current position, switches are attached to the surroundings, which become triggered by contact with the gate. Topmost (1) and bottommost (3) limit switches bring the gate's movement to a halt, if the gate is moving. The key position switches (2) indicate, when the gate is near the bottom limit, an intermediate or reversal position, which are to be described later. Depending on the flood gate's current state, at a key position the control system may switch to the slow motion motor, to avoid hard impacts or invert the motors rotational direction.

Support Devices Part of the information about the gate's current position is also obtained via switches attached to the support devices (4). Depending on the hinges' angles, the support clamps trigger switches in different positions. These positions are chosen in accordance to the support clamp deflections, which occur for particular gate positions as has been illustrated by figure 1.2.5 in the introduction. According to this, the PLC judges when to reverse or slow down the gate's motion to softly bring it into the latched, supported opened state. The latter is detected by additional switches mounted to the bars of the support devices, on which the gate rests.

In the supporting angular deflection, the support clamps can be manually locked by bolts. Whether these bolts are in place or the support clamps can rotate freely is identified by the manual lock detection switches (5) mounted to the support device stands.

Automatic Lock When the gate rests in openend position, the automatic lock can be engaged. Two switches (6) detect the engaged and disengaged positions of the automatic lock bolt.

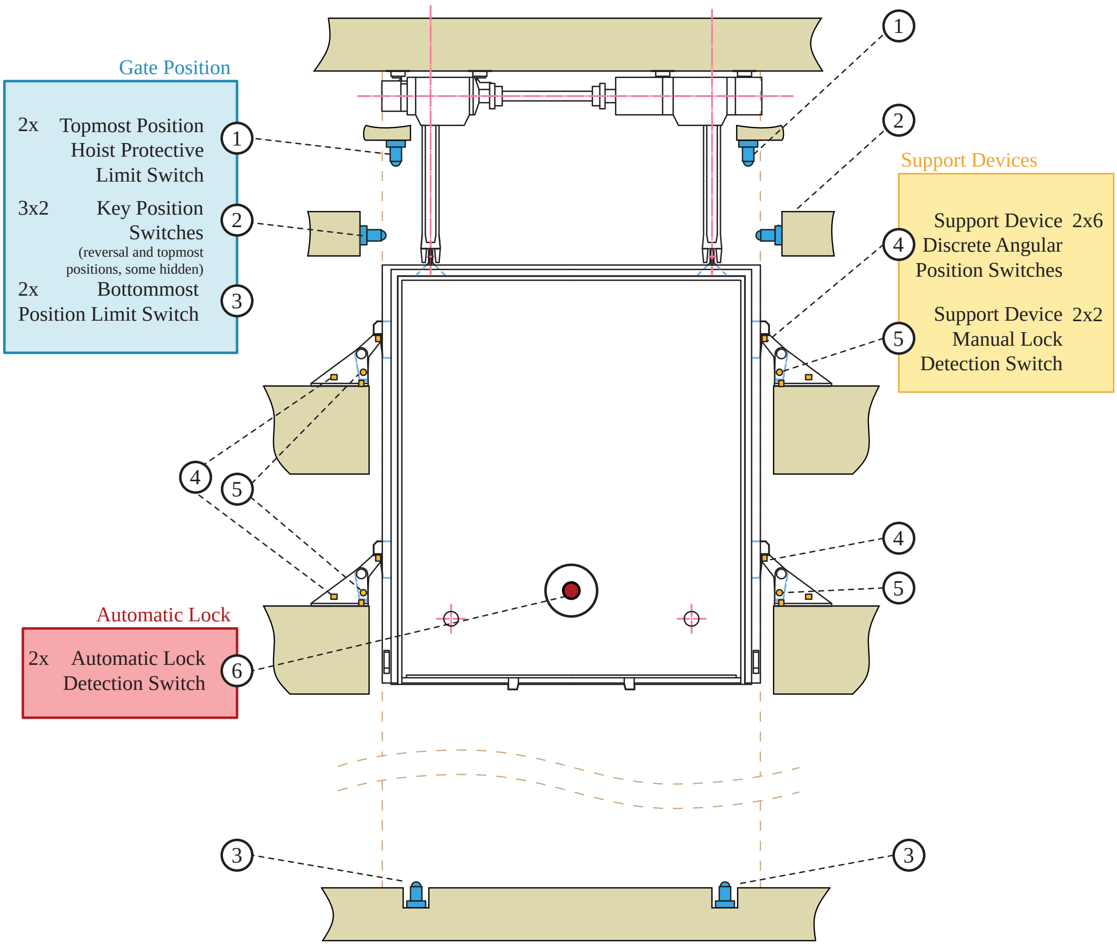

Figure 2.1.3.: System Instrumentation Layout of the Realised System

2.2. Flowchart of Process Operation

In the course of the programming of the PLC, detailed flowcharts of all possible modes of operation have been drawn. Prior to this a motion diagram has been employed to visualise the switching conditions, that occur for the different modes of operation. This motion diagram is pictured in figure 2.2.1. It visualises the sequences of motion triggered by the key position switches described in section 2.1.3 and the support devices' possible deflections in each key position. It becomes apparent, that there exist four main modes of motion: *Open*, *close*, *reset* and *maintenance*.

The close and open motions are predefined to begin in the supported opened or the closed positions, respectively. If the operator desires to close or open the gate from a position different from these, the reset sequence of motion has to be carried out first, which is designed to safely bring back the gate to the supported opened position from any starting point. The maintenance mode leaves the gate in total control of the operator enabling manual raising and lowering.

Taking the motion diagram as a basis, a high-level sequential function chart[1] has been derived as the next step. The SFC presented in figure 2.2.2 distinguishes between two operation states: *Working state* and *maintenance state*.

The operator can switch between these states enabling or disabling their respective modes of motion. In working state, the operator can control the gate to open, close or reset. The motions are then carried out automatically until the final event or transition fires. In maintenance state, the operator can manually lower or raise the gate in two distinct speeds or reset to opened position. The automatic lock can be manually engaged, to support the flood gate from beneath for maintenance purposes.

[1] Sequential function chart will be abbreviated with SFC in the following.

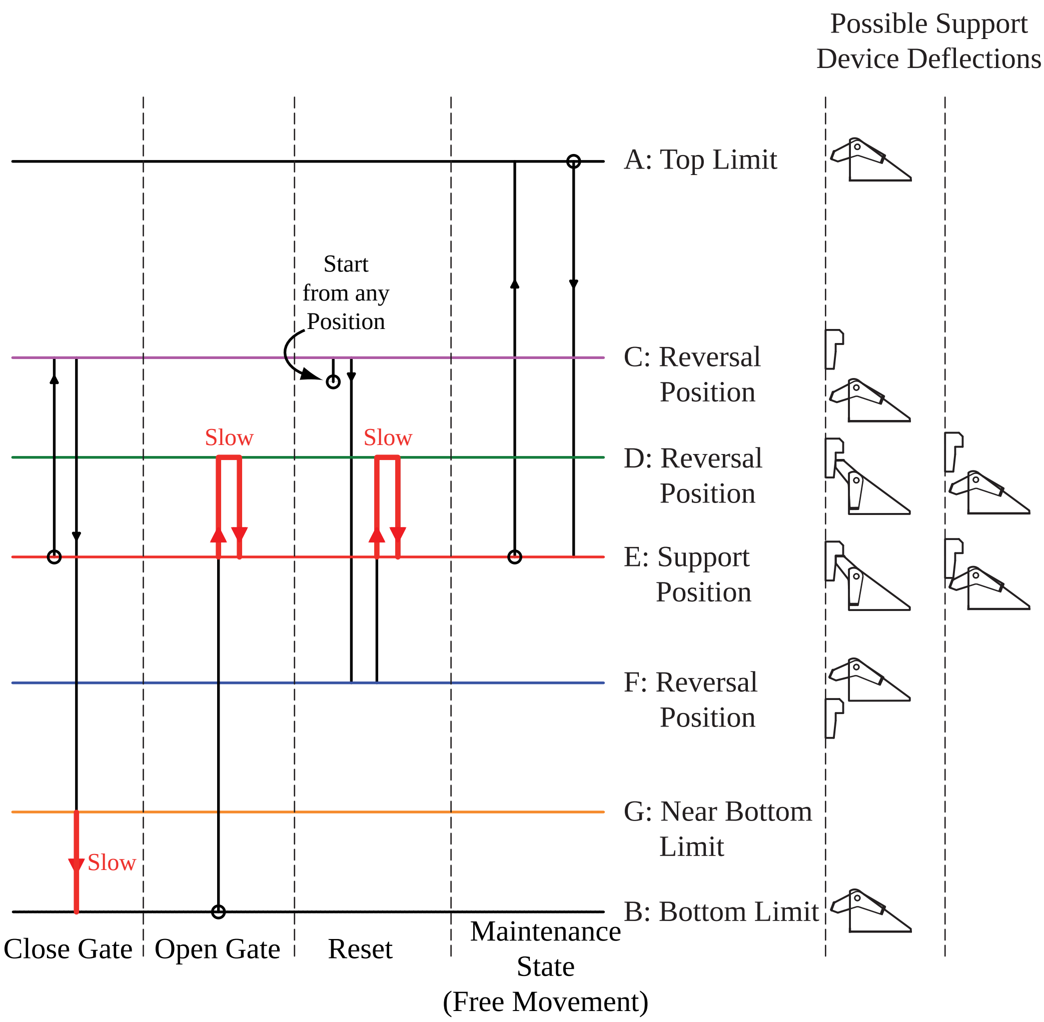

Figure 2.2.1.: Motion Diagram: Key Position Switch Triggered Basic Sequences of Motion

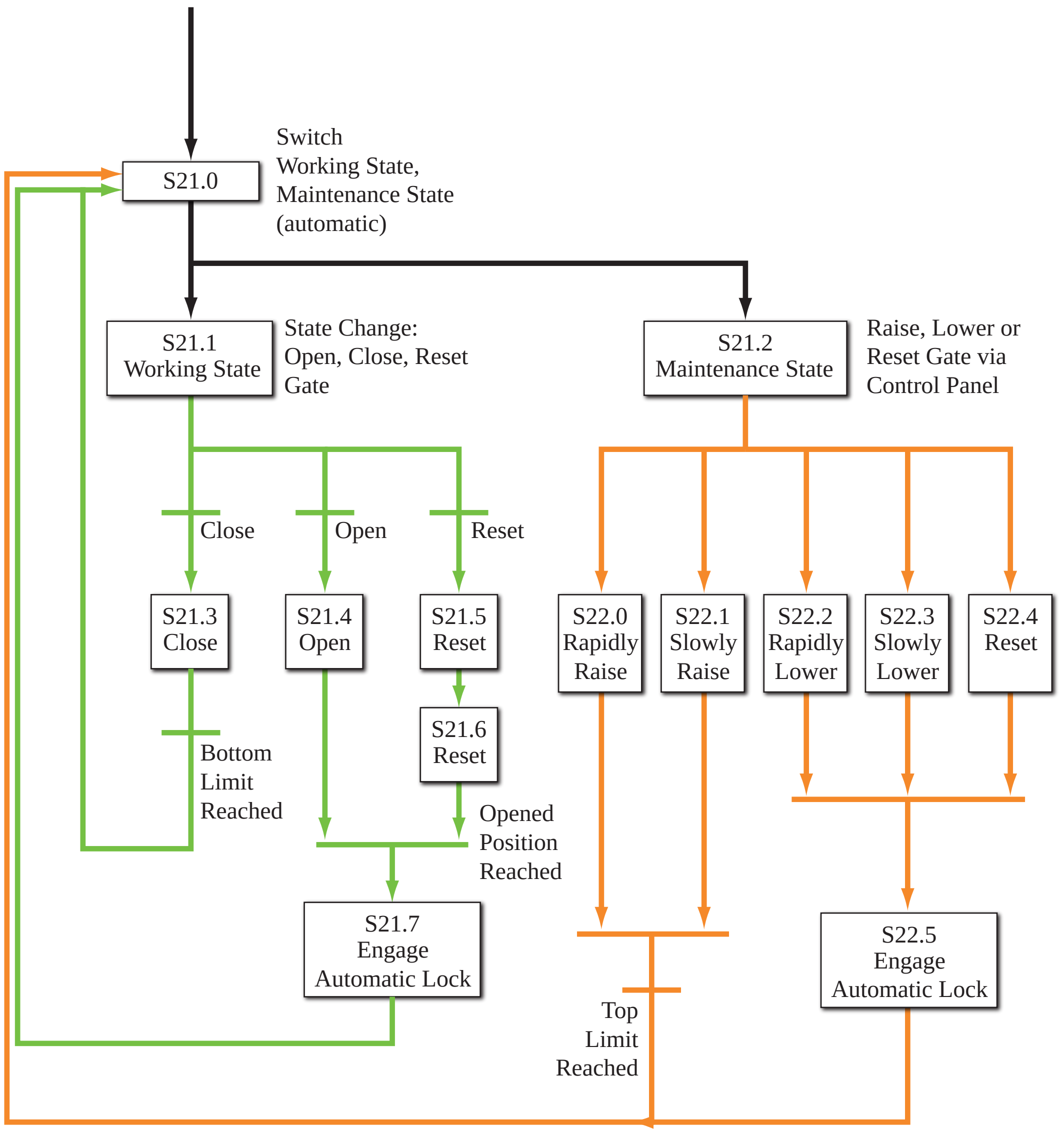

Figure 2.2.2.: High Level Process Operation Sequential Function Chart

2.2.1. Control Panel and Cabinet Design

The control panel is a vital part of the control cabinet's components. It allows operation or maintenance personell to perform all necessary actions. It has been designed in a safe, simple and straightforward manner, such as not to confuse and enable for unambiguous monitoring and control. Figure 2.2.3 shows a scheme of the control panel design. The terms occurring in the SFC in figure 2.2.2 directly map to the labels printed on the control panel.

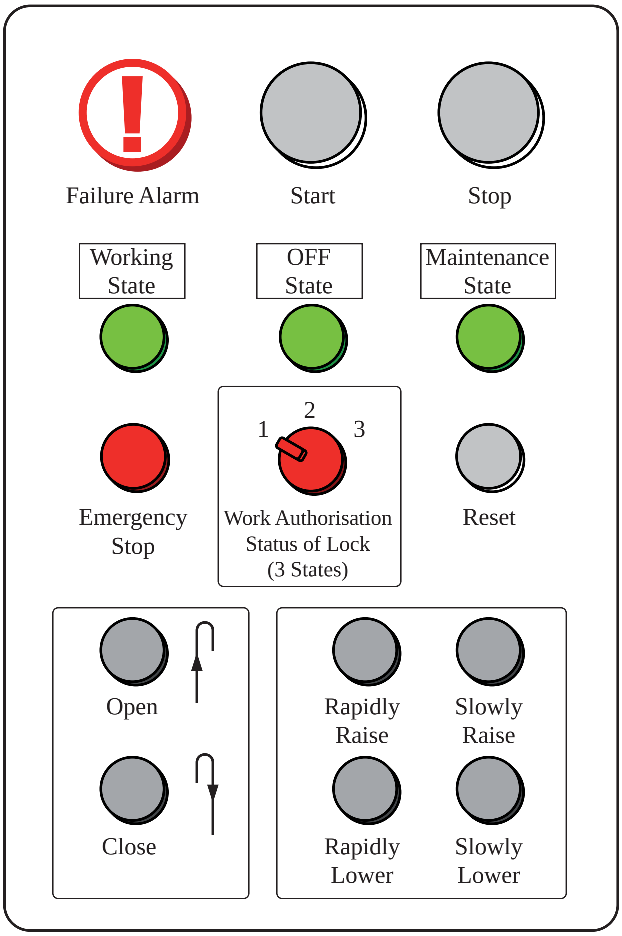

Figure 2.2.3.: Control Panel Design of Main Control Room Control Cabinet

With respect to the control cabinet, the following design specifications have been imposed and the cabinet production company RITTAL has been assigned to set it up:

- Protection level IP66, control door thickness of about 3.0 mm with good moisture, vibration, dust and splash water features; Elevated floor to provide protection against moisture; Sealed backplane; Internally sealed cabinet.

- Control system uses a two-way access to 380 V power supply; The power supply requires two automatic switching devices and a main circuit power supply for the motor, PLC control loop and video surveillance.
- PLC SIEMENS S7-200 Series, CPU 226 and I/O expansion module; Total number of PLC I/O points: DI: 40, DO: 10 – 15. Remaining components are selected SCHNEIDER products.

2.3. Prototype Testing

The control system described in the previous sections has been tested on a prototype of the flood gate. Apart from being smaller, this experimental version closely resembles the actual flood gate. The control cabinet, hoisting device and switches are practically unchanged. Figure 2.3.1 shows a photograph of the control cabinet used for the experiment and a total of the experimental flood gate.

(a)

(b)

Figure 2.3.1.: Experimental Prototype of the Shànghǎi Flood Gate: (a) Prototype Control Cabinet, (b) Total of the Experimental Flood Gate

2.3.1. Issues Occurring During Testing

During testing some issues occurred, that required adjustments for the experiment to be successfully conducted. These will be briefly outlined in the following.

Difficult Switch Placement and Surface Treatment For all switches only one type of switch has been used. Figure 2.3.2 shows a close-up of the type of switch used and switches mounted on a support device. It has been observed, that while the limit switches are well suited for making contact with obstacles coming from the front, they can make the support clamp get stuck or fail to trigger, when the impact is sliding in from the side. The surfaces have been subsequently grinded and bevelled to enable better triggering conditions. It can be assumed, that the switches will stop working reliably

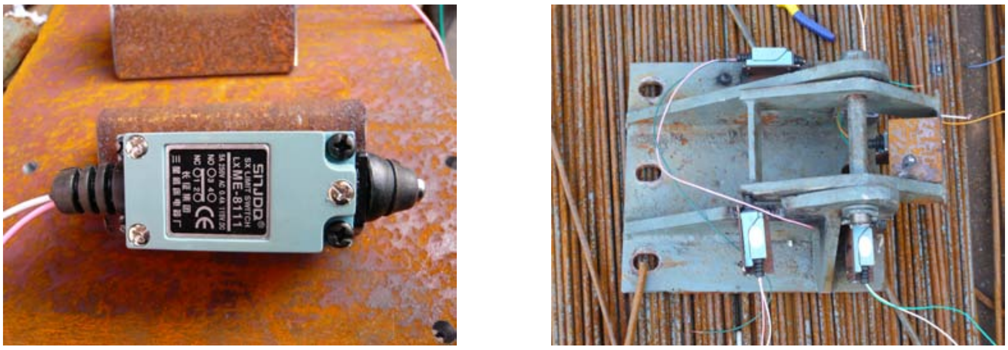

(a) (b)

Figure 2.3.2.: Limit Switches: (a) Unmounted Limit Switch, (b) Limit Switches Mounted on Support Device

when the surfaces become dirty, though. Switches with ball trigger heads might be more suited.

Unbalancing of the Support Clamps and High Forces Acting on the Switch in Opened, Supported Position Figure 2.3.3 shows a support clamp supporting the flood gate. A limit switch has been attached to the bar of the clamp to be triggered in the completely opened and supported position. During the experiments it has been observed, though, that the mounting of the switch and the switch itself has a high force applied to it when supporting the flood gate. Before the flow of forces goes to the clamp bar, the switch solely supports the gate. This is probable to become an issue after several impacts.

Misalignment of the Wire-Rope Connection to the Flood Gate Because of imprecisely positioned ears on top of the flood gate or a non-matching distance between the wire-ropes, the connection to the flood gate has become misaligned to a degree, which has been difficult to fix by using spacer bushings. This resulted in the flood gate main body canting against the support beams on either side and thus getting stuck. A solid metal guide could keep the flood gate in place and prevent canting.

Figure 2.3.3.: Support Device Supporting the Experimental Flood Gate in Closed Position

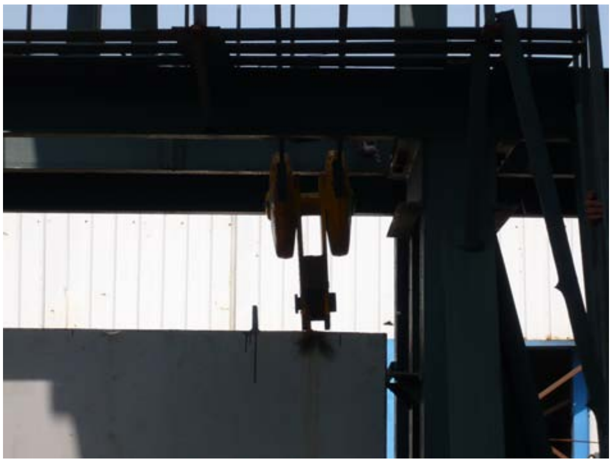

Figure 2.3.4.: Misaligned Clevis on Top of the Experimental Flood Gate

2.4. Suggestions on Improvements to the Control System

The Shànghǎi flood gate control system as described in the previous sections will be installed into the subway network. Some issues have been pointed out, but with some minor adjustments, the control system will be workable and fulfills the given requirements. However, there is still some room for improvement, which might be included in future generations. To investigate these improvements is the main task of this thesis.

2.4.1. Simplified Instrumentation Layout Based on Rotary Encoders

The control of the flood gate's position with the help of limit switches has several downsides:

Liability to Wear As mechanical parts the switches are liable to wear. Strong forces exerted onto the trigger may eventually damage it.

Environmental Hazards In an environment, which may be subject to flood hazards or an accumulation of dirt, the continuous and safe operation of these switches might become impaired. False-positive or positive-false triggerings might occur.

Maintenance The number of switches used in the control system is relatively high. Their redundancy is intentional: If only one switch fails, an alarm is issued and the switch has to be replaced. With continued operation, it is likely that replacements become frequent and maintenance tedious.

To overcome these issues, a completely new paradigm may be implemented with respect to the measurement of the flood gate's position. Instead of using switches, a set of four rotary encoders for the support devices and another rotary encoder attached to the motor can be utilised to determine the gate's position and ensure, that the latching mechanism works properly.

Since it is vital, that the gate's position is readily and instantly available after control system shutdown and reboot, absolute measurement is necessary. Rotary encoders are common in lift applications and provide sufficient accuracy for the task. The mounting to the shaft is easily done and does not involve any tolerance issues.

Instead of using rotary encoders as a support device angular sensor, a rotary potentiometer might be a considered a cost-effective alternative. Rotary potentiometers are passive devices and thus, do not need a dedicated power supply. They have a limited linear range, though, which might be easily dealt with considering the small sensing region necessary. Figure 2.4.1 shows an exemplary division of angles marked with their respective occurrance.

Figure 2.4.2 depicts an updated version of figure 2.1.3, which contains the abovementioned instrumentation paradigm employing rotary encoders.

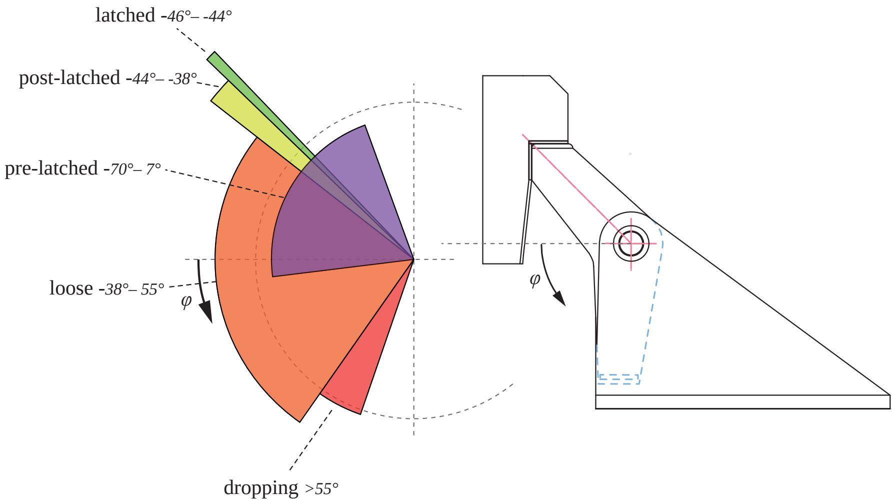

Figure 2.4.1.: Angular Ranges of Phases That Occur During Nominal Motion

The next section deals with further possible advantages induced by a rotary encoder based position control system.

2.4.2. Possible Advantages of a Control System Based on a Rotary Encoder Position Sensor

Using rotary encoders for position measurement not only overcomes the liabilities of a switch based system. It has numerous further advantages:

Continuous Positioning Instead of only being able to position the flood gate at certain predefined positions automatically, it would also be possible to assume any desired position, for example just by typing in the distance above ground level. The reset motion sequence would be obsolete.

Time-Optimised Motion Sequences Because of the support device mechanism it would still be necessary to follow certain trajectories to assume opened or closed positions. By measuring the support device clamp angles and the gate's position more accurately the motion sequences can be time-optimised in case of impending flood.

Time-Optimised Trajectory Tracking by Sophisticated Control Algorithms Instead of employing a two stage motor system, a single AC motor controlled by a drive can be utilised. A torque control based control algorithm using modern control theory synthesis approaches can minimise positioning time, steady state error and control effort, while also attenuating disturbances to a degree, where they do not present a harm to the actuators.

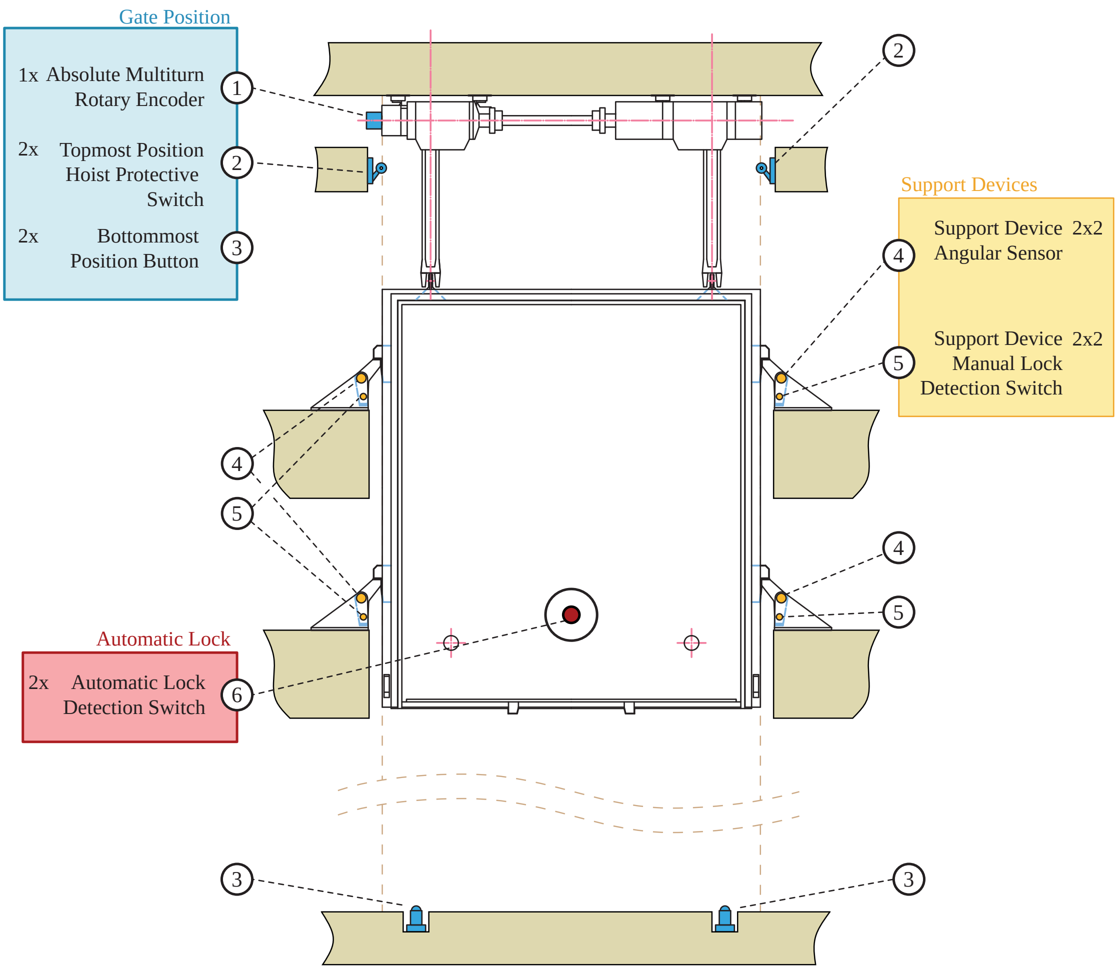

Figure 2.4.2.: Suggested Improved System Instrumentation Layout

Steady State Accuracy Besides the benefits mentioned above, it should be considered, that it is still possible to employ a rotary encoder, run the motors at constant speeds and just stop them, if the desired position is reached. This might require a very short sampling time, though, as time delays add up and create a steady state error as follows:

$$\begin{bmatrix} \text{Steady State} \\ \text{Error} \end{bmatrix} = \begin{bmatrix} \text{Slow Motor} \\ \text{Movement Speed} \end{bmatrix} \cdot \left(\begin{bmatrix} \text{Sampling} \\ \text{Time} \end{bmatrix} + \begin{bmatrix} \text{Motor Braking} \\ \text{Delay} \end{bmatrix} \right)$$

Taking the motor braking delay as a fixed constant, either the sampling time or the fixed slow movement speed has to be small. A drive controlled motor can have variable rotating speeds, thus providing a high potential to avoid any steady state error. In the later chapters a controller with a sampling time of 0.8 s will be designed, which is able to easily keep the positioning error below 10 mm. With the same sampling time and under the assumption of a slow movement speed of $v_{\text{slow}} = 0.7 \cdot v_{\text{fast}} = 0.7 \cdot 4 \frac{\text{m}}{\text{min}} \approx 0.5 \frac{\text{m}}{s}$, the steady state error adds up to approximately 37 mm even when neglecting the motor braking delay. This illustrates the advantage of a more sophisticated control algorithm over simple on-off switching with regard to steady state accuracy. The sampling time can be easily lowered to 0.1 s, though.

These benefits together with being a promising solution to the issues raised by the use of switches show, that it is worth investigating a feasible controller algorithm synthesis approach. The following chapters present the result of this research.

3. Mathematical Modelling of a Lifting Device Using a Wire-Rope Hoist

Based on the actual realisation of the Shànghǎi flood gate system and the used electromechanical components, this chapter's aim is to find a mathematical representation for all parts relevant to apply control theory calculations. The derived equations are generalised to ensure applicability to similar problems, i.e. wire-rope hoist lifting devices. After assumptions have been made concerning the drive system, a mechanical model of the hoist is derived, which is then given in terms of differential equations, both continuous and discrete time transfer functions and finally formulated as a simple linear parameter-varying state space model using the lifted mass as a time-varying parameter. The latter is of importance for simulation purposes in chapter 5, which deals with the derivation of an adaptive position controller in the case of unknown loads.

3.1. Assumptions

In this thesis a position controller is regarded as a device, which generates a torque reference command from a user-input desired position. This torque reference command is then fed into a drive, which controls an electric motor, such that it assumes and exerts the torque on a mechanical system. The torque reference command has to be calculated in a way, such that the deviation from the desired position by disturbances or position reference input changes is driven to zero.

Figure 3.1.1 depicts the general control device configuration considered in this thesis. This configuration may be enhanced in later chapters, especially with regard to the PLC, which may turn out to be a strong limitation when it comes to the implementation of controllers with are computationally demanding. In later chapters, when different controllers are discussed, this issue will be picked up again.

3.1.1. Assumptions on the Instrumentation

Suggestions on the improvement of the current realisation of the flood gate security system have been given in section 2.4. The enhancements concerning the instrumentation and control algorithm, which are investigated further in this thesis, have an impact on the mathematical modelling process, which can be summarized as follows:

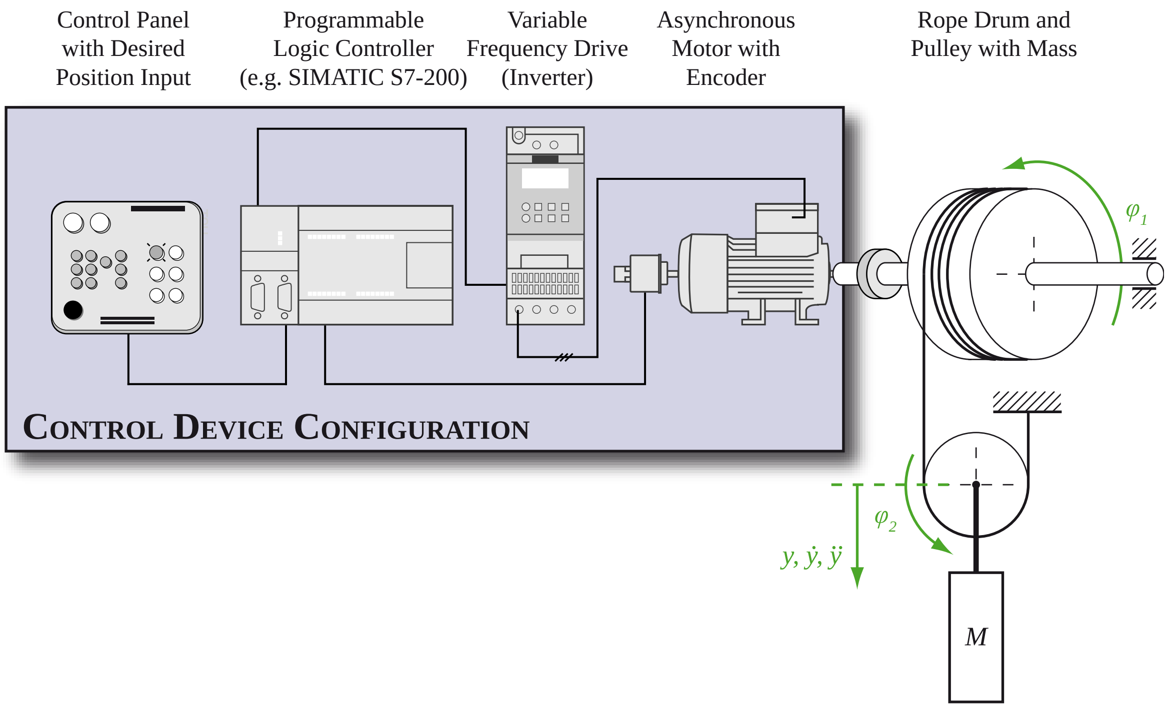

Figure 3.1.1.: Assumed Control Device Configuration for the Position Control of a Lifting Device

- The flood gate position will be measured by a rotary encoder on the motor shaft. By an appropriate gain, this can be translated into the assumed flood gate position.
- The gain on the rotary encoder will be assumed constant. Any minor oscillations that may occur, because of the wire rope elasticity, are neglected, because they can not be measured.

3.1.2. Assumptions on the Drive System

For the controller design and modelling, several assumptions have been made with regard to the electrical motor and the drive, which comprise the drive or servomotor system:

- The torque transient resulting from the inner control loop between electrical motor and drive is assumed to be faster than the position transient by at least one order of magnitude. Therefore, the drive can be modelled as a simple gain without introducing a time delay. Modern drive systems fullfill these requirements and operate at a bandwidth of about $f_{\text{Drive}} = 1\,\text{kHz}$ [15, p. 149ff].

- Only drive systems are considered, which are capable of a torque control operating mode. Very different – yet presumably also feasible — solutions to the position control problem can be found by employing direct position or even speed control operating modes of a given drive system, all of which can be found on modern equipment. However, they will not be considered in this thesis.
- The servomotor system can maintain torque at zero to very low speed at least for a short period of time. Electrical motors, which are not designed for the use together with modern drives tend to be controllable only upwards of a given minimum rotating speed. It is assumed, that this minimum rotating speed is sufficiently small.
- The maximum and minimum torque limits are supervised by the drive system.

A discussion on this topic can be found in [15, p. 147ff], which validates the assumptions.

3.1.3. Assumptions on the Transmission System

For the controller design and modelling, assumptions have been made with regard to the transmission system:

- As is the case with at least some electrical motors [3, ch. 4-15], overhanging loads, which tend to continuously rotate the motor are not allowed. Therefore, it is assumed, that the transmission system exerts the equilibrium torque T^0 to keep the hanging load from moving. A possible solution would be to employ a worm gear, which is self-locking.
- Because backlash and elasticity issues are less emphasized, when the position control aims for a strictly aperiodic transient [15, p. 149], the transmission system can be modelled by a static gain.
- No hysteresis occurs.
- The unwinding from the wire rope drums is assumed to take place in a linear fashion. Mechanical measures are taken to minimise the error introduced when the wire is — in reality — not completely vertical from hoist to flood gate.

3.2. Mechanical Model

Figure 3.2.1 shows a technical drawing of the wire-rope hoist lifting device as used in the actual realisation of the flood gate control system. Unrolling from the rope drums the wire-ropes pass two parallel pulleys attached to the hook and another pulley attached to the drum housing. The design has been chosen, such that the hook is lowered and raised on a non-moving vertical axis as opposed to a design without the third centered pulley.

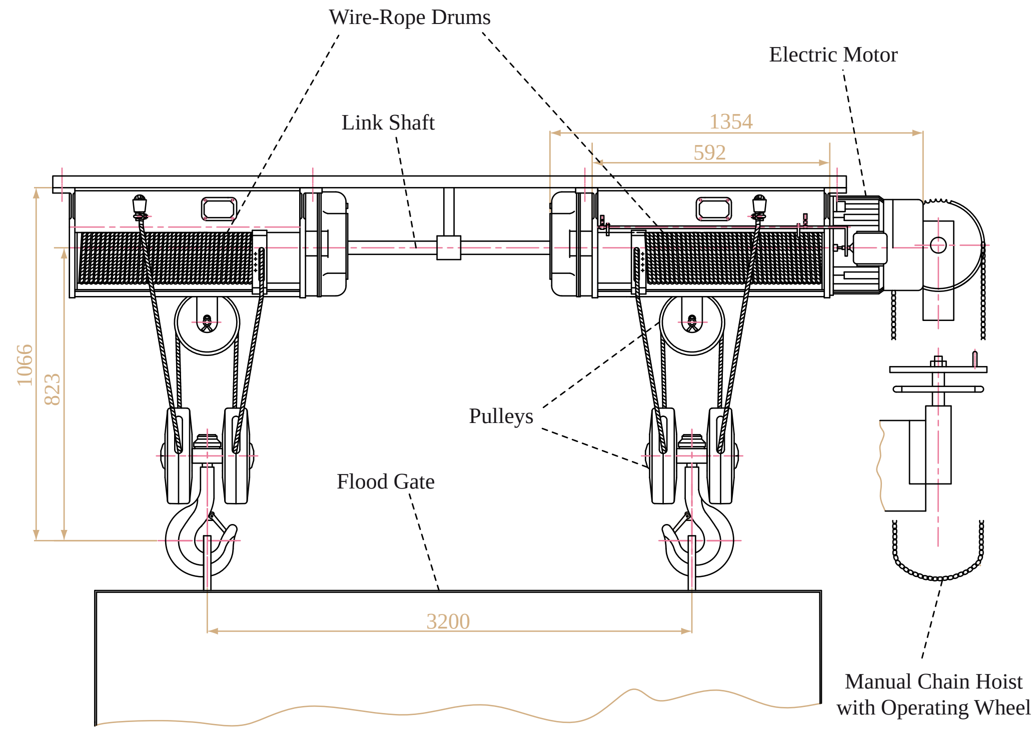

Figure 3.2.1.: Technical Drawing of the Wire-Rope Hoist Lifting Device as Used in the Actual Realisation

3.2.1. Free Body Diagram and Derivation of the Differential Equation

Figure 3.2.2 shows a simplified model, which considers all three pulleys, and a free body diagram of the flood gate hoisting device loosely following [12]. Please note, that it is sufficient to model only a single hook as both hooks can be mirrored on a centered vertical axis.

The following assumptions have been made:

- The rope is completely stiff.
- The flood gate mass is a point mass.
- The drum and pulleys are homogenous cylinders with inertia $\Theta_i = m_i \frac{d_i^2}{4}$.
- No friction occurs and the rope does not slip.

From the free body diagram (3.2.2), the following relevant equations can be derived:

$$M \cdot \ddot{y} = G_L - F_L \tag{3.2.1}$$

$$m_1 \frac{d_1^2}{4} \cdot \ddot{\varphi}_1 = T_h - b_1 \dot{\varphi}_1 + S_1 \frac{d_1}{2} \tag{3.2.2}$$

$$m_2 \frac{d_2^2}{4} \cdot \ddot{\varphi}_2 = S_2 \frac{d_2}{3} - S_1 \frac{2d_2}{3} + F_L \frac{d_2}{12} \tag{3.2.3}$$

$$m_3 \frac{d_3^2}{4} \cdot \ddot{\varphi}_3 = S_3 \frac{d_3}{2} - S_2 \frac{d_3}{2} \tag{3.2.4}$$

$$m_4 \frac{d_4^2}{4} \cdot \ddot{\varphi}_4 = F_L \frac{d_4}{4} - S_3 d_4 \tag{3.2.5}$$

It has been made use of the fact, that the instantaneous centre of rotation of pulley 2 is set between both margins, dividing the diameter by the ratio 2:1. Thus $a = \frac{2d_2}{3}$ and $b = \frac{d_2}{3}$. Solving 3.2.1 for F_L and eliminating F_L in all equations, enables to solve 3.2.2 for S_1, 3.2.5 for S_3 and subsequently both 3.2.4 and 3.2.3 for S_2. Equating these last two equations leads to a single differential equation, which depends on $\ddot{y}, \ddot{\varphi}_1, \ddot{\varphi}_2, \ddot{\varphi}_3$ and $\ddot{\varphi}_4$.

$$2M \cdot \ddot{y} + m_4 d_4 \cdot \ddot{\varphi}_4 + 2m_3 d_3 \cdot \ddot{\varphi}_3 + 3m_2 d_2 \cdot \ddot{\varphi}_2 + 4m_1 d_1 \cdot \ddot{\varphi}_1 + \frac{16}{d_1} b_1 \cdot \dot{\varphi}_1 = 2G_L + \frac{16}{d_1} T_h$$

The analysis of the system inherent kinematics reveals the dependencies

$$\ddot{y} = \frac{d_1}{8} \ddot{\varphi}_1 = \frac{d_2}{6} \ddot{\varphi}_2 = \frac{d_3}{4} \ddot{\varphi}_3 = \frac{d_1}{2} \ddot{\varphi}_4, \tag{3.2.6}$$

which can be used for further elimination of states:

$$(M + m_4 + 4m_3 + 9m_2 + 16m_1) \cdot \ddot{y} + \frac{64}{d_1^2} b_1 \cdot \dot{y} = G_L + \frac{8}{d_1} T_h. \tag{3.2.7}$$

Considering 3.2.7 it becomes obvious, that under the above-mentioned assumptions, the pulley inertias and the inertia induced by the lifted mass add up with weighing factors determined by the kinematics. Furthermore, the hoisting torque T_h can be expressed as the motor torque T multiplied by an appropriate gain factor $\hat{k}$. Thus the differential equation can be written in more general terms:

$$\hat{M} \cdot \ddot{y} + \hat{b} \cdot \dot{y} = G_L + \hat{k} \cdot T. \tag{3.2.8}$$

$$\text{with } \hat{M} = M + m_4 + 4m_3 + 9m_2 + 16m_1,$$

$$\hat{k} = \frac{8 \cdot i \cdot \eta_{mech} \cdot k_D}{d_1}$$

$$\text{and } \hat{b} = \frac{64}{d_1^2} b_1,$$

while i is the gear transmission,

η_{mech} is the mechanical coefficient of performance

and k_D is the drive gain.

The system can be formulated for the equilibrium, where

$$T^0 = -\frac{G_L}{\hat{k}} \quad \Delta T = T - T^0.$$

Since y does not explicitly occur in the differential equation, in equilibrium y may attain any value.

$$\hat{M} \cdot \ddot{y} + \hat{b} \cdot \dot{y} = \hat{k} \cdot \Delta T. \tag{3.2.9}$$

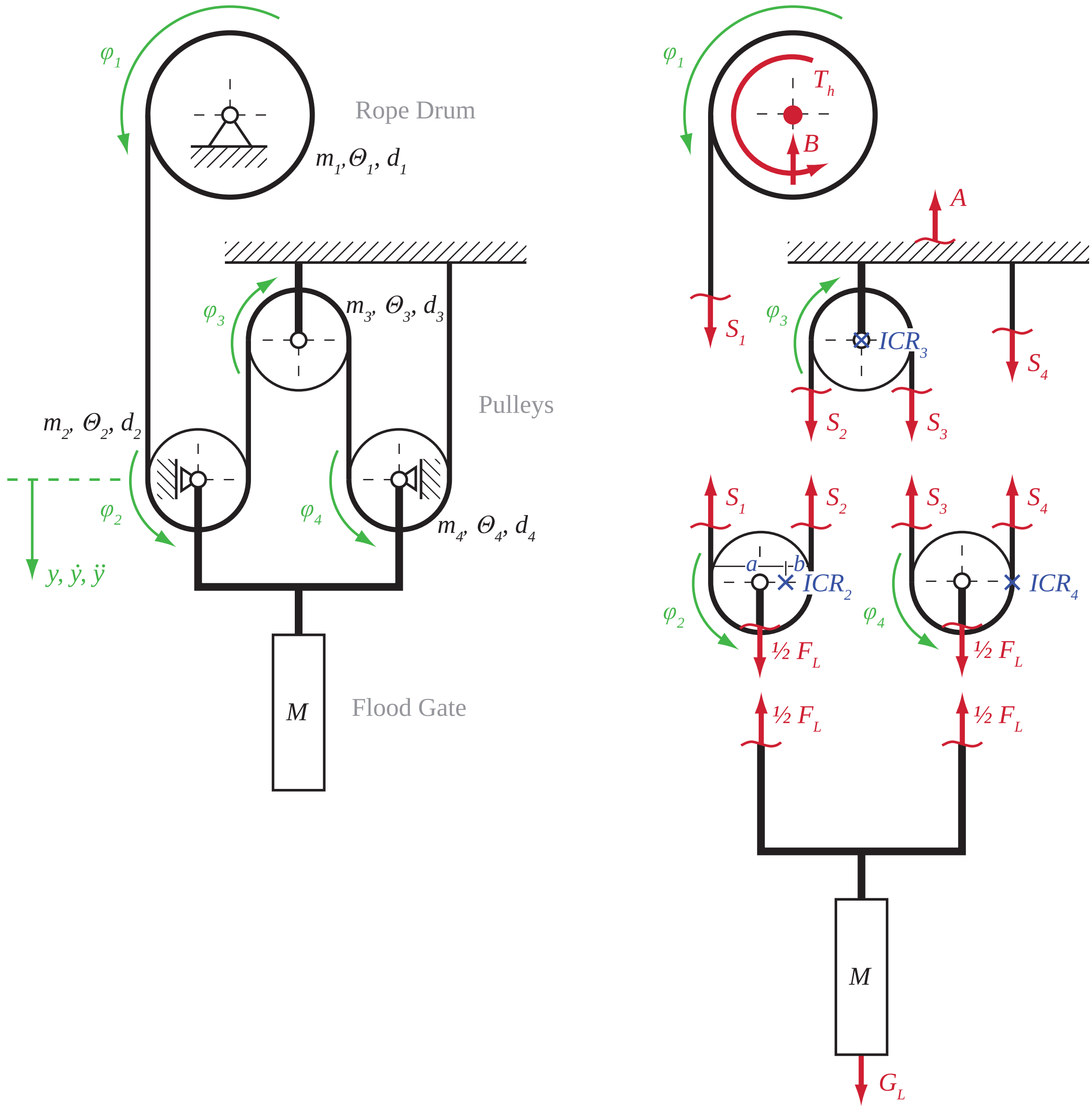

Figure 3.2.2.: Simplified Mechanical Model and Free Body Diagram of the Flood Gate Hoisting Device

3.2.2. Continuous and Discrete Time Transfer Function Representation

The controller design will be carried out directly in discrete time in the following chapters. To facilitate this, the system can be analysed with the help of the transfer functions or in state space notation. In this thesis, the transfer function approach is chosen and prefered over the state space approach, because it suits classical system identification techniques better and an exact discretisation in the state space form is not possible, as will be shown.

In continuous time the LaPlace-Transform yields the following transfer function:

$$G(s) = \frac{\Delta Y(s)}{\Delta T(s)} = \frac{\hat{k}}{\hat{M} \cdot s^2 + \hat{b} \cdot s} \tag{3.2.10}$$

The system has $n = 2$ poles and $m = 0$ zeros, a pole excess of two. By rewriting the transfer function the poles become directly obvious:

$$\begin{aligned} G(s) &= \frac{\hat{k}}{\hat{b}} \cdot \frac{\frac{\hat{b}}{\hat{M}}}{s \cdot \left(s + \frac{\hat{b}}{\hat{M}}\right)}, \\ s_0 = 0, &\quad s_1 = -\frac{\hat{b}}{\hat{M}}. \end{aligned}$$

[16, Table 6.1, p. 120] provides a direct way of transforming this into the discrete z-domain:

$$\frac{a}{s \cdot (s+a)} \quad ○\!\!-\!\!● \quad \frac{T_s}{2} \cdot \frac{(1 - e^{-aT_s}) \cdot z^{-1}}{(1 - z^{-1}) \cdot (1 - e^{-aT_s} \cdot z^{-1})} \tag{3.2.11}$$

This, however, does not account for the sampling zeros, which are introduced during discretisation because of the pole excess. The discrete time system has $n - 1 = 1$ regular zeros, because of non-existent direct feedthrough. Had the continuous time system $m \neq 0$ zeros, they would approach the continuous time zeros, whereas the remaining $n - m - 1 = 1$ zeros approach the discrete time zeros of a zero-order-hold discretisation of a pure integrator of degree $n - m = 2$ as the sampling time $T_s \to 0$ [16, p. 134]. The discrete time zeros of a pure integrator of degree 2 have to be calculated by utilising the continuous state space formulation

$$\begin{aligned} \dot{\boldsymbol{x}} &= \boldsymbol{A} \cdot \boldsymbol{x} + \boldsymbol{b} \cdot u, \\ \boldsymbol{A} &= \begin{bmatrix} 0 & 1 \\ 0 & 0 \end{bmatrix} \quad \boldsymbol{b} = \begin{bmatrix} 0 \\ 1 \end{bmatrix}, \end{aligned}$$

which is then to be converted into discrete time. The discrete time state space system matrix Φ is calculated by the matrix exponential series expansion, whereas for the input gain vector Γ an integral has to be solved:

$$\begin{aligned}
\dot{\boldsymbol{x}} &= \boldsymbol{\Phi} \cdot \boldsymbol{x} + \boldsymbol{\Gamma} \cdot u, \\
\boldsymbol{\Phi} &= e^{\boldsymbol{A}T_s} = \boldsymbol{I} + \boldsymbol{A}T_s + \boldsymbol{A}^2 \frac{T_s^2}{2!} + \ldots = \begin{bmatrix} 1 & T_s \\ 0 & 1 \end{bmatrix} \\
\boldsymbol{\Gamma} &= \int_0^{T_s} e^{\boldsymbol{A}t} \boldsymbol{b} \, \mathrm{d}t = \begin{bmatrix} \frac{T_s^2}{2} \\ T_s \end{bmatrix}.
\end{aligned}$$

The discrete time transfer function of the double integrator is thus calculated as

$$\begin{aligned}
H(z) &= \boldsymbol{C} \left(z\boldsymbol{I} - \boldsymbol{\Phi}\right)^{-1} \boldsymbol{\Gamma} = \begin{bmatrix} 1 & 0 \end{bmatrix} \begin{bmatrix} z-1 & -T_s \\ 0 & z-1 \end{bmatrix}^{-1} \begin{bmatrix} \frac{T_s^2}{2} \\ T_s \end{bmatrix} \\
&= \frac{T_s^2}{2} \cdot \frac{(z+1)}{(z-1)^2}.
\end{aligned} \tag{3.2.12}$$

From equation 3.2.13 it becomes obvious, that the additional *sampling zero* approaches $z_0 = -1$ as $T_s \to 0$. Despite the fact, that the double integrator's zero is invariant with regard to T_s, the sampling zero of the hoist system is not, which is shown in figure 3.2.3. As has already been mentioned, it is not possible to analytically discretise the continuous time transfer function via the formulas used for the double integrator. When trying to do so, the matrix exponential series expansion appeared to be infinitely long and the values of the sampling zeros shown in figure 3.2.3 are thus only approximations.

As a conclusion to the observations, the sampling zero is assumed to be $z_0 = -1$ in all further analytical representations of the transfer function:

$$\begin{aligned}
H(z^{-1}) &= \frac{T_s}{2} \cdot \frac{\hat{k}}{\hat{b}} \cdot \frac{z^{-1}\left(1 - e^{-\frac{\hat{b}}{\hat{M}}T_s}\right) \cdot \left(z^{-1} - z_0\right)}{\left(1 - z^{-1}\right) \cdot \left(1 - e^{-\frac{\hat{b}}{\hat{M}}T_s} \cdot z^{-1}\right)} \\
&= \frac{T_s}{2} \cdot \frac{-\frac{\hat{k}}{\hat{b}}\left(1 - e^{-\frac{\hat{b}}{\hat{M}}T_s}\right) z_0 \cdot z^{-1} + \frac{\hat{k}}{\hat{b}}\left(1 - e^{-\frac{\hat{b}}{\hat{M}}T_s}\right) \cdot z^{-2}}{1 - \left(1 + e^{-\frac{\hat{b}}{\hat{M}}T_s}\right) \cdot z^{-1} + e^{-\frac{\hat{b}}{\hat{M}}T_s} \cdot z^{-2}} \\
&= \frac{b_1 \cdot z^{-1} + b_2 \cdot z^{-2}}{1 + a_1 \cdot z^{-1} + a_2 \cdot z^{-2}}
\end{aligned} \tag{3.2.13}$$

$$\text{with} \quad \begin{matrix} b_1 = -\frac{T_s}{2}\frac{\hat{k}}{\hat{b}}\left(1 - e^{-\frac{\hat{b}}{\hat{M}}T_s}\right) z_0 & b_2 = \frac{T_s}{2}\frac{\hat{k}}{\hat{b}}\left(1 - e^{-\frac{\hat{b}}{\hat{M}}T_s}\right) \\ a_1 = -\left(1 + e^{-\frac{\hat{b}}{\hat{M}}T_s}\right) & a_2 = e^{-\frac{\hat{b}}{\hat{M}}T_s} \end{matrix} .$$

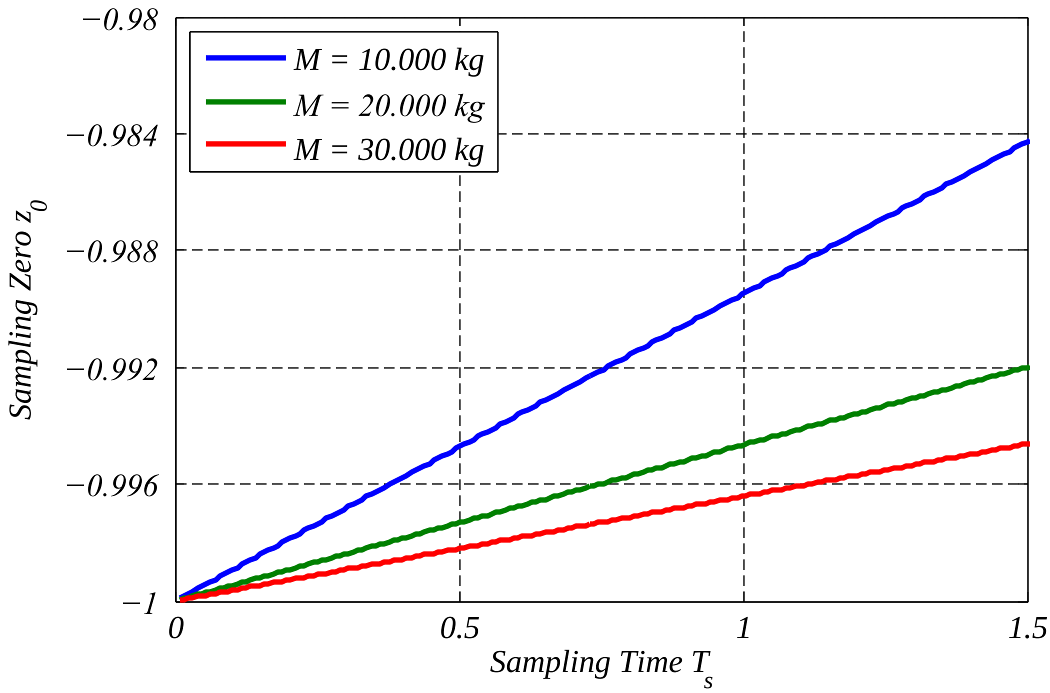

Figure 3.2.3.: Sampling Zero Vs. Sampling Time in Discrete Time Representation of the Hoist Mechanical System

Later, it will be made use of the fact, that for varying and unknown inertias $\hat{M}$ only the exponential term changes and can be treated as an identifiable parameter p. Under the assumption that the damping is known and constant, the inertia can even be easily calculated from an identified transfer function.

$$\begin{aligned} b_1 &= -\frac{T_s}{2}\frac{\hat{k}}{\hat{b}}(1-p)\, z_0 & \qquad b_2 &= \frac{T_s}{2}\frac{\hat{k}}{\hat{b}}(1-p) \\ a_1 &= -(1+p) & a_2 &= p \end{aligned}$$

$$\text{with } p = e^{-\frac{\hat{b}}{\hat{M}}T_s}. \tag{3.2.14}$$

3.2.3. Linear Parameter-Varying State Space Model Representation

In the last section, a discrete time representation has been derived, which suits controller synthesis and design both in the case of known and unknown loads. For the simulation of the controlled plant under various time-varying loading conditions, a linear parameter-varying[1] state space modelling approach has been used, which will be explained quickly in this section. For a good introduction into linear parameter-varying modelling refer to [8] or [13, in German]. Only a very basic definition of the aspects used in this thesis will be provided next.

General Formulation of a LPV System

Generally a LPV system takes the form

$$\begin{aligned}\dot{\boldsymbol{x}} &= \boldsymbol{A}(\boldsymbol{\theta}(t)) \cdot \boldsymbol{x} + \boldsymbol{B}(\boldsymbol{\theta}(t)) \cdot \boldsymbol{u} \\ \boldsymbol{y} &= \boldsymbol{C}(\boldsymbol{\theta}(t)) \cdot \boldsymbol{x} + \boldsymbol{D}(\boldsymbol{\theta}(t)) \cdot \boldsymbol{u}.\end{aligned}$$

So called quasi-LPV systems have representations, in which the parameter dependent system and gain matrices $\boldsymbol{A}(\boldsymbol{\theta}(t)), \boldsymbol{B}(\boldsymbol{\theta}(t)), \boldsymbol{C}(\boldsymbol{\theta}(t)), \boldsymbol{D}(\boldsymbol{\theta}(t))$ can be formulated as affine linear combinations. Assuming a number of m time-varying parameters, the system matrix can then be decomposed into products of a constant matrix times a parameter:

$$\boldsymbol{A}(\boldsymbol{\theta}(t)) = \boldsymbol{A} \cdot \boldsymbol{\theta}(t) = \boldsymbol{A}_0 + \boldsymbol{A}_1\theta_1(t) + \boldsymbol{A}_2\theta_2(t) + \cdots + \boldsymbol{A}_m\theta_m(t).$$

3.2.4 shows a block diagram realisation of an exemplary LPV system, whose only parameter dependency can be found in the system matrix.

Application to the Simulation Model

It is the goal to formulate the system $G(s)$ as a state space system, which is dependent on the supposedly time-varying parameter $\hat{M}$.

Starting from the generalised formulation of the equation of motion

$$\hat{M} \cdot \ddot{y} + \hat{b} \cdot \dot{y} = \hat{k} \cdot \Delta T + d(y, \dot{y}), \tag{3.2.15}$$

a state space representation is as follows:

$$\begin{aligned}\underbrace{\begin{bmatrix} \dot{x} \\ \ddot{x} \end{bmatrix}}_{\dot{\boldsymbol{x}}} &= \underbrace{\begin{bmatrix} 0 & 1 \\ 0 & -\frac{\hat{b}}{\hat{M}} \end{bmatrix}}_{\boldsymbol{A}(\theta(t))} \cdot \underbrace{\begin{bmatrix} x \\ \dot{x} \end{bmatrix}}_{\boldsymbol{x}} + \underbrace{\begin{bmatrix} 0 \\ \frac{\hat{k}}{\hat{M}} \end{bmatrix}}_{\boldsymbol{B}(\theta(t))} \cdot \underbrace{\Delta T}_{u} + \underbrace{\begin{bmatrix} 0 \\ \frac{1}{\hat{M}} \end{bmatrix}}_{\boldsymbol{D}(\theta(t))} \cdot d(y, \dot{y}) \\ \boldsymbol{y} &= \underbrace{\begin{bmatrix} 1 & 0 \end{bmatrix}}_{\boldsymbol{C}} \cdot \boldsymbol{x}\end{aligned} \tag{3.2.16}$$

[1] Linear parameter-varying will be called LPV for short in the following sections

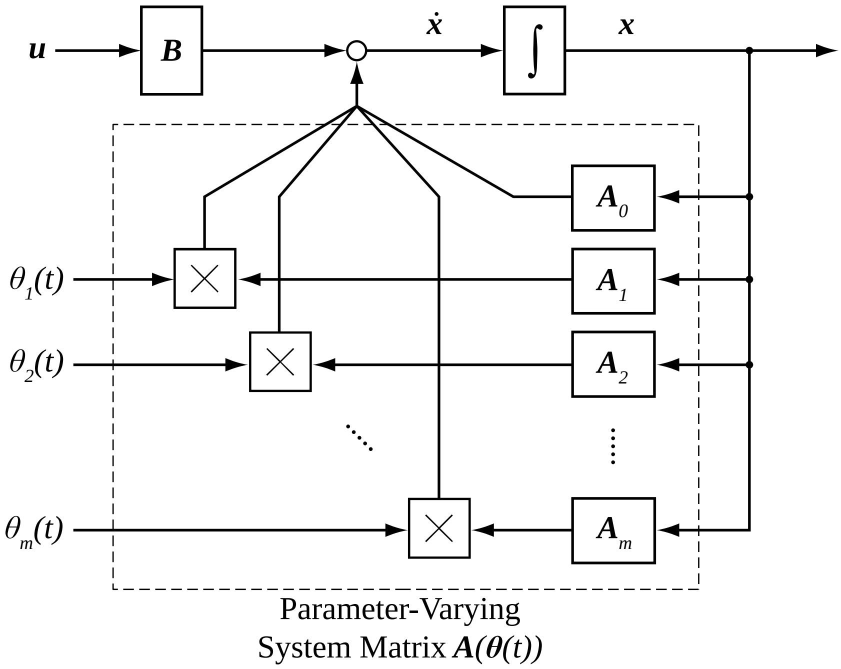

Figure 3.2.4.: Block Diagram Realisation of an Exemplary LPV System

Please note, that a new unknown disturbance input $d(y, \dot{y})$ has been introduced at this point. It is either used to represent input disturbance or model uncertainties like neglected non-linear behaviour.

Defining

$$\theta(t) := \frac{1}{\hat{M}} \quad \hat{M} > 0, \tag{3.2.17}$$

the system can be rewritten in quasi-LPV form:

$$\begin{aligned} \dot{\boldsymbol{x}} &= \left(\underbrace{\begin{bmatrix} 0 & 1 \\ 0 & 0 \end{bmatrix}}_{\boldsymbol{A}_0} + \underbrace{\begin{bmatrix} 0 & 0 \\ 0 & -\hat{b} \end{bmatrix}}_{\boldsymbol{A}_1} \cdot \theta(t) \right) \cdot \boldsymbol{x} + \left(\underbrace{\begin{bmatrix} 0 \\ \hat{k} \end{bmatrix}}_{\boldsymbol{B}_1} \cdot \theta(t) \right) \cdot u + \left(\underbrace{\begin{bmatrix} 0 \\ 1 \end{bmatrix}}_{\boldsymbol{D}_1} \cdot \theta(t) \right) \cdot d(y, \dot{y}) \\ \boldsymbol{y} &= \boldsymbol{C} \cdot \boldsymbol{x} \end{aligned} \tag{3.2.18}$$

Assuming $\hat{M} > 0$ is feasible, since at the very least, the motor's, pulleys' and rope drums' inertias will define the dynamics, even when no load is applied. It is then important to note, that in the case of a very small inertia, the non-linearities or input disturbances are also affected by a larger gain. It can be concluded, that — from this representation — they will have a similar influence on the system behaviour for any value of $\theta(t)$.

Figure 3.2.5 shows the actual block diagram used for all forthcoming simulations of designed controllers, whether the system parameter $\theta(t)$ is set constant or is time-varying. An additional time delay d can be applied to the input of the system, acting as an actuator delay.

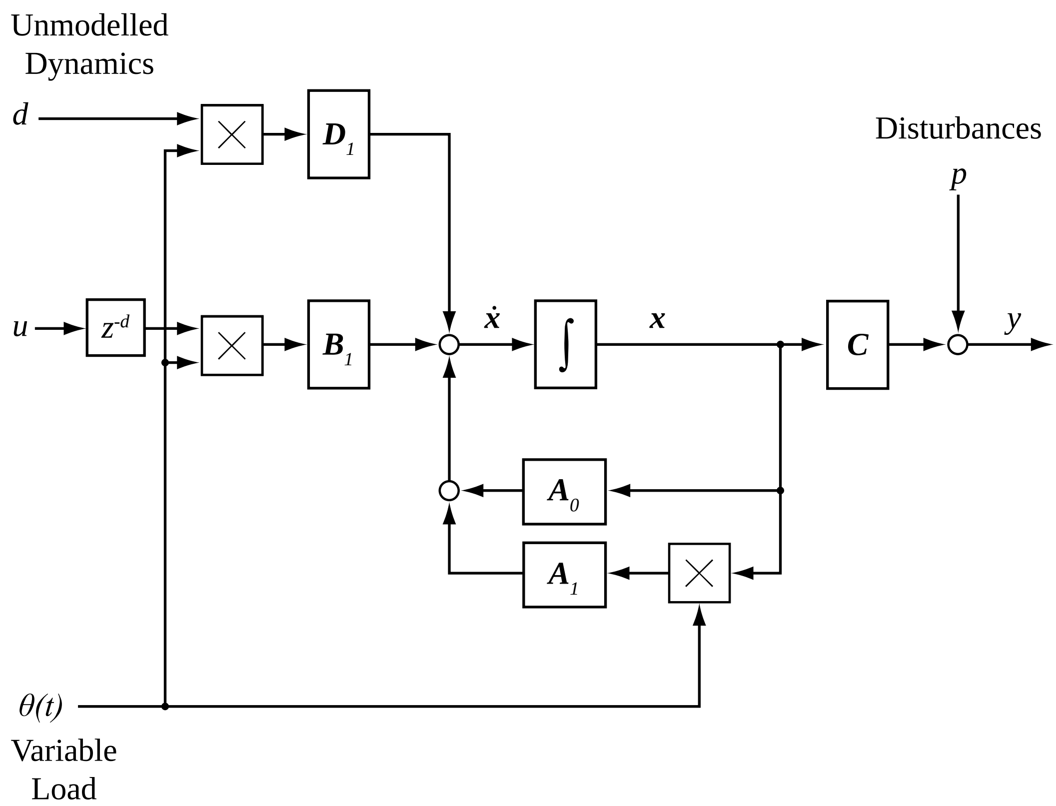

Figure 3.2.5.: Lifting Device Continuous LPV Model

4. Design of a Fixed Digital RST-Structure Controller for the Case of Known Loads

In this chapter a fixed order RST-structure controller is designed to improve the position control algorithm of the flood gate security system. As has been mentioned before, the problem is generalised, in order to be also applicable to any kind of hoist driven lifting device similar to the one, which has been mathematically modelled in the previous chapter.

Before the actual controller is designed and evaluated, a brief overview of the properties of RST-structure controllers is given and an explanation of the manual sensititvity shaping pole placement synthesis approach is provided. The controller will be analysed in terms of robustness against possible occuring time delays and parameter uncertainties.

The solution derived within this chapter does not maintain to be unique or optimal, but feasible in a way, that it supports the suggestions made on the improvement of the Shànghǎi flood gate control system. The generalisation and abstraction from this control system to general hoist driven lifting devices is done in the hope, that it may be of use in further, possibly more demanding, projects.

4.1. RST-Structure Controllers

A structure for discrete time controllers often refered to as the *digital controller canonical structure*, is the RST controller [9, p. 61]. Its block diagram for a closed-loop system is given in figure 4.1.1.

The RST-structure controller consists of three different transfer functions $R(z^{-1})$, $S(z^{-1})$ and $T(z^{-1})$ — hence the name. At the summation port, the equation

$$S(z^{-1}) \cdot u_k = -R(z^{-1}) \cdot y_k + T(z^{-1}) \cdot r_k \tag{4.1.1}$$

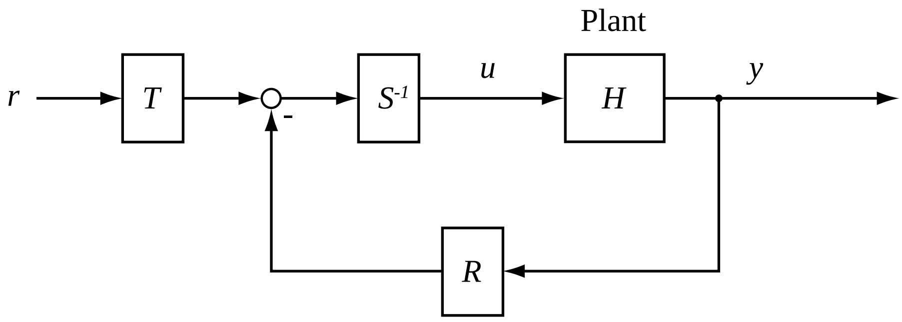

Figure 4.1.1.: Digital Controller Canonical Structure (RST-Structure)

can be derived. Bearing in mind, that z^{-1} can be interpreted as the time shift operator, this form yields a particularly suitable way of calculating the most recent controller output:

$$\begin{aligned} u_k = &-(s_1 u_{k-1} + s_2 u_{k-2} + \cdots + s_{n_S} u_{k-n_S}) - \cdots \\ &\cdots (r_0 y_k + r_1 y_{k-1} + r_2 y_{k-2} + \cdots + r_{n_R} y_{k-n_R}) + \cdots \\ &\cdots (t_0 r_k + t_1 r_{k-1} + t_2 r_{k-2} + \cdots + t_{n_R} r_{k-n_T}), \end{aligned} \tag{4.1.2}$$

$$\begin{aligned} \text{with } S(z^{-1}) &= 1 + s_1 z^{-1} + s_2 z^{-2} + s + s_{n_S} z^{-n_S}, \\ R(z^{-1}) &= r_0 + r_1 z^{-1} + r_2 z^{-2} + s + r_{n_R} z^{-n_R} \\ \text{and } T(z^{-1}) &= t_0 + t_1 z^{-1} + t_2 z^{-2} + s + t_{n_R} z^{-n_T} \end{aligned}$$

This is basically a weighted sum of past plant outputs y, controller outputs u and reference inputs r and ready to implement on even very basic processors under the constraint of limited memory or sample buffers.

RST-structure controllers have a few benefits and properties [9, p. 62]:

- The RST-structure controller provides *two degrees of freedom*, since $T(z^{-1})$ allows to impose specifications for tracking separately from desired performance requirements with regard to regulation.
- It can be used as a standardised controller framework, whose representation may yield many differently synthesised controllers and controller types (P, PI, PID, Pole Placement, ...).
- As mentioned before, the representation lends itself to an easy implementation process.

Especially due to the last point, the RST-structure representation has been chosen, in order to make sure, that the control algorithm designed in this chapter can be implemented on the already existing equipment of the flood gate control system (i.e. a PLC) with minimum effort.

4.1.1. Notation

Since RST-structure controller synthesis can always be basically formulated in terms of pole placement, a certain terminology will be used as follows. The discrete time plant transfer function $H(z^{-1})$ is a rational polynomial in z^{-1}

$$H(z^{-1}) = \frac{B(z^{-1})}{A(z^{-1})} = \frac{b_0 + b_1 z^{-1} + b_2 z^{-2} + \cdots + b_m z^{-m}}{1 + a_1 z^{-1} + a_2 z^{-2} + \cdots + a_n z^{-n}} \tag{4.1.3}$$

with $n \geq m$.

The open-loop transfer function can be computed as

$$H_{\mathrm{ol}}(z^{-1}) = \frac{B(z^{-1})T(z^{-1})}{A(z^{-1})S(z^{-1})}. \tag{4.1.4}$$

From where it follows for the closed-loop transfer function that

$$H_{\mathrm{cl}}(z^{-1}) = \frac{B(z^{-1})T(z^{-1})}{A(z^{-1})S(z^{-1}) + B(z^{-1})R(z^{-1})} = \frac{B(z^{-1})T(z^{-1})}{P(z^{-1})}. \tag{4.1.5}$$

The polynomial

$$P(z^{-1}) = A(z^{-1})S(z^{-1}) + B(z^{-1})R(z^{-1}) \tag{4.1.6}$$

appears in this context as the polynomial, which defines the closed-loop poles. This polynomial is to be shaped in a pole placement approach.

4.1.2. Synthesis-Relevant Sensitivity Functions

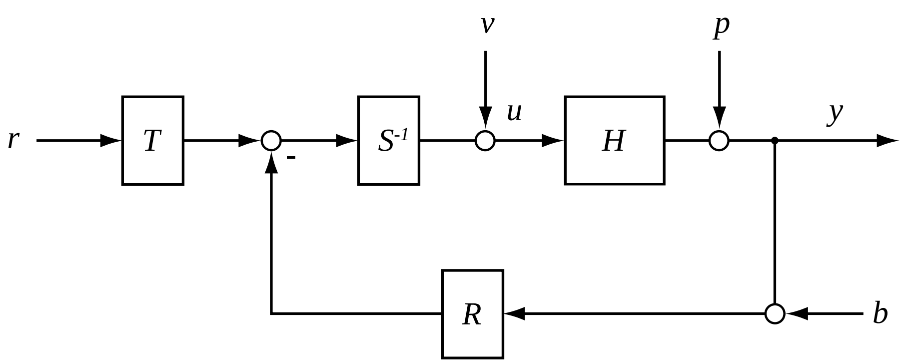

Figure 4.1.2.: Digital Controller Canonical Structure (RST-Structure)

For the controller design, several sensitivity functions are of importance, in order to evaluate the performance and the robustness. A short overview shall define the relevant ones in accordance to [9]. Figure 4.1.2 indicates the signal names and where they enter the loop.

Complementary Sensitivity Function (Closed-Loop Transfer Function)

$$S_{yr}(z^{-1}) = H_{\mathrm{cl}}(z^{-1}) = \frac{B(z^{-1})T(z^{-1})}{A(z^{-1})S(z^{-1}) + B(z^{-1})R(z^{-1})} = \frac{B(z^{-1})T(z^{-1})}{P(z^{-1})} \tag{4.1.7}$$

Output Sensitivity Function

$$S_{yp}(z^{-1}) = \frac{A(z^{-1})S(z^{-1})}{A(z^{-1})S(z^{-1}) + B(z^{-1})R(z^{-1})} = \frac{A(z^{-1})S(z^{-1})}{P(z^{-1})} \tag{4.1.8}$$

Input Sensitivity Function

$$S_{up}(z^{-1}) = \frac{-A(z^{-1})R(z^{-1})}{A(z^{-1})S(z^{-1}) + B(z^{-1})R(z^{-1})} = \frac{-A(z^{-1})R(z^{-1})}{P(z^{-1})} \tag{4.1.9}$$

Noise-Output Sensitivity Function

$$S_{yb}(z^{-1}) = \frac{-B(z^{-1})R(z^{-1})}{A(z^{-1})S(z^{-1}) + B(z^{-1})R(z^{-1})} = \frac{-B(z^{-1})R(z^{-1})}{P(z^{-1})} \tag{4.1.10}$$

Input Disturbance-Output Sensitivity Function

$$S_{yv}(z^{-1}) = \frac{B(z^{-1})S(z^{-1})}{A(z^{-1})S(z^{-1}) + B(z^{-1})R(z^{-1})} = \frac{B(z^{-1})S(z^{-1})}{P(z^{-1})} \tag{4.1.11}$$

4.2. Sensitivity Shaping Pole Placement Synthesis Approach

The sensitivity shaping pole placement controller synthesis method has been programmed and adapted in accordance to [9, p. 105] in MATLAB. It has proven to be a very versatile method, that once automated, can provide an intuitive and responsive way of synthesising a SISO controller by having full control over the controller order and the resulting closed-loop behaviour. It has been chosen, because of the resulting RST controller structure and because the computation can to a certain extend even be comprehended analytically, which encouraged the adaptive controller design covered in the next chapter.

The pole placement approach works for any plant $H(z^{-1}) = \frac{z^{-d} \cdot \hat{B}(z^{-1})}{A(z^{-1})} = \frac{B(z^{-1})}{A(z^{-1})}$ with no restrictions on

- the time delay d,
- plant stability,
- stable or unstable zeros,

as long as the nominator and the denominator do not have common factors.

Choice of Closed-Loop Poles The desired closed-loop poles can be chosen by discretising a continuous time transfer function of second order, whose damping and frequency parameter ζ and ω_0 have been determined in accordance with the desired behaviour.

$$P_D(s) = \frac{\omega_0^2}{s^2 + 2\zeta\omega_0 \cdot s + \omega_0^2} \tag{4.2.1}$$

Only the denominator of the discretisation is of interest. It calculates to

$$P_D(z^{-1}) = 1 - 2e^{-\zeta\omega_0 T_s}\cos(\omega_0 T_s) \cdot z^{-1} + e^{-2\zeta\omega_0 T_s} \cdot z^{-2}. \tag{4.2.2}$$

The dominant poles $P_D(z^{-1})$ can be enhanced by faster auxiliary poles $P_F(z^{-1})$, which have the ability to facilitate the quality of the closed-loop response.

$$P(z^{-1}) = P_D(z^{-1}) \cdot P_F(z^{-1}) = 1 + p_1 z^{-1} + p_2 z^{-2} + \cdots + p_{n_p} z^{-n_p} \tag{4.2.3}$$

Sensitivity Shaping Parts of the controller can be prespecified, in order to achieve desired performance and robustness margins. Mathematically, it is the easiest way, to act like the prespecified parts $H_R(z^{-1})$ and $H_S(z^{-1})$ of $R(z^{-1})$ and $S(z^{-1})$, respectively, are part of the plant to be controlled:

$$\begin{aligned} \tilde{B}(z^{-1}) &= B(z^{-1}) \cdot H_R(z^{-1}) \\ \tilde{A}(z^{-1}) &= A(z^{-1}) \cdot H_S(z^{-1}). \end{aligned} \tag{4.2.4}$$

The controller transfer functions are composed of the fixed polynomials $H_R(z^{-1})$ and $H_S(z^{-1})$ and the calculated polynomials $\tilde{R}(z^{-1})$ and $\tilde{S}(z^{-1})$:

$$\begin{aligned} R(z^{-1}) &= \tilde{R}(z^{-1}) \cdot H_R(z^{-1}) \\ S(z^{-1}) &= \tilde{S}(z^{-1}) \cdot H_S(z^{-1}). \end{aligned} \tag{4.2.5}$$

There are certain typical choices as to the fixed parts of the controller. Those applied during the actual controller design will be explained later.

Solution to the Bezout Identity To determine the controller transfer functions $S(z^{-1})$ and $R(z^{-1})$, the equation

$$\tilde{A}(z^{-1})\tilde{S}(z^{-1}) + \tilde{B}(z^{-1})\tilde{R}(z^{-1}) = P(z^{-1}) \tag{4.2.6}$$

has to be solved for the polynomials $\tilde{R}(z^{-1})$ and $\tilde{S}(z^{-1})$. This equation is called the Bezout Identity and is a linear diophantine equation. The problem can be posed in matrix notation, such that for the solution only a matrix inversion is needed.

$$\underbrace{\begin{bmatrix} 1 & 0 & \cdots & 0 & 0 & \cdots & \cdots & 0 \\ \tilde{a}_1 & 1 & & \vdots & \tilde{b}_1 & 0 & & \vdots \\ \tilde{a}_2 & \ddots & \ddots & 0 & \tilde{b}_2 & \ddots & \ddots & \vdots \\ \vdots & & \ddots & 1 & \vdots & & \ddots & 0 \\ \vdots & & & \tilde{a}_1 & \vdots & & & \tilde{b}_1 \\ \tilde{a}_{n_{\tilde{a}}} & & & \tilde{a}_2 & \tilde{b}_{n_{\tilde{b}}} & & & \tilde{b}_2 \\ 0 & & & \vdots & 0 & & & \vdots \\ 0 & \cdots & 0 & \tilde{a}_{n_{\tilde{a}}} & 0 & \cdots & 0 & \tilde{b}_{n_{\tilde{b}}} \end{bmatrix}}_{\boldsymbol{M}\in\mathbb{R}^{((n_{\tilde{b}}+d)+n_{\tilde{a}})\times((n_{\tilde{b}}+d)+n_{\tilde{a}})}} \cdot \boldsymbol{k} = \underbrace{\begin{bmatrix} 1 \\ p_1 \\ p_2 \\ \vdots \\ \vdots \\ p_{n_p} \\ 0 \\ \vdots \\ 0 \end{bmatrix}}_{\boldsymbol{p}\in\mathbb{R}^{(n_{\tilde{b}}+d)+n_{\tilde{a}}}} \tag{4.2.7}$$

Then the coefficients of the calculated parts of the controller transfer functions $\tilde{S}(z^{-1})$ and $\tilde{R}(z^{-1})$ can be extracted from the vector $\boldsymbol{k}$.

$$\begin{aligned} \boldsymbol{k} &= \boldsymbol{M}^{-1} \cdot \boldsymbol{p} \\ &= \begin{bmatrix} 1 & \tilde{s}_1 & \tilde{s}_2 & \cdots & \tilde{s}_{n_{\tilde{S}}} & \tilde{r}_0 & \tilde{r}_1 & \cdots & \tilde{r}_{n_{\tilde{R}}} \end{bmatrix}^T \end{aligned} \tag{4.2.8}$$

Eventually, the final controller transfer functions $S(z^{-1})$ and $R(z^{-1})$ have then to be generated by multiplication of the polynomials:

$$\begin{aligned} R(z^{-1}) &= \tilde{R}(z^{-1}) \cdot H_R(z^{-1}) = \left(\tilde{r}_0 + \tilde{r}_1 z^{-1} + \cdots + \tilde{r}_{n_{\tilde{R}}} z^{-n_{\tilde{R}}}\right) \cdot H_R(z^{-1}) \\ S(z^{-1}) &= \tilde{S}(z^{-1}) \cdot H_S(z^{-1}) = \left(1 + \tilde{s}_1 z^{-1} + \cdots + \tilde{s}_{n_{\tilde{S}}} z^{-n_{\tilde{S}}}\right) \cdot H_S(z^{-1}). \end{aligned} \tag{4.2.9}$$

Choice of the Prefilter $T(z^{-1})$ A RST pole placement controller with only two selected dominant poles and $T(z^{-1}) = R(z^{-1})$, is the discrete equivalent to a continuous time PID controller. However, new zeros are introduced this way, which results in an overshoot and cannot be avoided, however small it may be.

By directly designing a discrete controller via the RST pole placement approach, it is possible to circumvent the addition of new zeros to the closed-loop system by choosing

$$T(z^{-1}) = R(1). \tag{4.2.10}$$

Since then the closed-loop transfer function becomes

$$S_{yr}(z^{-1}) = R(1) \cdot \frac{B(z^{-1})}{P(z^{-1})} = R(1) \cdot \frac{B(z^{-1})}{A(z^{-1})S(z^{-1}) + B(z^{-1})R(z^{-1})}$$

and since $S(1) = 0$, this results in an unit gain between reference input and plant output in case of no disturbances:

$$S_{yr}(1) = R(1) \cdot \frac{B(1)}{P(1)} = R(1) \cdot \frac{B(1)}{A(1)S(1) + B(1)R(1)} = R(1) \cdot \frac{B(1)}{B(1)R(1)} = 1.$$

4.3. Design by Robustness Templates

When manually choosing auxiliary poles via $P_F(z^{-1})$ or defining fixed controller parts $H_S(z^{-1})$ and $H_R(z^{-1})$, the effect can be analysed by bode plots of the resulting sensitivity functions. [9] suggests templates, in which to fit the bode plots to ensure gain, phase and delay margins, which can let the designer anticipate a certain degree of robustness. These templates could also prove useful in an approach to find an optimal solution by employing genetic algorithms.

Since, the controller could not be tested on a real plant, all further designs have been done using these templates, to achieve feasible controllers.

Robustness templates can be expressed for the sensitivity functions $S_{yp}(z^{-1})$, $S_{yb}(z^{-1})$ and $S_{up}(z^{-1})$, which all state, that for a certain deviation from the used plant model $\left|H_{ol}^{tol}(z^{-1}) - H_{ol}(z^{-1})\right|$, the gains with regard to the disturbance signal p may only have a certain magnitude. More specific, the templates are as follows.

Robustness against Additive Plant Uncertainties The criteria for the controlled plant with a controller computed for the nominal plant to be robust with respect to some different plant parameters or other additive uncertainties can be expressed as inequalities. With $H_{\text{ol}}^{\text{tol}}(z^{-1}) = \frac{B^{\text{tol}}(z^{-1})T(z^{-1})}{A^{\text{tol}}(z^{-1})S(z^{-1})}$ computed with controller coefficients derived from the nominal plant, the following inequalities have to hold:

$$\left|S_{yp}^{-1}(z^{-1})\right| > \left|H_{\text{ol}}^{\text{tol}}(z^{-1}) - H_{\text{ol}}(z^{-1})\right|. \tag{4.3.1}$$

$$\left|S_{yb}^{-1}(z^{-1})\right| > \frac{\left|H^{\text{tol}}(z^{-1}) - H(z^{-1})\right|}{\left|H(z^{-1})\right|}. \tag{4.3.2}$$

$$\left|S_{up}^{-1}(z^{-1})\right| > \left|H^{\text{tol}}(z^{-1}) - H(z^{-1})\right|. \tag{4.3.3}$$

Robustness against Time Delays Specific templates can be found for imposing a time delay d_{tol} to be tolerated. Then $H^{\text{tol}}(z^{-1}) = z^{-d_{\text{tol}}} \cdot H(z^{-1})$ and thus

$$\frac{\left|H^{\text{tol}}(z^{-1}) - H(z^{-1})\right|}{\left|H(z^{-1})\right|} = \left|z^{-d_{\text{tol}}} - 1\right|, \tag{4.3.4}$$

which can be used to simplify the expressions from the preceding paragraph. In particular, the time delay margin criterion with respect to the output sensitivity function becomes

$$1 - \left|z^{-d_{\text{tol}}} - 1\right|^{-1} < \left|S_{yp}(z^{-1})\right| < 1 + \left|z^{-d_{\text{tol}}} - 1\right|^{-1} \tag{4.3.5}$$

General Gain Margin As a rule of thumb, a gain margin of $\Delta M \geq 0.5$ (approximately -6dB) is sufficient. The template can be formulated as

$$\left|S_{yp}(z^{-1})\right| < -\Delta M \tag{4.3.6}$$

and should be considered together with a time delay margin. In control theory literature, the maximum of the output sensitivity function is also often called the $\mathcal{H}_\infty$-norm, whereas the gain margin becomes an upper bound on the $\mathcal{H}_\infty$-norm.

Robust Design Rules Imposing these robustness margins is often not enough to succesfully design a feasible controller. First of all, plant uncertainties have to be identified or anticipated. Furthermore, when manually selecting fixed controller parts, the effects should be known and used purposefully. Much can already be dealt with, by always thinking of the sensitivity functions in terms of gains from input to output. With respect to this point of view, the following rules should be observed:

Zero Steady State Error To enforce integral action, which means constant (i.e. zero frequency) disturbances are completely rejected $|S_{yp}(z^{-1})|$ should be made zero ($-\infty$dB) at low frequencies. Therefore $H_S(z^{-1})$ can be chosen to include $(1-z^{-1})$.

Actuator Stress To avoid actuator stress, $|S_{up}(z^{-1})|$ should be made small at high frequencies. Therefore $H_R(z^{-1})$ can be chosen to include factors $(1+\beta z^{-1})^i, 0 < \beta \leq 1$, where $\beta = 1$ lets the system work like in open loop at half the sampling frequency $f = 0.5 f_s$.

Figure 4.3.1 shows typical templates for time delay and gain margins, as well as boundaries to consider, in order to avoid excessive control action in high frequencies and achieve zero steady state error.

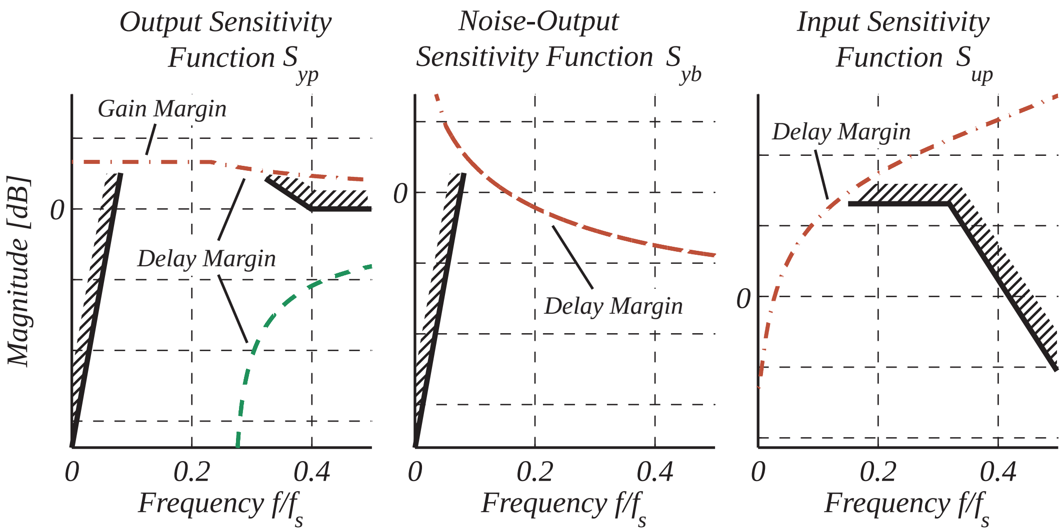

Figure 4.3.1.: Robustness Templates for Sensitivity Shaping. *(Hatched boundaries show desirable margins for feasible control)*

4.4. Controller Design and Simulation Results

In this section, the sensitivity shaping pole placement approach is applied to the plant given in chapter 3. The process of designing a feasible controller manually involves some trial and error and analysis of simulation results as well as sensitivity function plots. After the control objectives and the controller requirements are listed, the final design is presented. Please bear in mind, that it is based on some uncertain and assumed values. Before implementing the results, the design should be carried out anew, but in a very similar way, in order to adapt the controller to the actual circumstances. The assumed values, however, are deemed realistic and without loss of generality, the results can be interpreted as a feasibility study.

4.4.1. Control Objectives and Corresponding Controller Requirements

With regard to the suggested improvement to incorporate a feedback control architecture into the flood gate control system, the control objectives given in the system abstract (ref. to 1.3) are reviewed and reconsidered from a control theory point of view. The respective attributes of the controller are directly given.

Ramp Reference Tracking The position controller has to be able to track a ramp shaped reference input, which will be generated and fed to the controller. The maximum movement speed of the gate is limited by the reference input.

Steady State Accuracy The position controller has to achieve a zero steady state error within the limits of measurement accuracy, which is assumed to include noise of ± 10 mm magnitude. This corresponds to the controlled closed-loop having integral action.

Fully Aperiodic Behaviour When approaching the reference input, absolutely no overshoot is permitted, in order to protect the mechanical equipment. This corresponds to a choice of a purely real dominant pole pair with damping coefficient $\zeta = 1$. Also the prefilter $T(z^{-1})$ has to be deprived of any dynamics and chosen as $T(z^{-1}) = R(1)$.

Avoidance of Excessive Control Action The controller output should not oscillate violently to prevent actuator stress. Therefore the input sensitivity function $S_{up}(z^{-1})$ should have a low gain at high frequencies, which can be achieved by opening the loop near $f = 0.5f_s$.

Low Controller Order The controller order should be limited, to enhance the chance, that it can be implemented on existing equipment. This corresponds to imposing as little fixed parts on the controller as possible.

4.4.2. Choice of Sampling Frequency

All results presented later on are in some way obtained under the consideration of the flood gate control system. Still, since this and especially the following chapter generalises the problem to hoist based lifting devices, the choice of a sampling frequency or desired maximum velocities and thus induced desired rise-times do only devalue the results of this thesis if any of the assumptions posed in section 3.1 are violated.

As a general rule presented in [9], the sampling frequency can be chosen in accordance to the rise-time for first order systems. Since totally aperiodic behaviour is desired, the closed-loop system should behave close to a first order system. As such, the maximum velocity of the load can be used to calculate an approximate rise-time to a unit step:

$$t_{\text{rise}} = \frac{1}{\dot{y}_{\max}} \cdot 1\,\text{m} \qquad (4.4.1)$$

with $\dot{y}_{\max}$ in SI-units.

This corresponds to a closed-loop bandwidth of

$$f_0^{\text{cl}} = \frac{2}{p t_{\text{rise}}}. \qquad (4.4.2)$$

Shannon's theorem states, that a signal can be reconstructed, if it is sampled with at least double the highest occurring frequency. In control system applications, the sampling frequency is generally chosen even higher in a range

$$f_s = 5 \dots 30 \cdot f_0^{\text{cl}}. \qquad (4.4.3)$$

4.4.3. Sensitivity Shaping Solution

A maximum velocity of 6 m per 1 min is considered desirable for the Shànghǎi flood gate control system. Even higher values can easily be achieved, given the mechanical equipment and the actuator are capable to withstand the stress, because this leads to a rather long sampling interval of

$$T_s = \frac{1}{f_s} = \frac{1}{20 \cdot f_0^{\text{cl}}} \approx 0.8\,\text{s}.$$

This should in general provide more than enough time to perform all the needed computations on the existing control equipment.

Under consideration of all objectives from the previous section a manually derived solution incorporated the following parameters:

$$\omega_0 = 0.44 \frac{\text{rad}}{\text{s}} \quad \zeta = 1 \qquad (4.4.4)$$

and auxiliary poles chosen as

$$P_F(z^{-1}) = \left(1 - 0.7 \cdot z^{-1}\right)^2 . \tag{4.4.5}$$

This results in the desired closed-loop transfer function denominator

$$\begin{aligned} P(z^{-1}) = P_D(z^{-1}) \cdot P_F(z^{-1}) &= \left(1 - 1.416z^{-1} + 0.501z^{-2}\right) \cdot \left(1 - 1.4z^{-1} + 0.49z^{-2}\right) \\ &= \left(1 - 2.816z^{-1} + 2.973z^{-2} - 1.395z^{-3} + 0.2455z^{-4}\right) . \end{aligned} \tag{4.4.6}$$

Zero steady state error does not have to be enforced, since the controlled plant itself already has an integrator:

$$H_S(z^{-1}) = 1. \tag{4.4.7}$$

Opening the loop at high frequencies is mandatory, though.

$$H_R(z^{-1}) = \left(1 + z^{-1}\right)^4 . \tag{4.4.8}$$

Taking the term $\left(1 + z^{-1}\right)$ to the power of 4 is a choice based on the trade-off between a high controller order and noise attenuation with respect to the controller output u in the high frequency region. How much attenuation is actually needed in a real implementation, mainly depends on the sensor output quality. It has been assumed, that the rotary encoder signal is disturbed by a white noise signal, which has a magnitude of about 10 mm.

Figure 4.4.1 visualises the pole placement of auxiliary and dominant poles, where the dominant poles are only marginally faster than the auxiliary ones. The effect of the auxiliary poles is to further increase the amount of noise attenuation on the controller output.

Plots of the sensitivity functions are depicted in figure 4.4.2 for three different loads $M_i = i \cdot 10,000\,\mathrm{kg}, i = 1, 2, 3$. Robustness templates are plotted in with the standard gain margin and a delay margin of $2T_s$. With respect to the output sensitivity function $S_{yp}(z^{-1})$ and the noise-output sensitivity function $S_{yb}(z^{-1})$, there is no apparent difference in the dynamic behaviour for the different loads. With respect to the input sensitivity function $S_{up}(z^{-1})$, higher loads require for higher gains to compensate for a disturbance.

4.4.4. Simulation Setup

The derived controller is tested in presence of white noise signals entering as unmodelled dynamics $d(y, \dot{y}, t)$, random disurbance $p(t)$ and measurement noise $b(t)$. The linear parameter-varying state space representation of the lifting device depicted in figure 3.2.5 is used as a plant model, but with the system parameter $\theta(t)$ set to a constant value.

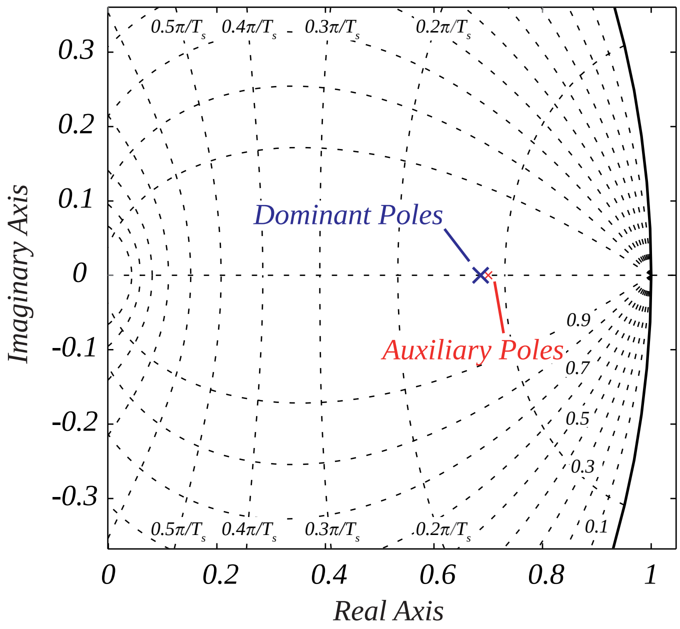

Figure 4.4.1.: Pole Placement for the Fixed RST Sensitivity Shaping Controller Design Visualised in the Complex z-Plane

All simulations have been done in MATLAB/SIMULINK. The basic simulation setup is depicted in figure 4.4.3, where it is obvious that the RST-structure controller needs to take as inputs the reference input $r(t)$, the controller output $u(t)$ and the plant output $y(t)$.

It is assumed, that only the plant output is a continuous signal, which is sampled inside the controller. In fact, the reference input would be also generated by the controller or a higher level control device as discrete values r_k, while the discrete controller output u_k could be directly feeded back or saved to a dynamic memory buffer. The sample buffers for all past plant outputs y_k and controller outputs u_k needed to compute the next controller output u_{k+1} have the length corresponding to the controller transfer function orders n_S and n_R and are visualised as delays of corresponding length, despite the fact, that the controller always receives full data vectors of length n_S and n_R, respectively.

A schematic of the fixed RST-structure controller inputs and outputs is given in figure 4.4.4. The buffers need to be initialised by suitable values, whereas the controller coefficients — denoted $R(z^{-1})$ and $S(z^{-1})$ in the schematic — are stored in the controller's memory.

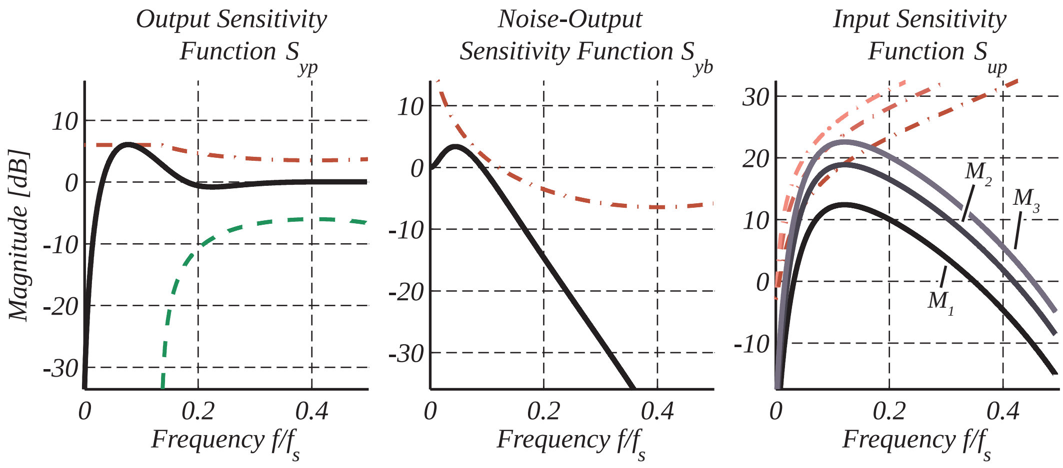

Figure 4.4.2.: Sensitivity Functions for the Fixed RST Sensitivity Shaping Controller Design for Constant and Known Loads $M_i = i \cdot 10,000\,\mathrm{kg}, i = 1, 2, 3$ under Tolerance of a Delay Margin of $2T_s$

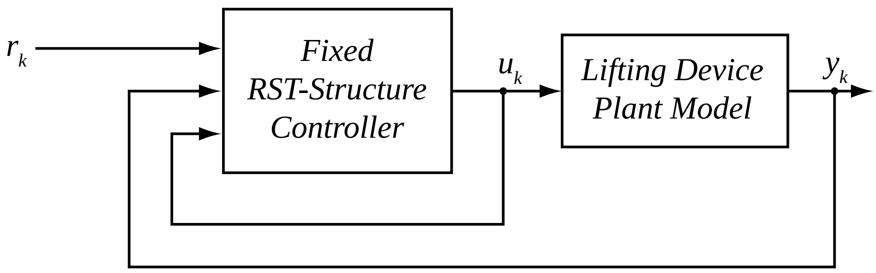

Figure 4.4.3.: Simulation Setup for the Fixed RST Sensitivity Shaping Controller Design

4.4.5. Simulation Results

Subject to a trapezoid reference input, determined by the maximum height of 6 m and the maximum movement speed of 6 m per 60 s, the controlled plant provides the simulation results provided by the graph 4.4.5.

The acceleration and deceleration is performed in a very smooth way and the reference input is tracked perfectly with regard to the zero steady state error and the slope. Note, that it is not desirable for the position to fully track the ramp-shaped reference input, in a way, that the position error becomes zero, while the load is still moving. The controller output u does not show excessive control action in the presence of white noise entering the ports for unmodelled dynamics d, disturbance p and measurement noise b.

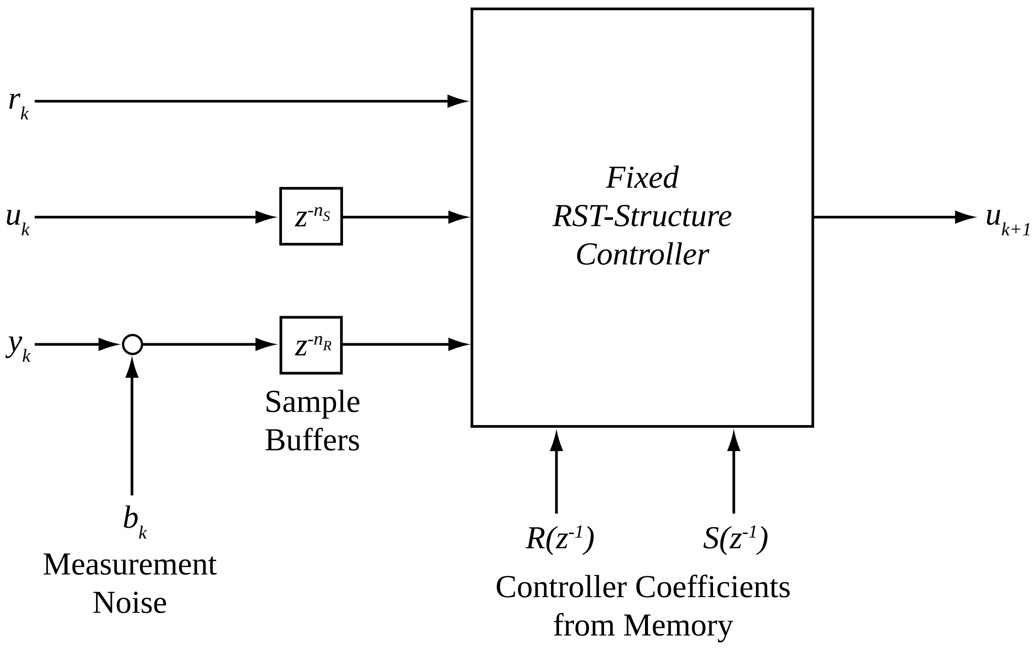

Figure 4.4.4.: Schematic of Inputs and Outputs to the Fixed RST-Structure Controller

Since the sensitivity function plots shown in figure 4.4.2 promised stability at least for a time delay of up to $d = 2$, the simulation results for $d = 1$ and $d = 2$ shall also be investigated. Figure 4.4.6 summarises the results.

For $d = 1$ the results are still satisfactory, in a sense, that only minor oscillations occur, which should not be harmful to the equipment. With increasing the delay, the oscillations become more pronounced and stability is finally lost for $d = 4$.

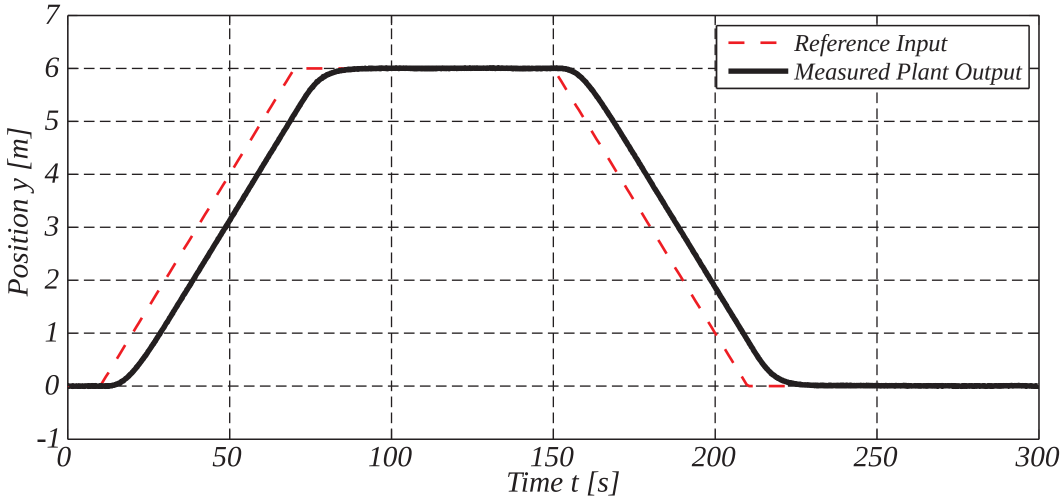

(a)

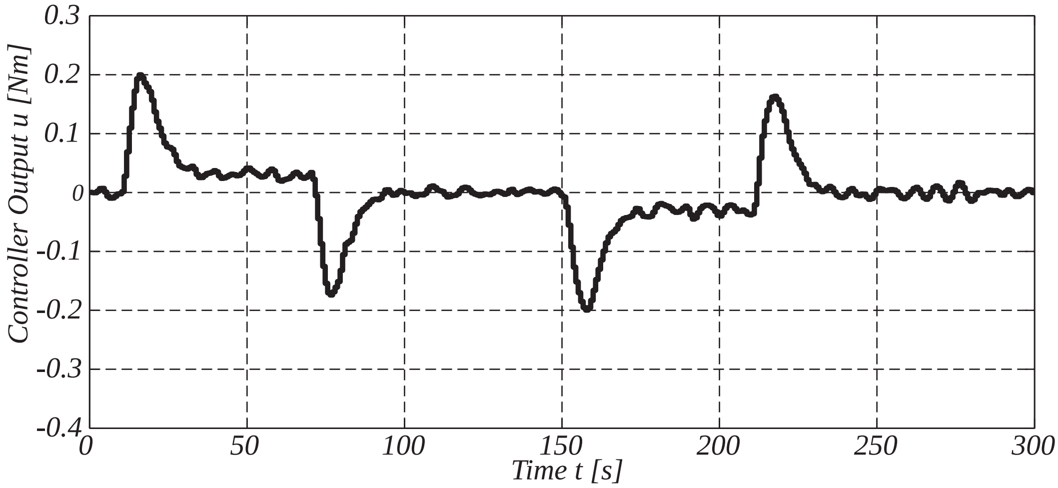

(b)

Figure 4.4.5.: Simulation Results for the Plant Controlled by a Fixed RST-Structure Controller under the Influence of Noise. *(a)* Plant Output y and Reference Signal r. *(b)* Controller Output u.

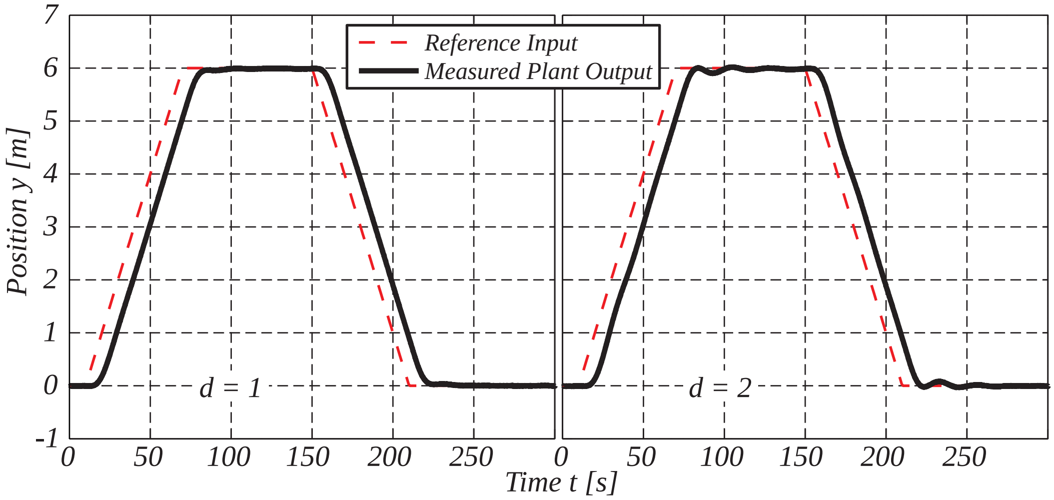

(a)

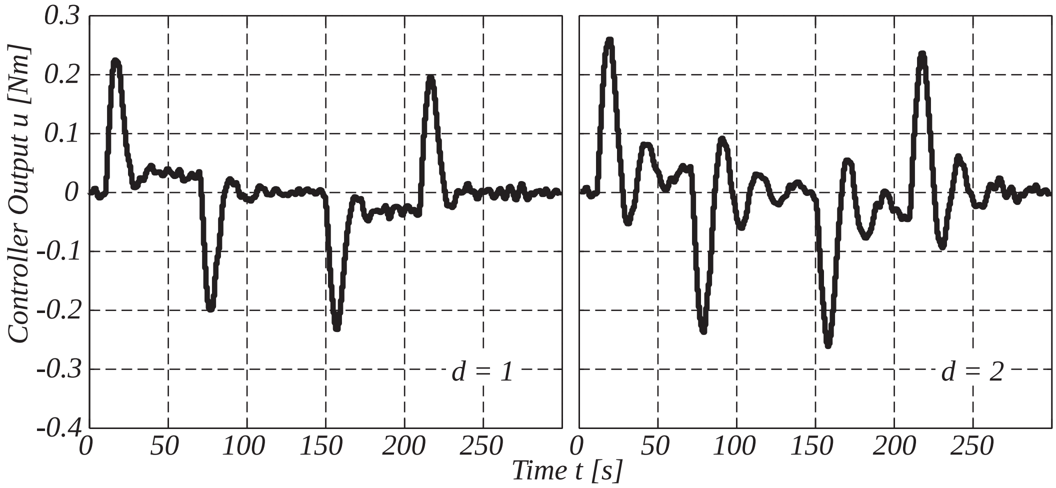

(b)

Figure 4.4.6.: Simulation Results for the Delayed Plant Controlled by a Fixed RST-Structure Controller under the Influence of Noise. *(a)* Plant Output y and Reference Signal r. *(b)* Controller Output u.

4.4.6. Extended Robustness Analysis

So far, the controller design has only taken into account time delay margins and a general gain margin to achive a certain degree of robustness. This can be interpreted as aiming for robustness against possible computational delays and delays originating from the drive system. Such an approach is sufficient, while in a situation, where the lifted load's mass and the system's inertia is well known or has been identified by established means of discrete system identification.

It is often the case, however, that various system parameters are only known within some certainty boundaries. With the synthesis and analysis tools described in the sections 4.2 and 4.3 it is possible to check the robustness margins of a given controlled plant against plant parameter variations. This can be included into the actual controller design process. Trying to achieve robustness against multiple deviations from the nominal plant, as well as optimising the closed-loop performance and dynamic behaviour can very quickly become a tedious task. This is especially true for MIMO systems, where more rigorous analytical or numerical optimisation techniques should be favoured over manual tuning.

For the sake of simplicity, an extended robustness analysis with respect to variations in the load mass $\hat{M}$ is given here post-hoc and only for a controller designed for the load mass $\hat{M}_2$. Figure 4.4.7 shows the sensitivity function plots of the controlled plant with robustness margins derived by varying the load mass parameter within boundaries, that still promise closed-loop stability. It is obvious that there is no upper boundary with respect to the load mass parameter for the system to become unstable. There is, however, no guarantee given by the fact, that the sensitivities remain below the robustness margins, that the dynamic behaviour is still strictly aperiodic. To investigate this, the sensitivity functions of the plant with varyied load mass and the controller computed for the nominal plant have to be regarded.

Figure 4.4.8 illustrates this point by showing simulation results for varyied plant parameters. While the controlled plant still provides protection against hard impacts, if the load mass is lower than expected, a larger plant parameter quickly results in an unwanted overshoot. Vice versa, the controller output has undesired oscillations, for a smaller load, while the amplitude in the case of an increased load is significantly higher but remains calmer.

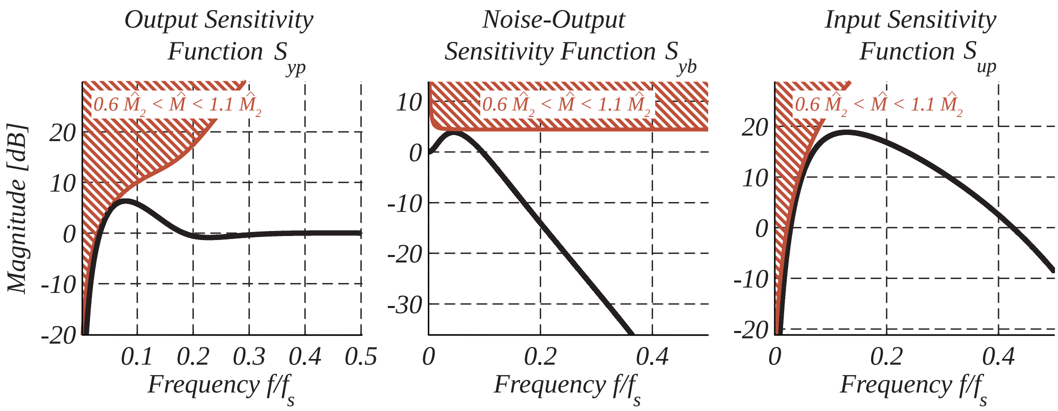

Figure 4.4.7.: Sensitivity Functions for the Fixed RST Sensitivity Shaping Controller Design with Robustness Margins against Load Parameter Variations

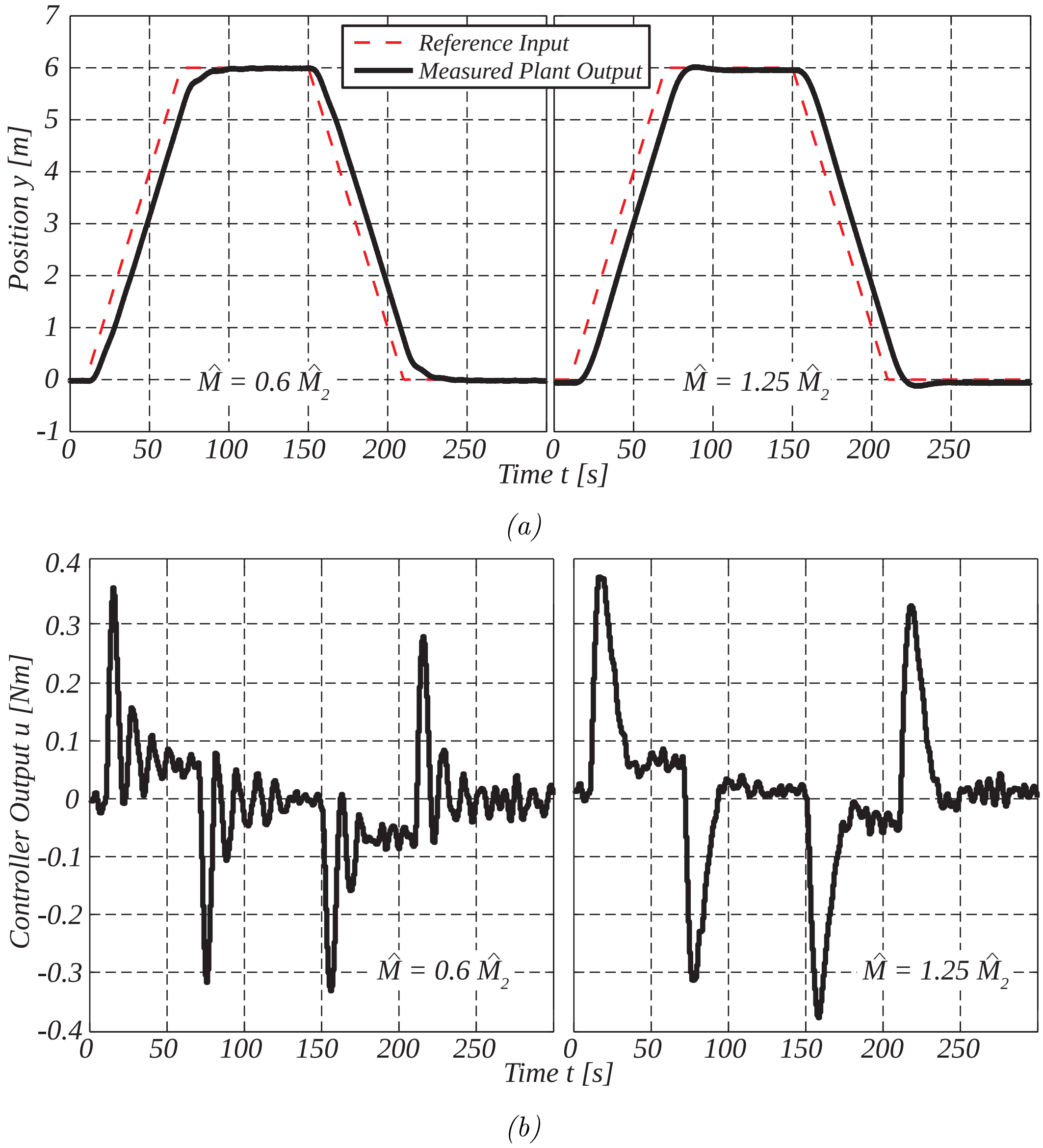

Figure 4.4.8.: Simulation Results for the Delayed Plant Controlled by a Fixed RST-Structure Controller and Varied Load Mass $\hat{M}$, while under the Influence of Noise. *(a)* Plant Output y and Reference Signal r. *(b)* Controller Output u.

4.5. Implementation Issues

PLCs like the SIEMENS S7-200 include optimised PID control loop functionality, which is usually executed without any influence on the performance of the other PLC computations. In this particular case, there is also support for hysteresis effects and exception handling. It would be advantageous if the control problem at hand could be solved by the integrated controllers. The controller designed in this chapter, however, meets two fundamental requirements, which impose two problems, when using the integrated PID functionality:

Avoiding the Introduction of Additional Controller Zeros A normal PID controller with all dynamic components in the feedforward path always introduces additional controller zeros into the closed-loop system. This leads to an undesireable overshoot. As a solution, it is usually possible to run several PID control loops at the same time, for which the P, I and D portions can be activated and deactivated separately [1]. Therefore, it is possible to reroute only the D portion into the feedback path, by using a PI and a pure D controller in parallel by adding their outputs. This basically has the same effect as setting $T(z^{-1}) = R(1)$ with the RST structure, i.e. avoiding to introduce new controller zeros. In other terms, it can be said, that state feedback is mandatory for the type of plant considered, since rerouting the D portion into the feedback path is actually the same as identifying the velocity state by taking the derivative of the position.

Avoiding Excessive Control Action in High Frequencies Normal PID controllers are generally not capable of having very low gains at high frequencies. This is why a sensitivity shaping approach has been followed in this thesis. If it is possible to reduce the amount of noise induced by the sensors, e.g. by filtering the signals, a PID controller might suffice.

If the requirements can be met by the solutions suggested above, the results presented in this thesis can be translated into P, I and D gains and an almost equivalent controller can be found. The trade-off between signal filtering, more expensive sensors versus the additional programming effort for a direct RST-structure controller implementation should be considered, though. When refering to equation 4.1.2, it becomes obvious, that the controller can be realised by simply buffering past inputs and outputs and doing a weighted summation to calculate the newest controller output. Some PLC manufacturers, like for instance ALLEN-BRADLEY, are even known to directly include RST-structure controller functionality just like the SIEMENS S7-200 supports PID loops.

For all reasons mentioned above, the solution presented in this chapter is deemed to be feasible and ready to implement on PLC controllers even without using an additional digital signal processor dedicated to the control algorithm.

5. Design of an Adaptive Digital RST-Structure Controller for the Case of Unknown Loads

In the previous chapter a control algorithm has been derived, which is feasible for controlling hoist-based lifting devices like the Shànghǎi flood gate security system under the assumption, that the load and the system parameters are known within certain tolerances.

This chapter aims at further generalising the problem, such that the control of lifting devices is possible without any knowledge about the load. It is the goal to provide very robust and safe control of potentially dangerous goods or in potentially hazardous environments with an amount of precision, which requires closed-loop torque-controlled position control.

As a typical example throughout this chapter, it will be refered to a crane lifting open containers carrying bulk cargo. The term *unknown loads* in this case is vague and can be more clearly specified by the three following phenomena:

1. **Unknown Constant Load** No, or only very uncertain information about the load's magnitude is available. The load will not change over time during movement, though. This can be imagined as the crane picking up a container of unknown weight.
2. **Unknown Pseudo-Constant Load** No, or only very uncertain information about the load's magnitude is available. The load will be constant for relatively long periods of time, but may change rapidly to a new constant level. This can be imagined as the crane moving a container, which suddenly looses part of its contents or is aquiring a higher load.
3. **Unknown Time-Varying Load** The load's magnitude is impossible to be known. It may change at constant or changing rates. This can be imagined as a crane lifting a container, which continuously looses parts of its contents or is continuously filled in small quantities.

Although the need for such a high precision, advanced control algorithm for lifting devices may appear only in few occasions, the above-mentioned cases may really depend on a very reliable control performance. Furthermore, modern equipment is able to deal with the computational effort [11]. With some optimisation with respect to the RST-structure controller synthesis, the algorithm can even be designed to be less demanding.

After a brief overview of the adaptive controller structure, the *recursive least squares*[1] online identification algorithm's principle will be explained as an example out of many possible online identification methods. Then follows an investigation on how to simplify the synthesis process for online use. Eventually, the adaptive control algorithm will be shown to perform well in simulations employing the three different load patterns mentioned above.

5.1. Adaptive Controller Scheme Using Online-Identification and –Synthesis

According to [11] adaptive control schemes can be grouped into two main approaches — model reference adaptive control and self-tuning control. Adaptive controllers can also be based on an heuristic approach or have a variable structure as two additional approaches mentioned by [14, p. 10]. With model reference adaptive control, the feedback law changes the dynamics of the given plant in such a way, that it corresponds to those of a particular reference model. Self-tuning control employs the measurement of input u_k and output signals y_k of a plant, in order to continuously retune a given type of controller.

Self-tuning control can be further divided into explicit and implicit self-tuning algorithms. An implicit self-tuning controller directly estimates controller coefficients from the measured data, while an explicit self-tuning controller first estimates the plant behaviour and uses this to calculate new controller parameters. In this thesis, explicit self-tuning control has been employed, since this allows to reuse the results derived in the last chapter. Figure 5.1.1 shows a schematic of an explicit self-tuning controller. Please note, that the double border around the plant block represents non-linear or time-varying behaviour.

A particular assumption has been made with regard to online controller synthesis in this thesis: The design specifications, specified in the desired closed-loop poles and — more importantly — in the fixed parts $H_R(z^{-1})$ and $H_S(z^{-1})$ of the controller polynomials $R(z^{-1})$ and $S(z^{-1})$, are assumed to be suitable for any parameter variation of the plant. The previous chapter briefly showed, that with respect to the lifting device model, this is a viable assumption, because identical specifications only resulted in higher gains in the input sensitivity function $S_{up}(z^{-1})$ and thus larger controller output amplitudes. While no limits on the actuator output have been imposed, it might be necessary for very large loads to restrict the controller output to prevent it from saturation. An additional remark is in order: Invariant controller specifications automatically result in an invariant controller order with respect to the RST controller sensitivity shaping approach employed in this thesis. This is in fact a welcome simplification and promotes this synthesis approach's applicability with self-tuning.

[1] From now on *recursive least squares* will be abbreviated with *RLS*

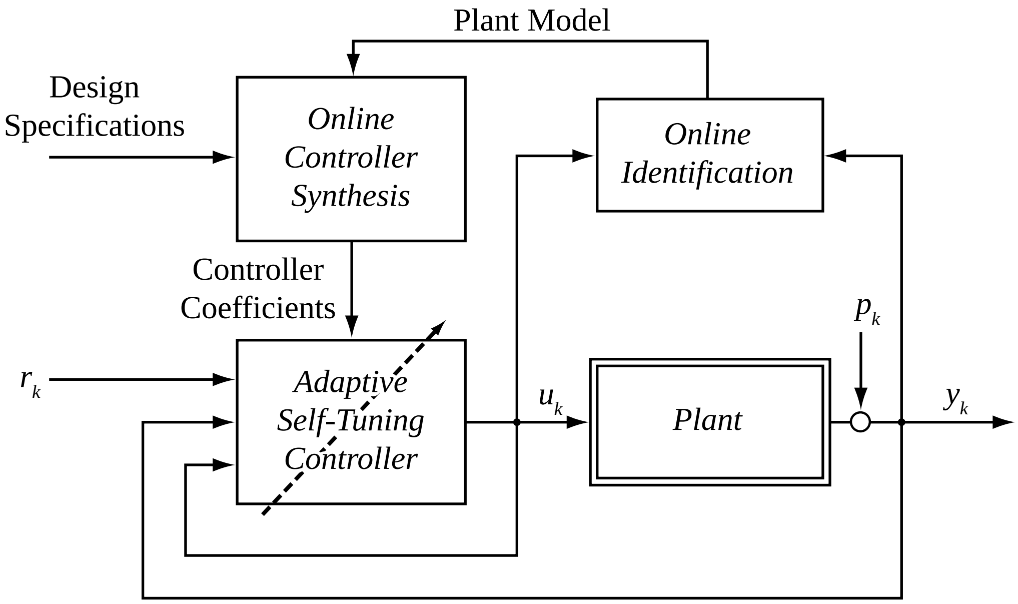

Figure 5.1.1.: Block Diagram of an Explicit Self-Tuning Controller Scheme

The underlying principle to the adaptive controller considered in this thesis is the Certainty Equivalence Principle. It states, that the control law design and the identification process can be separated. The control problem is solved for an estimated plant model, while it is treated as being known exactly [14, p. 16]. This separation evokes a common problem: While the control system is running, it cannot be made sure, whether the system input is sufficiently exciting, in order to correctly identify the plant.

5.2. Recursive Least Squares Identification Algorithm

The recursive least squares identification is only one of many identification algorithms suitable for online use, e.g. instrumental variable, maximum likelihood and stochastic approximation. All these algorithms have in common, that they estimate the plant parameters recursively, i.e. they update the model according to new data in every step, rather than recalculating the coefficients from a whole set of past input and output data. This reduces both the memory requirements and the computational effort to a level, modern microprocessor systems can handle.

The RLS algorithm invented by Ljung and Söderström has been chosen, because it has been applied with good effect in [11] for a trajectory tracking control problem and is said to achieve the best results for ARX model identification [14, p. 29]. The RLS algorithm used in this thesis shall be briefly outlined here.

ARX Model Structure A linear ARMAX model structure in the SISO case can be written as:

$$A(z^{-1}) \cdot y_k = z^{-d} B(z^{-1}) \cdot u_k + C(z^{-1}) \cdot e_k \tag{5.2.1}$$

It can be simplified to the ARX structure by assuming that the noise model $C(z^{-1}) = 1$. Furthermore, it will be assumed, that there is no additional time delay $d = 0$.

$$A(z^{-1}) \cdot y_k = B(z^{-1}) \cdot u_k + e_k \tag{5.2.2}$$

This model can be written in *regressor* form:

$$\begin{aligned} y_k &= \boldsymbol{\theta}_k^T \cdot \boldsymbol{\phi}_{k-1} + e_k \qquad (5.2.3)\\ \text{with } \boldsymbol{\theta}_k^T &= \begin{bmatrix} a_1 & a_2 & \dots & a_{n_A} & b_1 & b_2 & \dots & b_{n_B} \end{bmatrix}, \\ \boldsymbol{\phi}_{k-1}^T &= \begin{bmatrix} -y_{k-1} & -y_{k-2} & \dots & -y_{k-n_A} & u_{k-1} & u_{k-2} & \dots & u_{k-n_B} \end{bmatrix}. \end{aligned}$$

The Recursive Least Squares Algorithm with Forgetting Factor The recursive least squares algorithm with forgetting factor is comprised of the following set of formulas [10, c. 7-10], [14, p. 32], [15, p. 219]:

The estimated set of plant parameters is updated in each step by adding a correction term to the previous parameters. A bar on top a variable indicates, that its value is estimated.

$$\underbrace{\bar{\boldsymbol{\theta}}_k}_{\text{New Parameters}} = \underbrace{\bar{\boldsymbol{\theta}}_{k-1}}_{\text{Previous Parameters}} + \underbrace{\boldsymbol{K_k}(y_k - \bar{y}_k)}_{\text{Correction Term}} \tag{5.2.4}$$

The estimated output $\bar{y}_k$ is calculated from

$$\bar{y}_k = \bar{\boldsymbol{\theta}}_{k-1}^T \cdot \underbrace{\boldsymbol{\phi}_k}_{\text{Regressor}} . \tag{5.2.5}$$

The adaptation gain $\boldsymbol{K_k}$ is composed of

$$\boldsymbol{K_k} = \boldsymbol{Q}_k \cdot \boldsymbol{\phi}_k. \tag{5.2.6}$$

Where the inverse of $\boldsymbol{Q_k}$ is given by

$$\boldsymbol{Q_k}^{-1} = \underbrace{\lambda}_{\text{Forgetting Factor}} \cdot \boldsymbol{Q}_{k-1}^{-1} + \boldsymbol{\phi}_k \boldsymbol{\phi}_k^T. \tag{5.2.7}$$

It can be computed recursively by the matrix inversion lemma for $\boldsymbol{Q_{k-1}}$ regular to

$$\boldsymbol{Q_k} = \frac{1}{\lambda}\left(\boldsymbol{Q}_{k-1} - \frac{\boldsymbol{Q}_{k-1}\boldsymbol{\phi}_k\boldsymbol{\phi}_k^T\boldsymbol{Q}_{k-1}}{\lambda + \boldsymbol{\phi}_k^T\boldsymbol{Q}_{k-1}\boldsymbol{\phi}_k}\right). \tag{5.2.8}$$

By calculating $\boldsymbol{Q_k}$ the functional

$$V(\varepsilon_k) = \sum_{i=1}^{k} \lambda^{k-i} \cdot \varepsilon_k^2 \qquad (5.2.9)$$
$$\text{with } \varepsilon_k = y_k - \bar{y}_k$$

is minimised. The forgetting factor λ exponentially decreases the weight of past measurement data and can be tuned between $(0 \ldots 1]$ to achieve fast estimation or better averaging.

Simulation in Matlab For the simulations the MATLAB function `rarx` has been used to employ the RLS identification algorithm. The syntax requires $\bar{\boldsymbol{\theta}}_{k-1}$, $\boldsymbol{\phi}_k$ and $\boldsymbol{Q_k}$ to be initialised.

Figure 5.2.1 illustrates the RLS algorithm's iterative nature and its inclusion into the signal flow. The plant model's coefficients are contained inside the vector $\bar{\boldsymbol{\theta}}_k$ and are forwarded as signals indicated by $\bar{A}(z^{-1})$ and $\bar{B}(z^{-1})$ to the controller synthesis. In case of unexpected parameter behaviour, the coefficients are limited to certain bounds. This ensures an overall stability of the controlled plant.

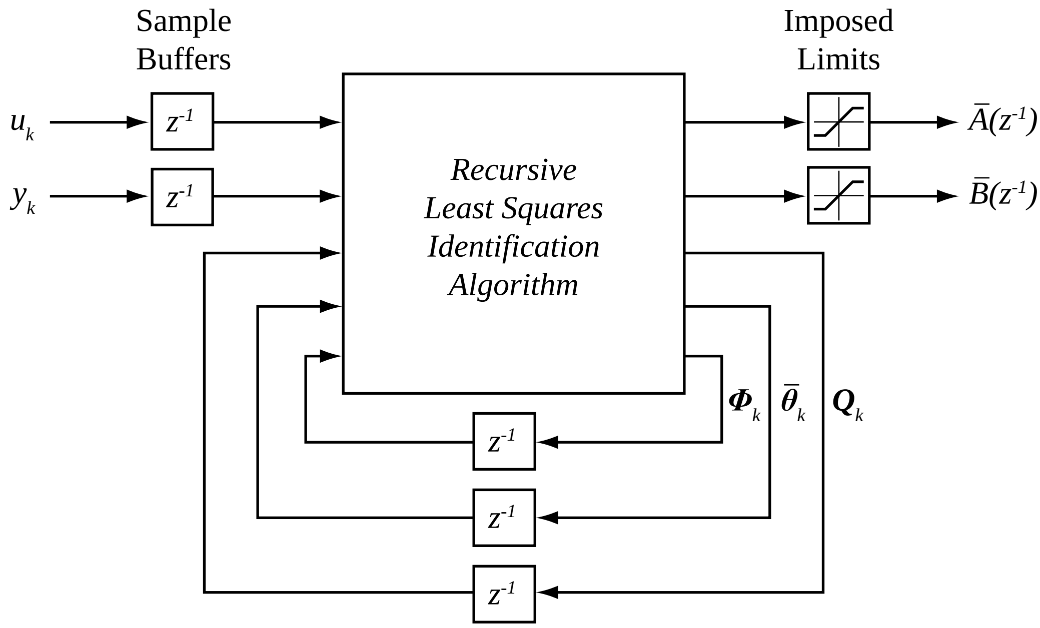

Figure 5.2.1.: Illustration of the RLS Algorithm's Iteration

5.3. Optimisation of the Synthesis Computations for Online Use

Since the recursive least squares algorithm already consumes additional processing power, the controller synthesis should be optimised. Currently the computation of the controller coefficients requires the solution of the Bezout Identity given in matrix notation by equation 4.2.7 via the inverse of the matrix $\boldsymbol{M}$. This matrix contains the plant model, as well as the fixed parts of the controller. Under the following restrictions, simplifications and assumptions, the inversion can be carried out symbolically.

Limitation of Fixed Controller Parts Limiting the fixed controller parts significantly reduces the dimensions of the matrix $\boldsymbol{M}$. Lowering the demands with regard to disturbance attenuation or more specifically its effect on the actuator stress, the controller design can be adjusted by decreasing the exponent in the fixed part of $R(z^{-1})$:

$$H_R(z^{-1}) = \left(1 + z^{-1}\right)^2. \tag{5.3.1}$$

Taking $H_S(z^{-1}) = 1$ as before gives $\boldsymbol{M} \in \mathbb{R}^{6\times 6}$, which suggests, that a symbolic inversion might be possible, while as a trade-off expectations with regard to the control quality have been slightly lowered.

$$\underbrace{\begin{bmatrix} 1 & 0 & 0 & 0 & 0 & 0 \\ \bar{a}_1 & 1 & 0 & 0 & \bar{\bar{b}}_1 & 0 \\ \bar{a}_2 & \bar{a}_1 & 1 & 0 & \bar{\bar{b}}_2 & \bar{\bar{b}}_1 \\ 0 & \bar{a}_2 & \bar{a}_1 & 1 & \bar{\bar{b}}_3 & \bar{\bar{b}}_2 \\ 0 & 0 & \bar{a}_2 & \bar{a}_1 & \bar{\bar{b}}_4 & \bar{\bar{b}}_3 \\ 0 & 0 & 0 & \bar{a}_2 & 0 & \bar{\bar{b}}_4 \end{bmatrix}}_{\boldsymbol{M}\in\mathbb{R}^{6\times 6}} \cdot \boldsymbol{k} = \underbrace{\begin{bmatrix} 1 \\ p_1 \\ p_2 \\ p_3 \\ p_4 \\ p_5 \end{bmatrix}}_{\boldsymbol{p}\in\mathbb{R}^{6}} \tag{5.3.2}$$

Note that the pole placement coefficients $p_i, i = 1 \dots 5$ can be left unchanged.

Reduction of Independent Variables The identification algorithm estimates the parameters of the plant model

$$H(z^{-1}) = \frac{\bar{b}_1 \cdot z^{-1} + \bar{b}_2 \cdot z^{-2}}{1 + \bar{a}_1 \cdot z^{-1} + \bar{a}_2 \cdot z^{-2}}. \tag{5.3.3}$$

Since in this application only variations with regard to the load mass $\hat{M}$ are of interest and subject to parameter identification, the number of independent variables can be reduced by mathematical means. The symbolic discretisation of the plant model given in section 3.2.2 yields a representation, where the polynomial coefficients can be expressed as functions of the parameter p. The relevant equations (3.2.14) will be reprinted here for convenience (for $z_0 = -1$):

$$\begin{aligned} \bar{b}_1 &= \frac{T_s}{2}\frac{\hat{k}}{\hat{b}}(1-\bar{p}) & \bar{b}_2 &= \frac{T_s}{2}\frac{\hat{k}}{\hat{b}}(1-\bar{p}) \\ \bar{a}_1 &= -(1+\bar{p}) & \bar{a}_2 &= \bar{p} \end{aligned}$$
$$\text{with } \bar{p} = e^{-\frac{\hat{b}}{\hat{M}}T_s}.$$

Please note, that a bar above the variables indicates, that their respective values are only estimated. With known sampling time T_s, damping $\hat{b}$ and input gain $\hat{k}$ — all of which could be estimated by an experiment with known load — the parameter $\bar{p}$ can be extracted from the estimated data. Furthermore the matrix $\boldsymbol{M}$ can now be written as $\boldsymbol{M}(\bar{p})$. This ultimately enables the controller coefficients to be dependent only on $\bar{p}$.

The resulting representation of $\boldsymbol{M}(p)$ and the associated equation is:

$$\underbrace{\begin{bmatrix} 1 & 0 & 0 & 0 & 0 & 0 \\ -(1+\bar{p}) & 1 & 0 & 0 & 0.7008(1-\bar{p}) & 0 \\ \bar{p} & -(1+\bar{p}) & 1 & 0 & 2.1020(1-\bar{p}) & 0.7008(1-\bar{p}) \\ 0 & \bar{p} & -(1+\bar{p}) & 1 & 2.1020(1-\bar{p}) & 2.1020(1-\bar{p}) \\ 0 & 0 & \bar{p} & -(1+\bar{p}) & 0.7008(1-\bar{p}) & 2.1020(1-\bar{p}) \\ 0 & 0 & 0 & \bar{p} & 0 & 0.7008(1-\bar{p}) \end{bmatrix}}_{\boldsymbol{M}\in\mathbb{R}^{6\times 6}} \cdot \boldsymbol{k} = \underbrace{\begin{bmatrix} 1 \\ -2.816 \\ 2.973 \\ -1.395 \\ 0.2455 \\ 0 \end{bmatrix}}_{\boldsymbol{p}\in\mathbb{R}^{6}}$$

Further Simplification of the Resulting Symbolic Expression The inversion $\boldsymbol{M}^{-1}(\bar{p})$ still yields a vast expression containing polynomials of $\bar{p}$ up to the power of 4. Under the assumption, that the load $\hat{M}$ is varied only within known constraints $\hat{M} \in \left[\hat{M}_{min} \dots \hat{M}_{max}\right]$, powers of $\bar{p}$ greater than 1 can be approximated:

For $\hat{M} \in [10,000\,\text{kg} \dots 30,000\,\text{kg}]$ the following approximations yield good results:

$$\begin{aligned} \bar{p}^2 &= 2.00 \cdot \bar{p} - 1.0000 \\ \bar{p}^3 &= 2.95 \cdot \bar{p} - 1.9495 \\ \bar{p}^4 &= 3.67 \cdot \bar{p} - 2.6729 \end{aligned}$$

Figure 5.3.1 visualises the goodness of fit.

Resulting Controller Coefficients The symbolic inversion yields a vector of the controller coefficients $k(\bar{p}$ dependent on the identified plant parameter $\bar{p}$.

$$\begin{aligned} \boldsymbol{k}(\bar{p}) &= \boldsymbol{M}^{-1}(\bar{p}) \cdot \boldsymbol{p} \\ &= \begin{bmatrix} 1 & \tilde{s}_1 & \tilde{s}_2 & \tilde{s}_3 & \tilde{r}_0 & \tilde{r}_1 \end{bmatrix}^T . \end{aligned} \tag{5.3.4}$$

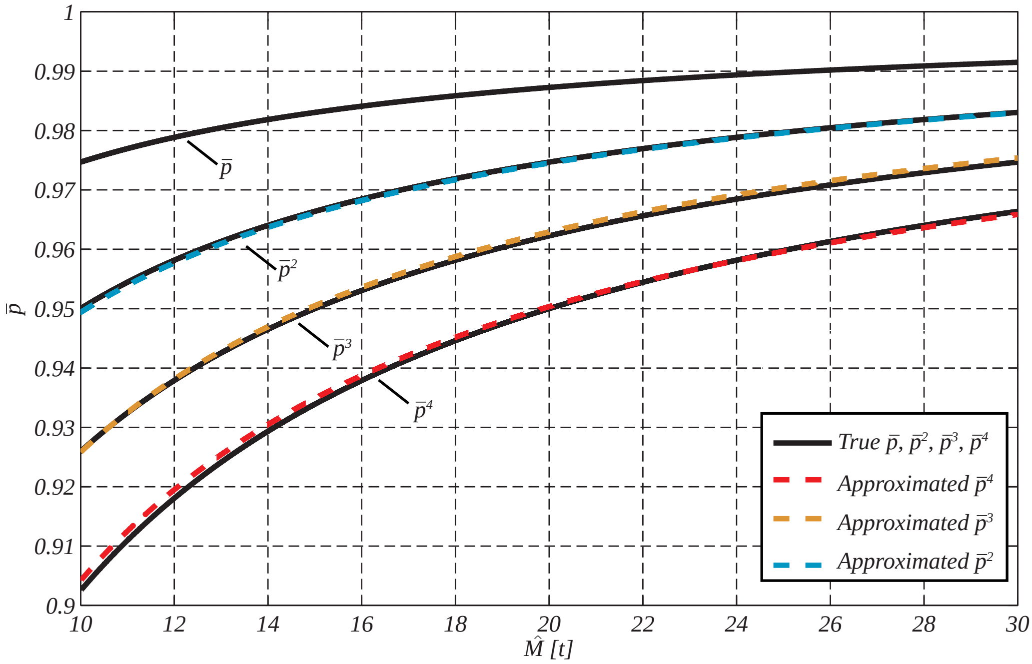

Figure 5.3.1.: Approximations of Higher Powers of the Fictitious Plant Parameter $\bar{p}$

$$\boldsymbol{k}(\bar{p}) = \begin{bmatrix} 1.0 \\ -\frac{0.6411\bar{p}+1.0153}{\bar{p}(\bar{p}+1.0)} \\ \frac{0.7035\bar{p}-0.1222}{\bar{p}(\bar{p}+1.0)} \\ \frac{0.1174\bar{p}-0.0943}{\bar{p}(\bar{p}+1.0)} \\ -\frac{0.0722\bar{p}-0.0542}{\bar{p}-1.0003} \\ \frac{\bar{p}(0.0885\bar{p}-0.0711)}{\bar{p}-1.0003} \end{bmatrix} \tag{5.3.5}$$

All symbolic calculations have been done with MATLAB/SIMULINK.

Avoiding Numerical Inaccuracies by Employing a Lookup Table Due to the nature of the dependency of $\bar{p}$ from $\hat{M}$, the values of $\bar{p}$ are all close to 1 (refer to figure 5.3.1). Thus the denominators for the coefficients $\tilde{r}_0$ and $\tilde{r}_1$ occurring in $\boldsymbol{k}(\bar{p})$ can be expected to be close to 0, which may lead to numerical inaccuracies. It is therefore a more feasible solution, to store precalculated coefficients into a lookup table, which has been calculated with suitably precise arithmetics.

To further reduce the amount of memory usage, it can be observed, that for varying load mass $\hat{M}$, the plant parameters a_1 and a_2 change almost unnoticably, and thus they are not vital to accurately describe the changes in the dynamics. As a consequence, the controller can remain invariant with regard to its transfer function $S(z^{-1})$ and only the coefficients of $R(z^{-1})$ need to be stored. Figure 5.3.2 depicts the change of $\tilde{r}_0$ and $\tilde{r}_1$ versus $\bar{p}$. A lookup table of about 20 distinct points has been stored and used to adapt the controller online.

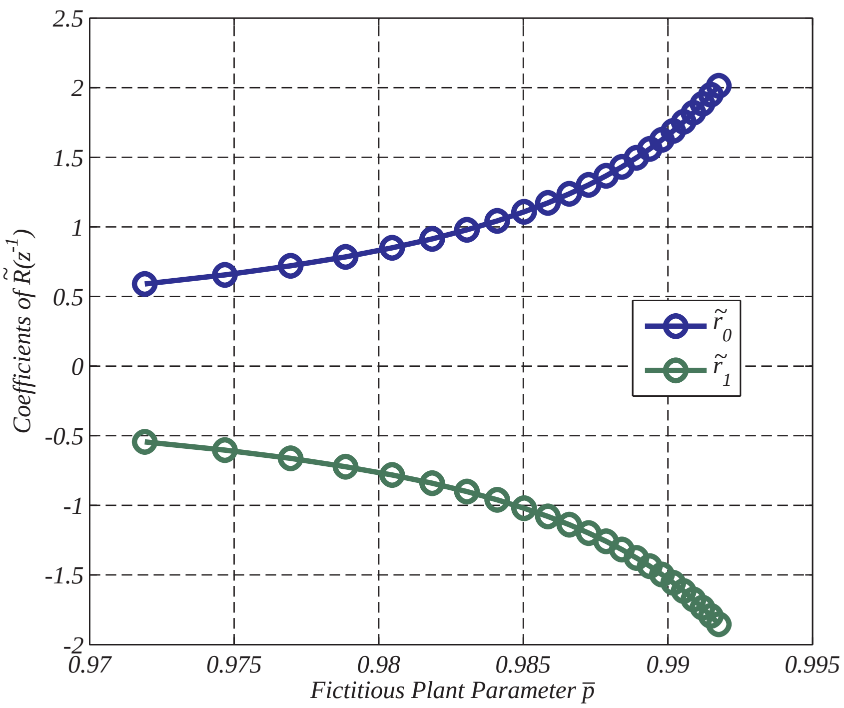

Figure 5.3.2.: Values of $\tilde{R}(z^{-1})$ Versus Fictitious Plant Parameter $\bar{p}$

The computed and the fixed part of the controller transfer function $R(z^{-1})$ still need to be multiplied:

$$R(z^{-1}) = \left(\tilde{r}_0 + \tilde{r}_1 z^{-1}\right) \cdot \left(1 + z^{-1}\right)^2 . \tag{5.3.6}$$

Identification of the Plant Parameter $\bar{p}$ Until now, the question of how to obtain the value of $\bar{p}$ from the estimated plant parameters $\bar{b_1}$, $\bar{b_2}$, $\bar{a_1}$ and $\bar{a_2}$ has been intentionally left unanswered, due to the fact, that $\bar{p}$ could be calculated from any of those. It is a somewhat arbitrary decision of which parameter or any combination of them to use.

It is straightforward to determine $\bar{p}(\bar{b_1})$, $\bar{p}(\bar{b_2})$, $\bar{p}(\bar{a_1})$ and $\bar{p}(\bar{a_2})$. After that, the resulting estimates have been grouped into those obtained from the plant numerator and the denominator and the arithmetic averages are taken:

$$\bar{p}_{\bar{B}} = \frac{\bar{p}(\bar{b_1}) + \bar{p}(\bar{b_2})}{2} \qquad \bar{p}_{\bar{A}} = \frac{\bar{p}(\bar{a_1}) + \bar{p}(\bar{a_2})}{2}. \tag{5.3.7}$$

A weighted sum of the parameter $\bar{p}$ determined by the respective group may give the final value:

$$\bar{p} = \alpha_B \cdot \bar{p}_{\bar{B}} + \alpha_A \cdot \bar{p}_{\bar{A}} \tag{5.3.8}$$

As has been mentioned before $\bar{a_1}$ and $\bar{a_2}$ are almost unaffected by load changes. To set $\alpha_A = 0$ would be an intuitive choice. It has been observed, though, that a small weight can render the identification a little more conservative and less prone to noise disturbances. A small gain below 1 further enhanced the accuracy of the identification, because $\bar{p}$ always appeared to be a little too large. The final weighting function has been chosen as follows:

$$\bar{p} = 0.9937 \cdot (0.875 \cdot \bar{p}_{\bar{B}} + 0.125 \cdot \bar{p}_{\bar{A}})\,. \tag{5.3.9}$$

In summary the above mentioned derivation yields an optimisation of the adaptive RST structure controller, which reduces the controller synthesis part to a mere lookup table and interpolation between values. An approximation of the lookup table values by a polynomial function of the parameter $\bar{p}$ would further render an increase of memory capacity unnecessary. This is a decision, which can be made according to available hardware.

5.4. Simulation Results

The adaptive RST-structure controller has also been tested without the simplified synthesis approach described in the last chapter. It has been observed, that the recursive least squares identification algorithm is very sensitive to output disturbances. For disturbances of the same strength as applied to the fixed RST-structure controller, the adaptive controller actually fails to provide acceptable results. Detailed plots of the result will be omitted here.

The optimised lookup table based solution has been able to provide better results, since oscillations in the estimated plant parameters can be evened out by adjusting the weighted sum of the fictitious plant parameter $\bar{p}$. Still, noise entering the output disturbance channel strongly affected the quality of control. The following simulations have therefore been done with a noise magnitude reduced to $\frac{1}{4}$. Under this constraint, the adaptive controller has been tested for three different scenarios as they have been introduced at the beginning of the chapter and are depicted by figure 5.4.1.

The choice of the forgetting factor λ has a high influence on the speed of estimation. A lower factor results in the identification algorithm to be able to track sudden parameter changes. For the simulations a value of $\lambda = 0.9$ has been used to provide fast decay of past measurement data and reasonable reduction of noise in the estimated parameters.

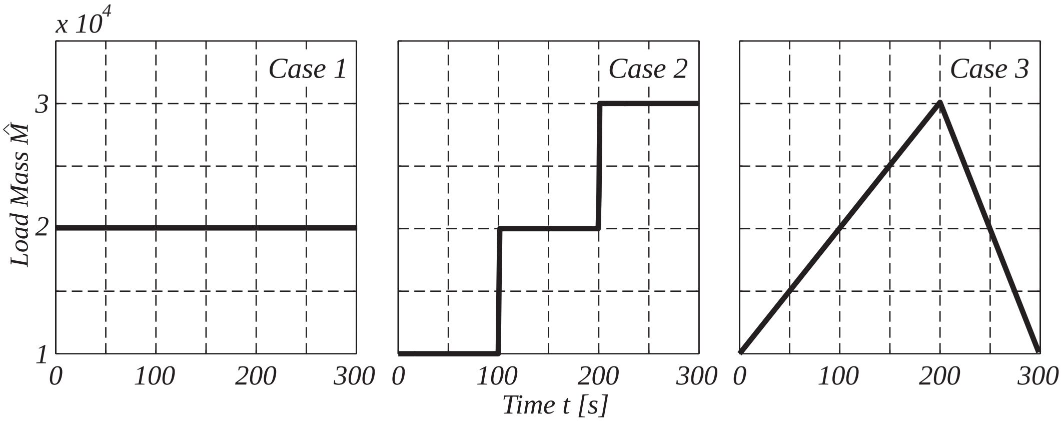

Figure 5.4.1.: Constant (Case 1), Pseudo-Constant (Case 2) and Time-Varying (Case 3) Load Scenarios

As can be seen in all cases, the controller almost perfectly tracks the desired trajectory in the sense of the design objectives independent of the load changes. Only minor overshoots can be observed. The controller output practically only varies in its maximum amplitude, which reflects the heavier load to be lifted.

The noise introduced to the controller coefficients via the plant parameter estimation can be attenuated by filtering the measurement data. In a real application more information with regard to the noise type and its predominant frequency is available, which could help smoothening the adaptation algorithm in certain frequency bands. In the simulations a filter obtained by discretising

$$F(s) = \frac{1}{(40 \cdot s + 1)^2}$$

effectively cut off the high frequency noise introduced at the output and subsequently smoothed the estimation signals. The quality of control remained the same.

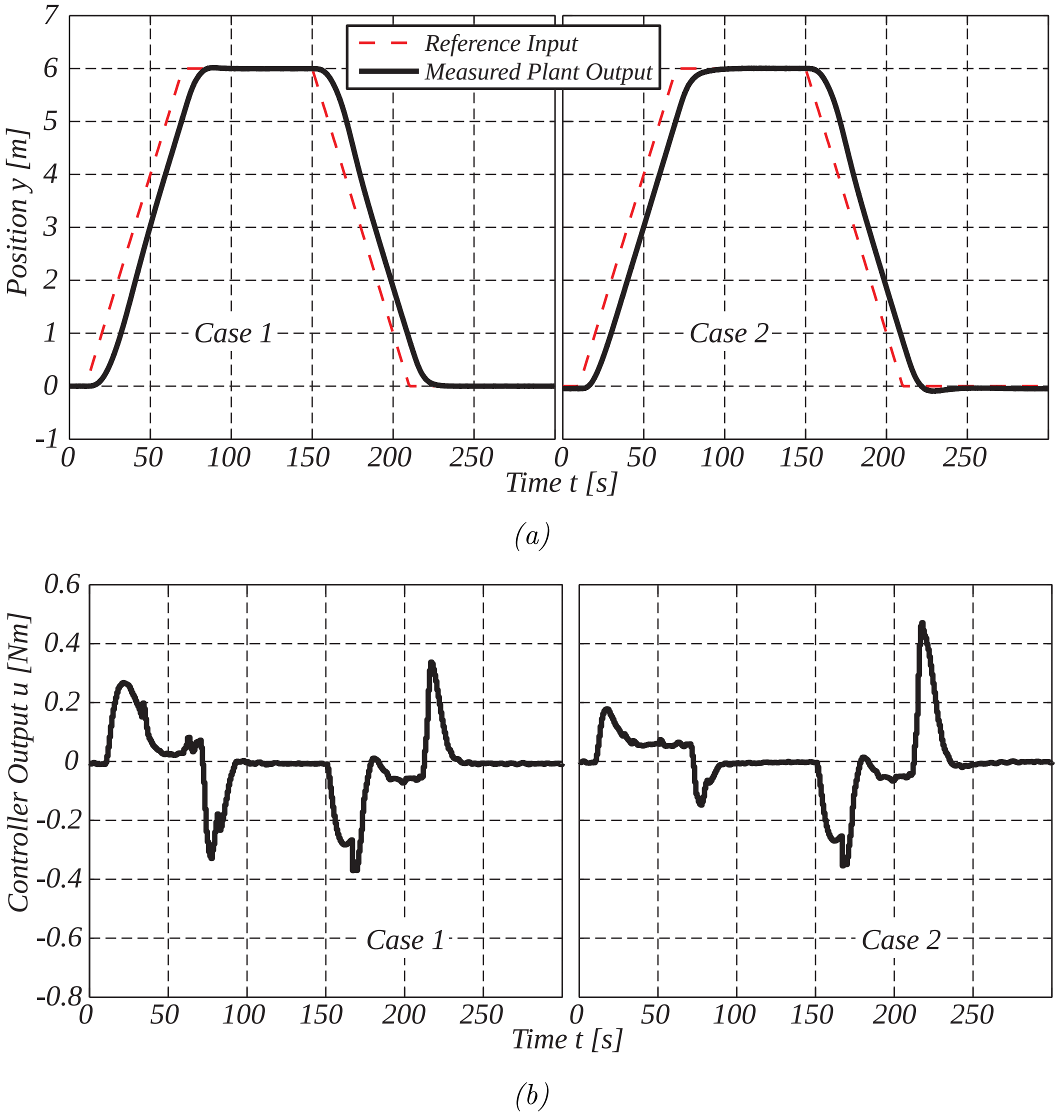

Figure 5.4.2.: Simulation Results for the Plant Controlled by an Adaptive RST-Structure Controller and Constant or Pseudo-Constant Load Mass $\hat{M}$, while under the Influence of Noise. *(a)* Plant Output y and Reference Signal r. *(b)* Controller Output u.

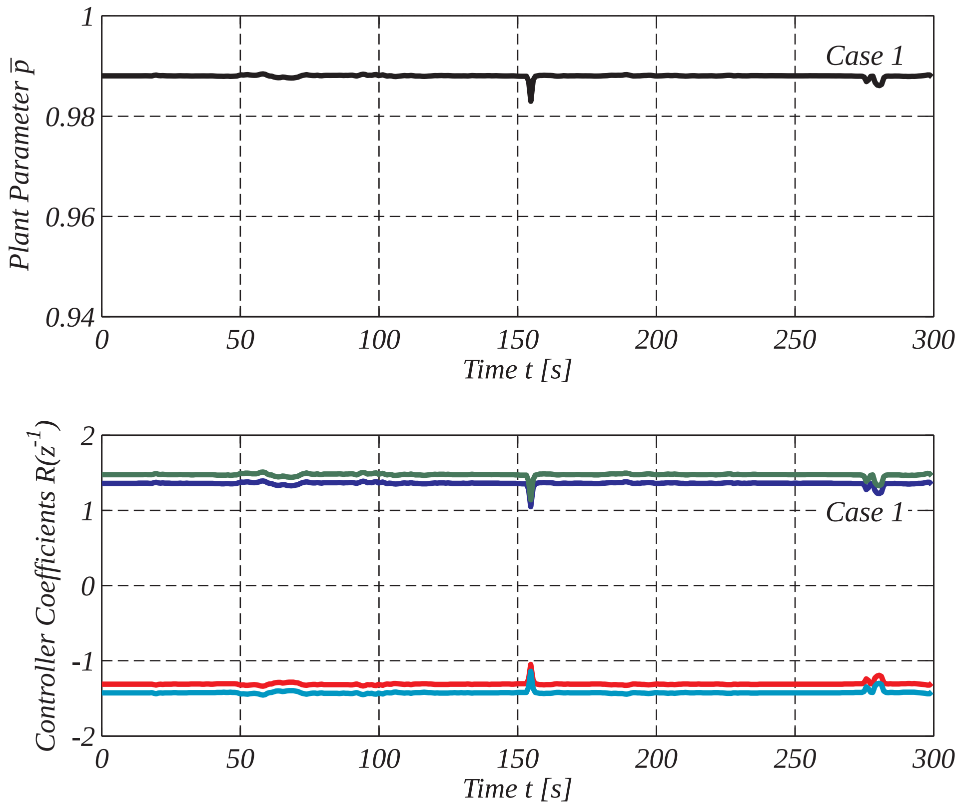

Figure 5.4.3.: Estimated Plant Parameter $\bar{p}$ and Resulting Controller Coefficients of $R(z^{-1})$ for the Plant Controlled by an Adaptive RST-Structure Controller and Constant Unknown Load Mass $\hat{M}$, while under the Influence of Noise.

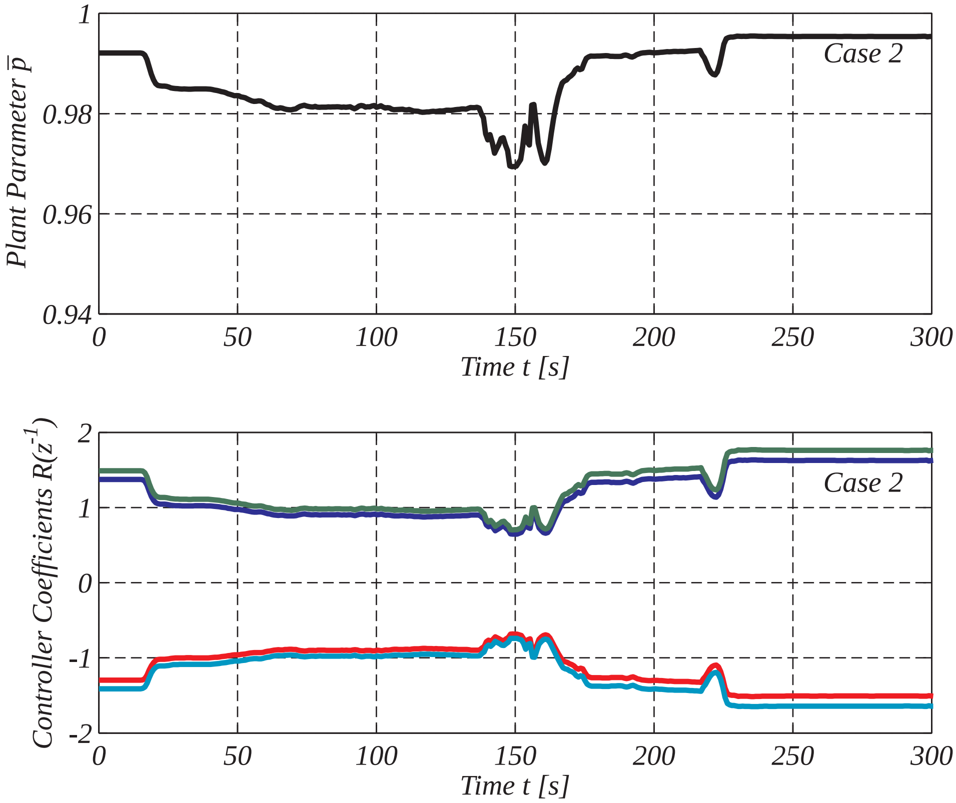

Figure 5.4.4.: Estimated Plant Parameter $\bar{p}$ and Resulting Controller Coefficients of $R(z^{-1})$ for the Plant Controlled by an Adaptive RST-Structure Controller and Pseudo-Constant Unknown Load Mass $\hat{M}$, while under the Influence of Noise.

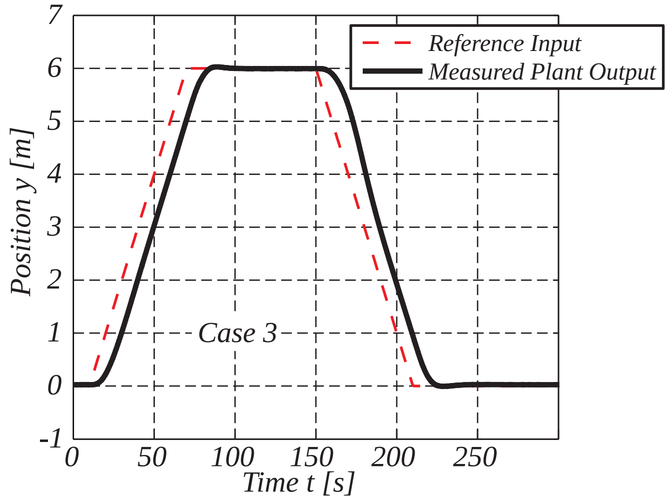

(a)

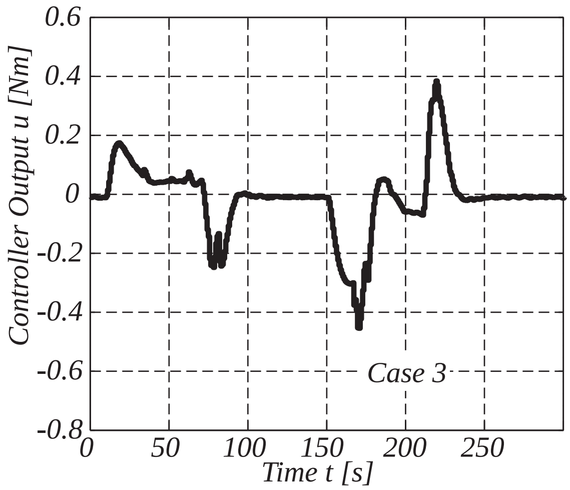

(b)

Figure 5.4.5.: Simulation Results for the Plant Controlled by an Adaptive RST-Structure Controller and Time-Varying Load Mass $\hat{M}$, while under the Influence of Noise. *(a)* Plant Output y and Reference Signal r. *(b)* Controller Output u.

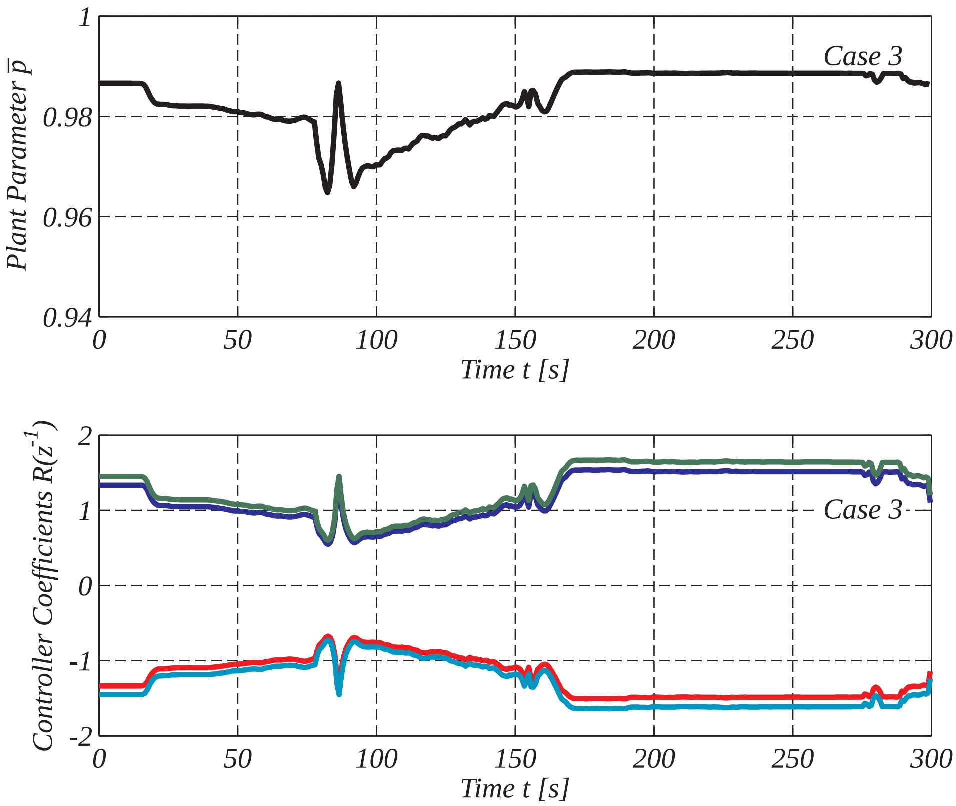

Figure 5.4.6.: Estimated Plant Parameter $\bar{p}$ and Resulting Controller Coefficients of $R(z^{-1})$ for the Plant Controlled by an Adaptive RST-Structure Controller and Time-Varying Load Mass $\hat{M}$, while under the Influence of Noise.

6. Conclusion and Outlook

The thesis at hand is divided into three parts. After an introduction to the overall principle of the Shànghǎi flood gate security device, the first part contained a description of the current realisation of its control system employing a Siemens S7-200 PLC and a wire-rope hoist driven by a two-speed electric motor.

An intermediate chapter containing the mathematical modelling of a general wire-rope hoist driven lifting device lays the foundation for the two subsequent parts.

The next chapter deals with the derivation of a more sophisticated control system which can still be implemented on the existing PLC. Changes to the instrumentation layout have to be made, though.

The final chapter abstracts from the Shànghǎi flood gate control system and aims for a simple, yet very versatile positioning control system to employ on lifting devices, which are supposed to lift unknown or time-varying loads.

The following conclusion will summarise the results in depth. An outlook gives a brief glimpse on work yet to be done and further possibilities to enhance the control system.

6.1. Conclusion

The current realisation of the Shànghǎi flood gate control system is a simple and cost effective solution, which — at the time of primary testing — has shown some flaws. With some engineering effort the control system can be finished and installed to the Shànghǎi subway network, which probably happens as this text is written.

However, useful suggestions on the improvement with regard to instrumentation and control algorithm have been outlined in section 2.4. It has been the aim of this thesis to further investigate the advantage and feasiblity of a discrete feedback based control algorithm, provide a design approach and present its explicit solution. It has been shown, that with the additional effort of employing a drive and an electric AC motor suitable for feedback torque control, a control algorithm in the form of a fixed discrete RST-structure controller is likely to provide excellent results on the real plant. This has been indicated by the fact, that the sensitivity shaping pole placement approach allows to achieve disturbance attenuation, steady state accuracy and robustness to a degree set by the designer. By manually designing the controller, this ensures that it is scalable to fit the computation hardware and actuator restrictions. The design presented in this thesis can also be optimised to achieve faster system response at the expense of higher torque amplitudes. The resulting control law is simple and only demands for sample buffering, additions and multiplications. In the outcome, the improved control system promises to provide a safer control system with more flexibility with regard to the possible automated positioning, a higher controlled movement speed, reduction of wear to the components by disturbance attenuation and soft impact approach of the reference position. The number of sensors can be drastically reduced, thus lessening the required amount of maintenance. On the downside, it is probably necessary to retune the control algorithm when the system parameters change, which might occur, for example, by aging components. However, the algorithm has been shown to be able to yield controllers, which inhere a certain amount of robustness, which can also be intentionally enlarged by imposing more strict robustness margins during design. In summary the sensitivity shaping RST-structure controller synthesis approach is deemed feasible with respect to the given problem.

A next step has been taken by generalising the problem to the control of a lifting device lifting unknown or time-varying loads. While this does not need to be applied to the Shànghǎi flood gate control system, it could offer a valid implementation scheme and algorithm applicable to many similar problems or it could even lay the basis for a stand-alone position control product envisioned by the head of the College of Mechanical Engineering of Tongji University, Shanghai, Professor Liu Haijiang. It has been the aim to find an adaptive control algorithm based on the previously introduced RST-structure controller synthesis approach, which still imposes only a few demands on the hardware. With the help of controller synthesis optimisations and simplifications a highly specialised solution has been found and successfully simulated under the influence of disturbances.

6.2. Outlook

The following outlook is comprised of two separate parts, which correspond to the achievements of chapters 4 and 5, respectively:

1. Equipping the Shànghǎi flood gate control system with the suggested improvements and implementing the RST-structure control algorithm.
2. Designing a controller hardware structure suitable for the implementation of the adaptive controller and finalising it as a stand-alone device.

6.2.1. Adjustments to the Existing Control System

The adjustments needed for the implementation of the RST-structure controller algorithms are few but indispensable. The most difficult and probably expensive part will be to find a suitable AC motor and corresponding drive, which can achieve high and constant torques at very low speeds. The transmission device might need a redesign to fulfill the assumptions imposed in section 3.1, especially with regard to self-locking or a motor brake. When the unwinding of the wire-rope does not take place in a linear fashion, a simple correction function can be applied, which can be obtained by preliminary and more accurate measurements incorporating the use of the encoder and an additional optical instrument for comparison.

The current PLC device layout needs to be enhanced by an analog I/O device, in order to feed the torque reference voltage command to the drive. The voltage command is computed inside the PLC, which needs to be reprogrammed. The reprogramming includes:

- Reading of the encoder output signal and transformation into linear position.
- Buffering of past controller output and plant input samples.
- Calculation of the RST control law.
- Voltage command output within voltage range specified by the drive.
- Storage of prespecified flood gate positions and update of the movement control logic.

While the above mentioned required adjustments are few and might seem simple, some possible issues with respect to hardware and programming might occur:

Limited Encoder Cable Length Encoders typically have a limited connection cable length, which can be increased by employing amplifiers. However, encoders as well as the amplifiers need additional power supply. This actually represents a disadvantage with regard to control system simplicity and liability to power failures.

Additional Power Supplies The drive and encoders need additional power supply. It is not guaranteed, that the existing power supply layout can provide sufficient possibilites for supply.

Analog-Output Extension to the PLC The Siemens S7-200 does not support native analog I/O. Additional components like the EM-235 are needed to extend its functionality.

Suitable and Economical AC Motor and Drive Solution A two-stage motor design, where each motor is responsible for a single fixed speed of motion, will be rendered unnecessary by a continuously torque-controlled AC motor approach. However, to substitute the motors by an economical motor and drive solution may be difficult. The benefits with respect to system reliability and the degree of protection the flood gates may provide could easily outweigh the higher costs, though.

Insufficient Computational Power Since the RST-structure controller can be enhanced by many fixed controller parts to support a high degree of robustness, limits are imposed by the computational performance of the PLC and its memory capacity. PLCs with dedicated RST controller support might be beneficial and even less expensive.

6.2.2. Design of an Adaptive Controller Hardware

It is assumed, that the recursive least squares identification algorithm can not be implemented on a PLC device. For this purpose, an additional piece of hardware has to be designed, which holds a processor capable of processing the data for identification and generating the torque reference command, which is then fed to the drive. The module should also be able to identify the damping parameter and adjust the lookup table accordingly. This has not to be done online, since it can be assumed, that the damping is a constant plant parameter. Input and output gain have to be able to be programmed manually.

Figure 6.2.1 illustrates the updated control device configuration with the adaptive controller module inserted. The development of the adaptive position control module still

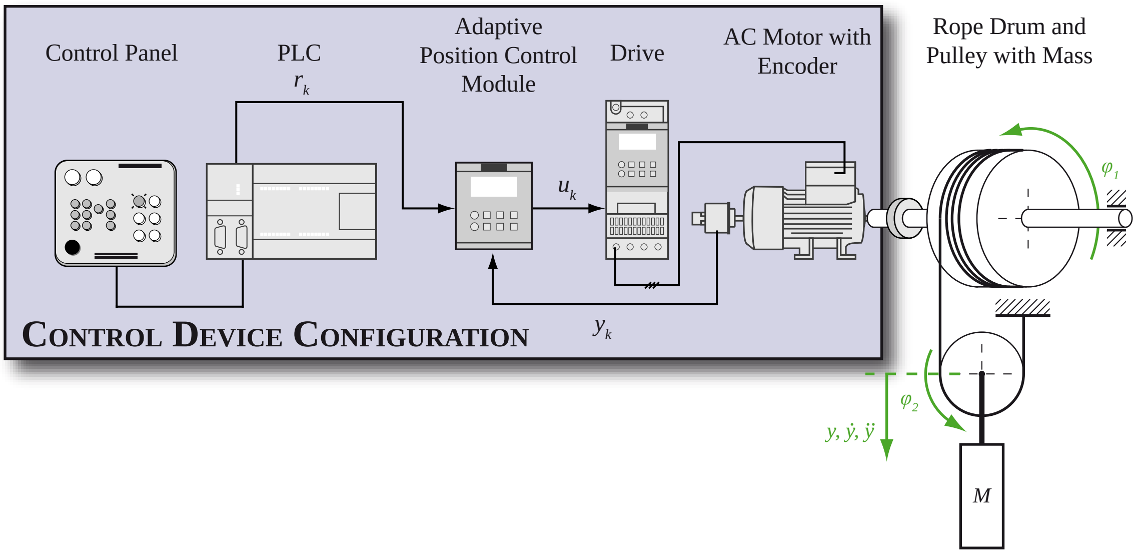

Figure 6.2.1.: Control Device Configuration Including a Dedicated Adaptive Torque Reference Command Generator Module

needs some remarkable engineering effort. To summarise the following steps have to be taken:

- Selection among implementation platforms for the recursive least squares and the control algorithm. Possible choices are: Microprocessors, digital signal processors, field programmable gate arrays.
- Implementation of the algorithms on chip and extending them.
- Design of all surrounding circuitry.
- Designing the control panel interface.

A discussion of the individual suitability of the platforms suggested and all electrical engineering necessary is beyond this thesis and is left for future work.

A. Contents of the Accompanying Disc

The CD ROM, which accompanies this thesis, contains the relevant *MATLAB* files created for the controller synthesis, design and simulation. The following will provide a quick overview of the files and their use. In order to easily run the *Simulink* simulations, it is recommended, that the disc is first copied to a hard drive, for instance to a directory `C:\LiftingDeviceControl`. In *MATLAB* the current working directory should be set to this path. The order, in which the files are executed is important. Please take heed of the remarks given below.

🗀 **.\LiftingDeviceControl** This folder contains all relevant MATLAB files.

- 🗋 **Parameters.m** Run this file first. It contains all needed parameters defining the plant.

- 🗋 **InitialiseFixedController.m** This file initialises all relevant variables for the fixed RST-structure controller simulation. It holds the computations for the controller coefficients and visualises the sensitivity plots.

- 🗋 **RSTSensitivityShaping.m** Controller computations in the sense of the sensitivity shaping pole placement approach are done by this function script. It is used by the initialisation scripts.

- 🗋 **RSTPolePlacementAnalysisPlots.m** A script, which generates sensitivity plots for the designer to analyse the closed-loop dynamics. This file is used by the initialisation scripts.

- 🗋 **FixedController.mdl** This SIMULINK model can be used to simulate the closed-loop system response of the linear parameter-varying model of the flood gate lifting device controlled by a fixed RST-structure controller.

- 🗋 **ParameterVariationRobustnessAnalysis.m** The MATLAB file calculates robustness margins for load mass plant parameter variations in a certain range. It thus provides a measure for the robustness of the fixed RST-structure controller against an inertial uncertainty.

- 🗋 **RSTPolePlacementExtendedRobustnessPlots.m** A script, which generates sensitivity plots for the designer to analyse the closed-loop robustness with respect to plant parameter variations. This file is used by the `ParameterVariationRobustnessAnalysis.m` script.

- 🗋 **InitialiseOptimisedAdaptiveController.m** This file initialises all relevant variables and the lookup table for the adaptive RST-structure controller simulation. It contains the computations for the initial controller coefficients and visualises the sensitivity plots.

\ **SelfTuningExplicitRSTControllerRecursiveFastLookUpTable.mdl** This SIMULINK model can be used to simulate the closed-loop system response of the linear parameter-varying model of the flood gate lifting device controlled by an adaptive RST-structure controller.

\ **RSTSensitivityShapingFastOnlineLookUpTable.m** A MATLAB function, which is used in an embedded function online to realise the adaptive controller.

\ **SymbolicDiscretisation.m** This file contains some calculations used in conjunction with the symbolic discretisation of the continuous transfer function given in chapter 3.

\ **HigherPowersApproximation.m** A script, which visualises the approximation of the fictitious plant parameter derived in section 5.3.

List of Figures

Bibliography

[1] Siemens AG. SIEMENS S7-200 *Programmable Controller System Manual.* Siemens AG, http://www.siemens.com, 2007.

[2] L. A. Bryan and E. A. Bryan. *Programmable Controllers - Theory and Implementation.* Industrial Text Company, 2nd edition edition, 1997.

[3] Yaskawa Electric Corporation. *$\Sigma - II$ Series SGM-H/SGDM User's Manual — SGMAH/SGMPH/SGMGH/SGMSH/SGMDH/SGMCS Servomotors SGDM SERVOPACK, Manual No. SIEPS80000015A.* Yaskawa Electric Corporation, http://www.yaskawa.com, 2003.

[4] CEng MIEE MInstMC E.A. Parr, MSc. *Programmable Controllers — An engineer's guide.* Self-published, 3rd edition edition, 2003.

[5] John R. Hackworth and Frederick D. Jr. Hackworth. *Programmable Logic Controllers: Programming Methods and Applications.* Self-published, unknown year.

[6] Shanghai Government City News http://www.shanghai.gov.cn Unknown Author. Shanghai gears up for the flood season. *Shanghai Government City News*, 2007.

[7] Zou Huilin and Wu Chong. Rising sea levels trigger fear over shanghai's future. *China Daily*, 2007.

[8] Andreas Kwiatkowski. *LPV Modelling and Application of LPV Controllers to SI Engines.* PhD thesis, Technische Universität Hamburg-Harburg, 2007.

[9] Ioan D. Landau and Gianluca Zito. *Digital Control Systems — Design, Identification and Implementation.* Springer-Verlag London Limited, 2006.

[10] The Mathworks, http://www.mathworks.com. *MATLAB System Identification 7 - User's Guide*, 2009.

[11] Mechanical Engineering Department, Gaziantep University, Turkey. *Self-Tuning Control as Conventional Method*, 2002.

[12] M. Schmittele and A. Bader. *Micromaster 4 Application Description — Conveyor Systems, Hoisting Gear Engineering and Commissioning.* Siemens AG, http://www.siemens.com, 2005.

[13] Steffen Sommer. *Regelung linearer parameterveränderlicher (LPV-) Systeme mit Hilfe klassischer Regelungsstrukturen und Anwendung auf nichtlineare Regelstrecken*. PhD thesis, Otto-von-Guericke-Universität Magdeburg, 2003.

[14] J. Fessl V. Bobal, J. Böhm and J. Machacek. *Digital Selt-Tuning Controllers — Algorithms, Implementation and Applications*. Springer-Verlag London Limited, 2005.

[15] Slobodan N. Vukosavic. *Digital Control of Electrical Drives*. Springer Science+Business Media, 2007.

[16] Herbert Werner. *Control Systems Theory And Design - Lecture Notes*. Institut für Regelungstechnik, ver. juli 2008 edition, 2008.